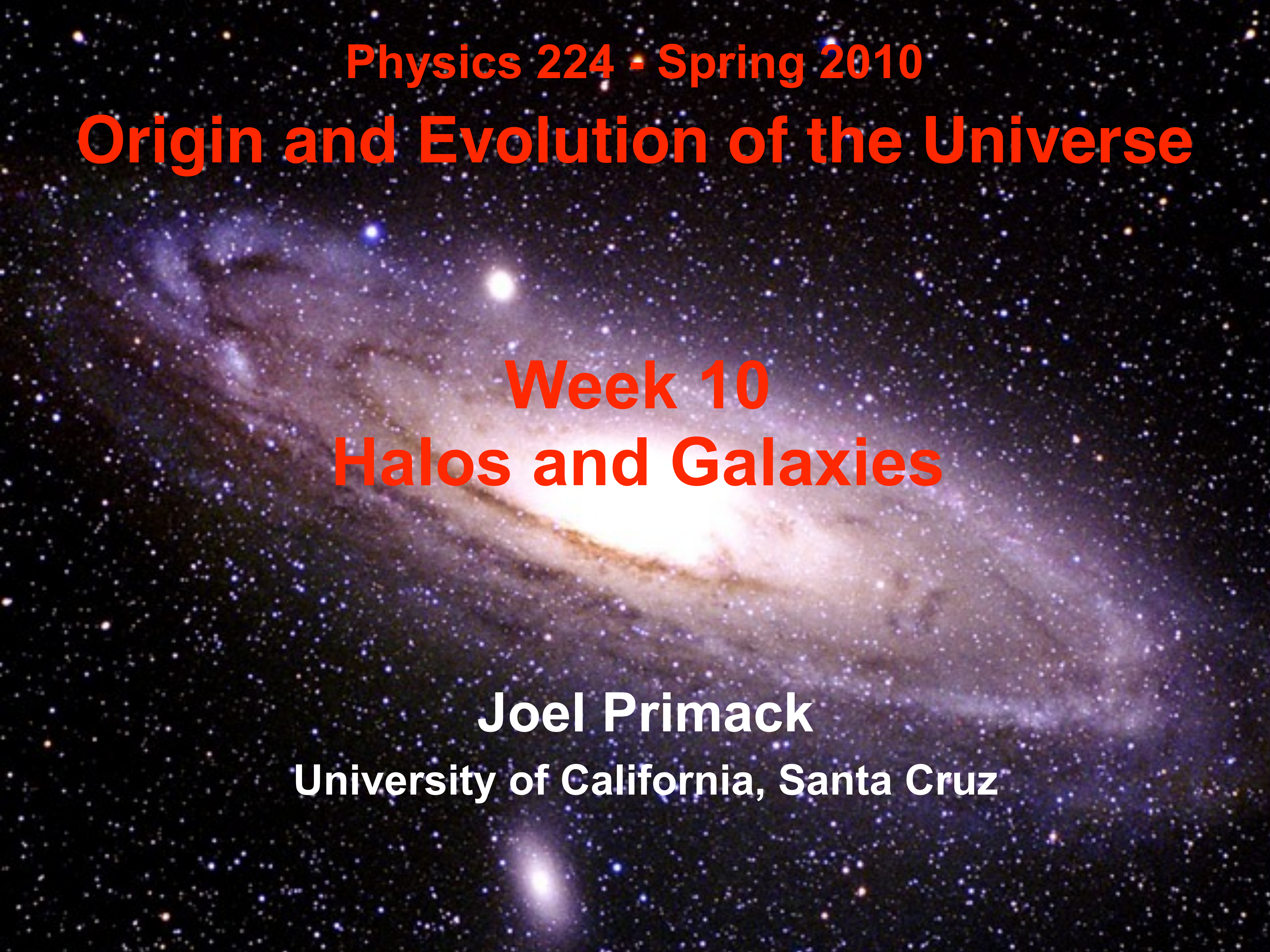

Physics 224 - Spring 2010

Origin and Evolution of the Universe

Week 10
Halos and Galaxies

Joel Primack

University of California, Santa Cruz

Student Presentations - Thursday June 10

ISB 231, 11 am - 4 pm

Laura Daniel – Eternal inflation, multiverses, and branes

Eddie Santos – SUSY WIMPs and LHC Detection

Jonathan Cornell – Detection of Dark Matter with Fermi

Rachel Rampy – Detection of dark matter using Ice Cube or other experiments (not LHC or Fermi)

Milton Bose – Extragalactic Background Light

Cosmological Simulation Methods

Dissipationless Simulations

Particle-Particle (PP) - NbodyN, N=1,...,6 (Aarseth)
Particle Mesh (PM) - see Klypin & Holtzman 1997
Adaptive PM (P3M) (Efstathiou et al.1985)
Tree - (Barnes & Hut 1986), PKDGRAV (Stadel)
TreePM - GADGET (Springel)
Adaptive Mesh Refinement (AMR) - Klypin (ART)

Hydrodynamical Simulations

Fixed grid (Cen & Ostriker)
Smooth Particle Hydrodynamics (SPH) - GADGET (Springel)
- Gasoline (Wadsley, Stadel, & Quinn)
Adaptive grid - hydro-ART (Klypin & Kravtsov)
- Enzo (Norman); RAMSES (Teyssier)

Initial Conditions

Standard: Gaussian P(k) realized uniformly, Zel'dovich displacement
Multimass - put lower mass particles in a small part of sim volume
Constrained realization - small scale: simulate individual halos (NFW)
large scale: simulate particular region

Reviews

Bertschinger ARAA 1998, Klypin lectures 2002, U Washington website,
UC-HIPACC Astro-Computing School, UCSC, July-August 2010

Empirical Models for Dark Matter Halos. II. Inner profile slopes, dynamical profiles, and ρ/σ^3

Alister Graham, David Merritt, Ben Moore, Jürg Diemand, Balša Terzić

Einasto's model is given by the equation

$$\rho(r) = \rho_e \exp\left\{-d_n\left[(r/r_e)^{1/n} - 1\right]\right\}.$$

Data on log slopes from innermost resolved radius of observed galaxies, not corrected for observational effects -- adapted from de Blok (2004).

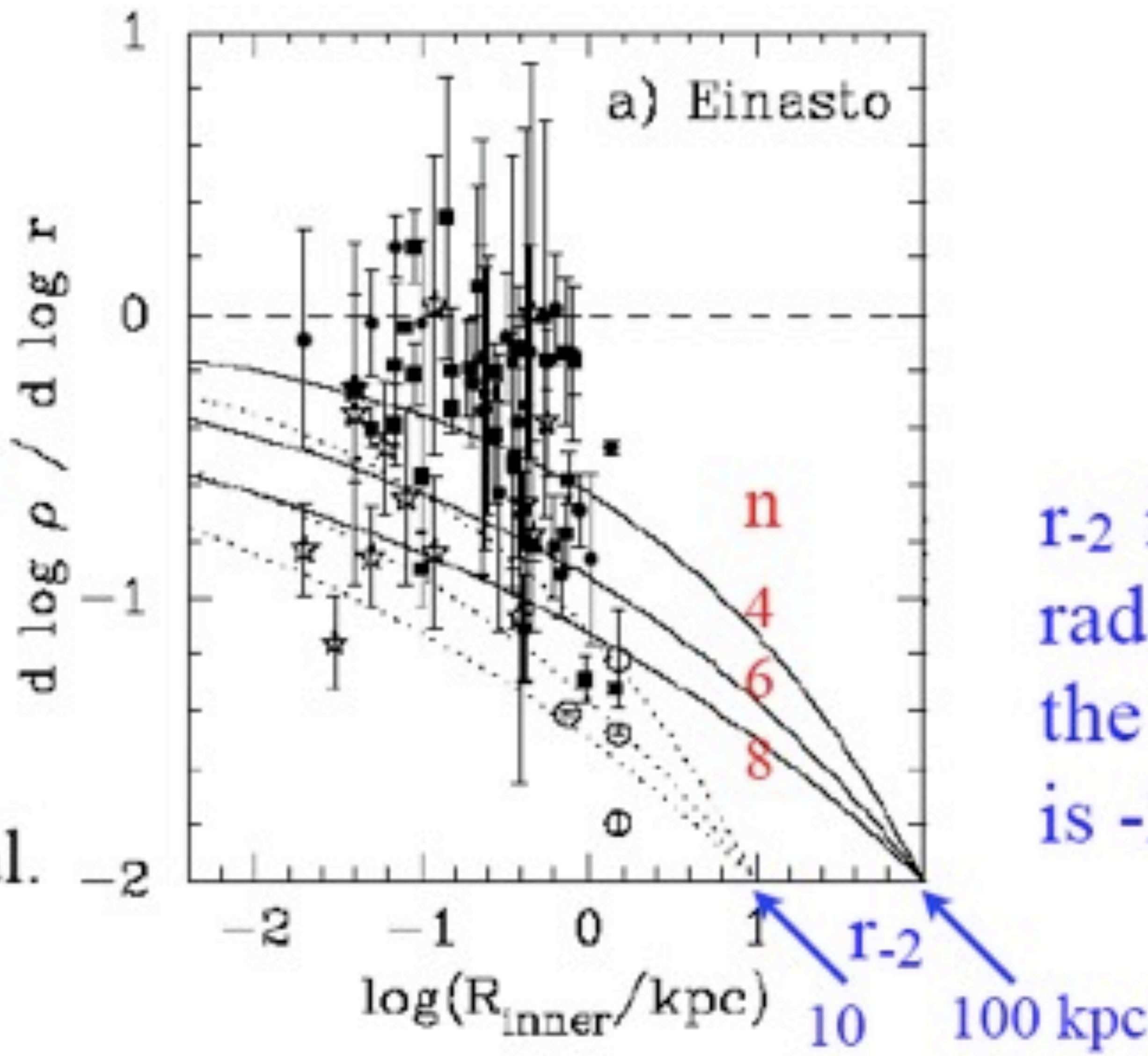

r_{-2} is the radius where the log-slope is -2

See also Navarro et al. Aquarius simulations arXiv:0810.1522

Evolution of Halo Maximum Circular Velocity

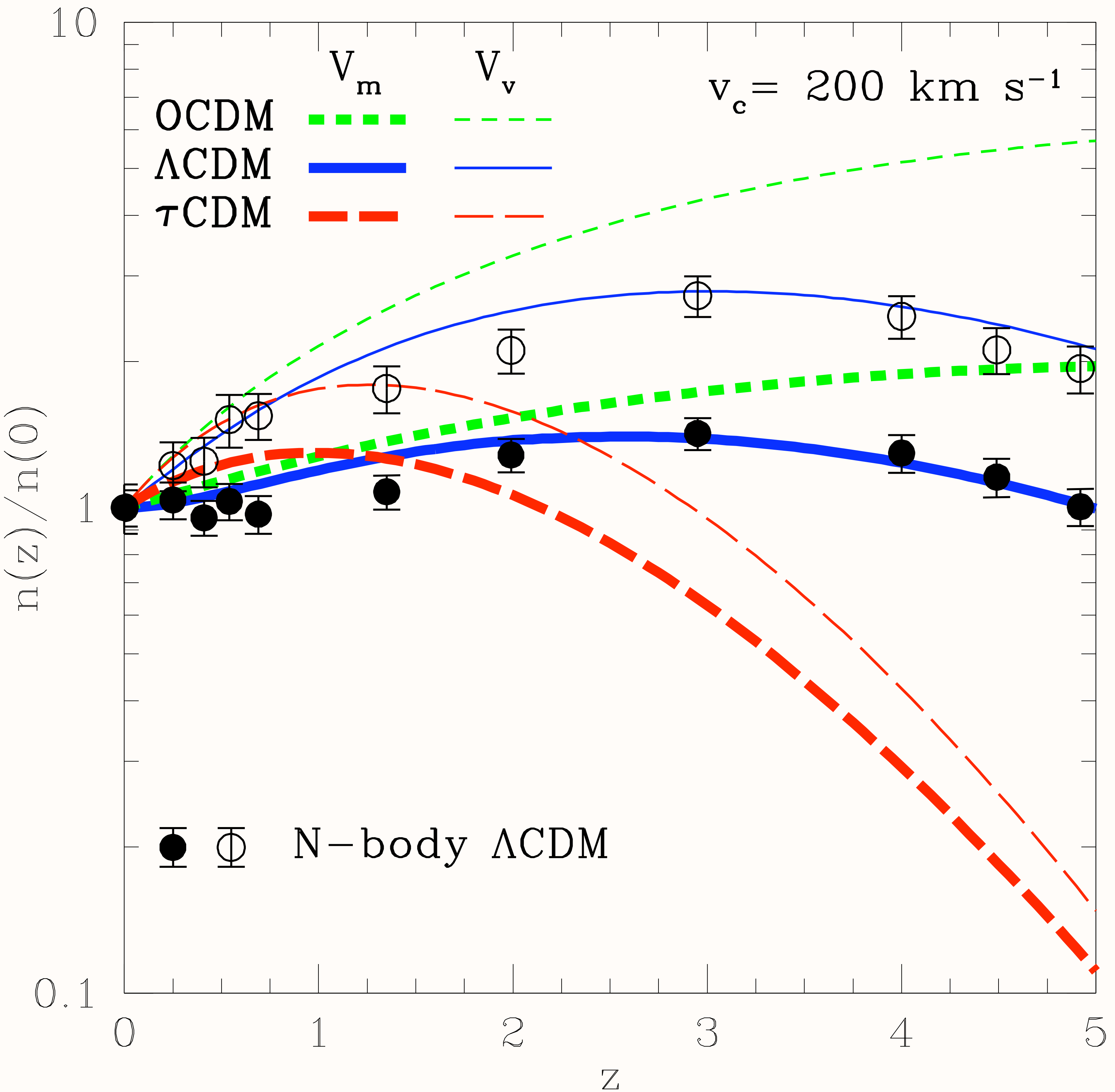

FIG. 1.— Evolution of relative comoving number density for fixed $v_{\rm m} = 200\,{\rm km\,s^{-1}}$ (bold curves) and $v_{\rm v} = 200\,{\rm km\,s^{-1}}$ halos in three cosmologies.

Bullock, Dekel, Kolatt, Primack, & Somerville 2001, ApJ, 550, 21

Dependence of Halo Concentration on Mass and Redshift

Profiles of dark haloes: evolution, scatter, and environment

J. S. Bullock[1,2], T. S. Kolatt[1,3], Y. Sigad[3], R.S. Somerville[3,4], A. V. Kravtsov[2,5★], A. A. Klypin[5], J. R. Primack[1], and A. Dekel[3] 2001 MNRAS 321, 559

ABSTRACT

We study dark-matter halo density profiles in a high-resolution N-body simulation of a ΛCDM cosmology. Our statistical sample contains ∼5000 haloes in the range $10^{11} - 10^{14} h^{-1} M_{\odot}$ and the resolution allows a study of subhaloes inside host haloes. The profiles are parameterized by an NFW form with two parameters, an inner radius r_s and a virial radius R_{vir}, and we define the halo concentration $c_{vir} \equiv R_{vir}/r_s$. We find that, for a given halo mass, the redshift dependence of the median concentration is $c_{vir} \propto (1+z)^{-1}$. This corresponds to $r_s(z) \sim$ constant, and is contrary to earlier suspicions that c_{vir} does not vary much with redshift. The implications are that high-redshift galaxies are predicted to be more extended and dimmer than expected before. Second, we find that the scatter in halo profiles is large, with a 1σ $\Delta(\log c_{vir}) = 0.18$ at a given mass, corresponding to a scatter in maximum rotation velocities of $\Delta V_{max}/V_{max} = 0.12$. We discuss implications for modelling the Tully-Fisher relation, which has a smaller reported intrinsic scatter. Third, subhaloes and haloes in dense environments tend to be more concentrated than isolated haloes, and show a larger scatter. These results suggest that c_{vir} is an essential parameter for the theory of galaxy modelling, and we briefly discuss implications for the universality of the Tully-Fisher relation, the formation of low surface brightness galaxies, and the origin of the Hubble sequence. We present an improved analytic treatment of halo formation that fits the measured relations between halo parameters and their redshift dependence, and can thus serve semi-analytic studies of galaxy formation.

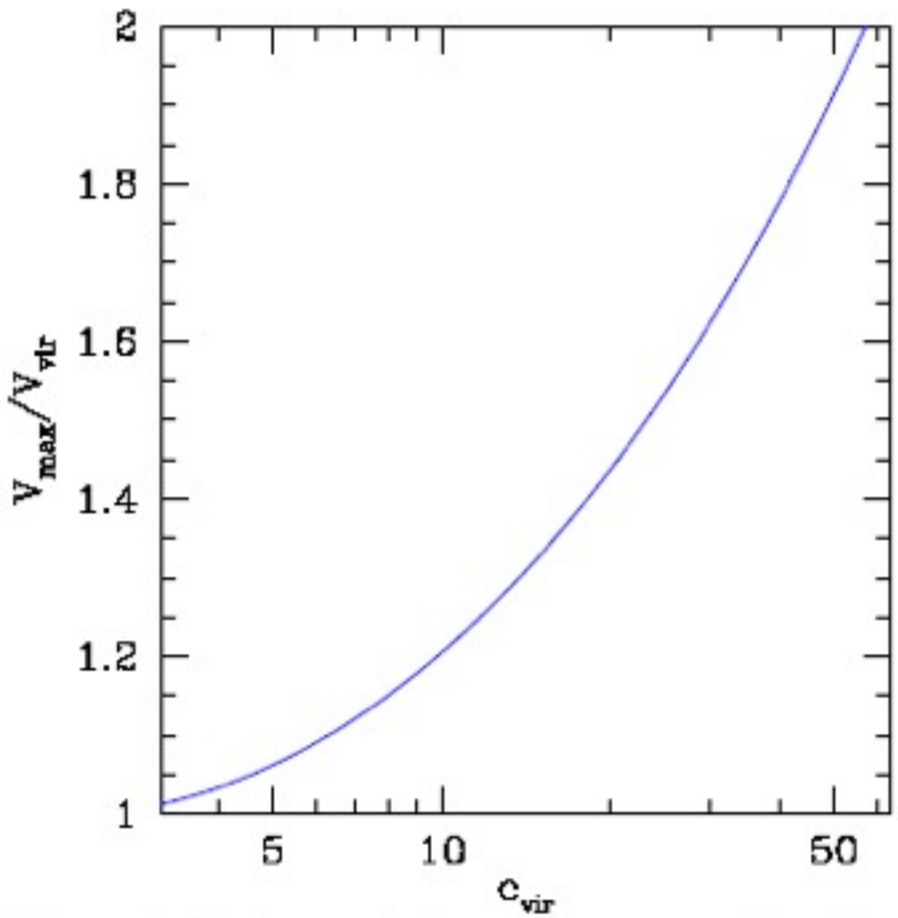

Figure 1. Maximum velocity versus concentration. The maximum rotation velocity for an NFW halo in units of the rotation velocity at its virial radius as a function of halo concentration.

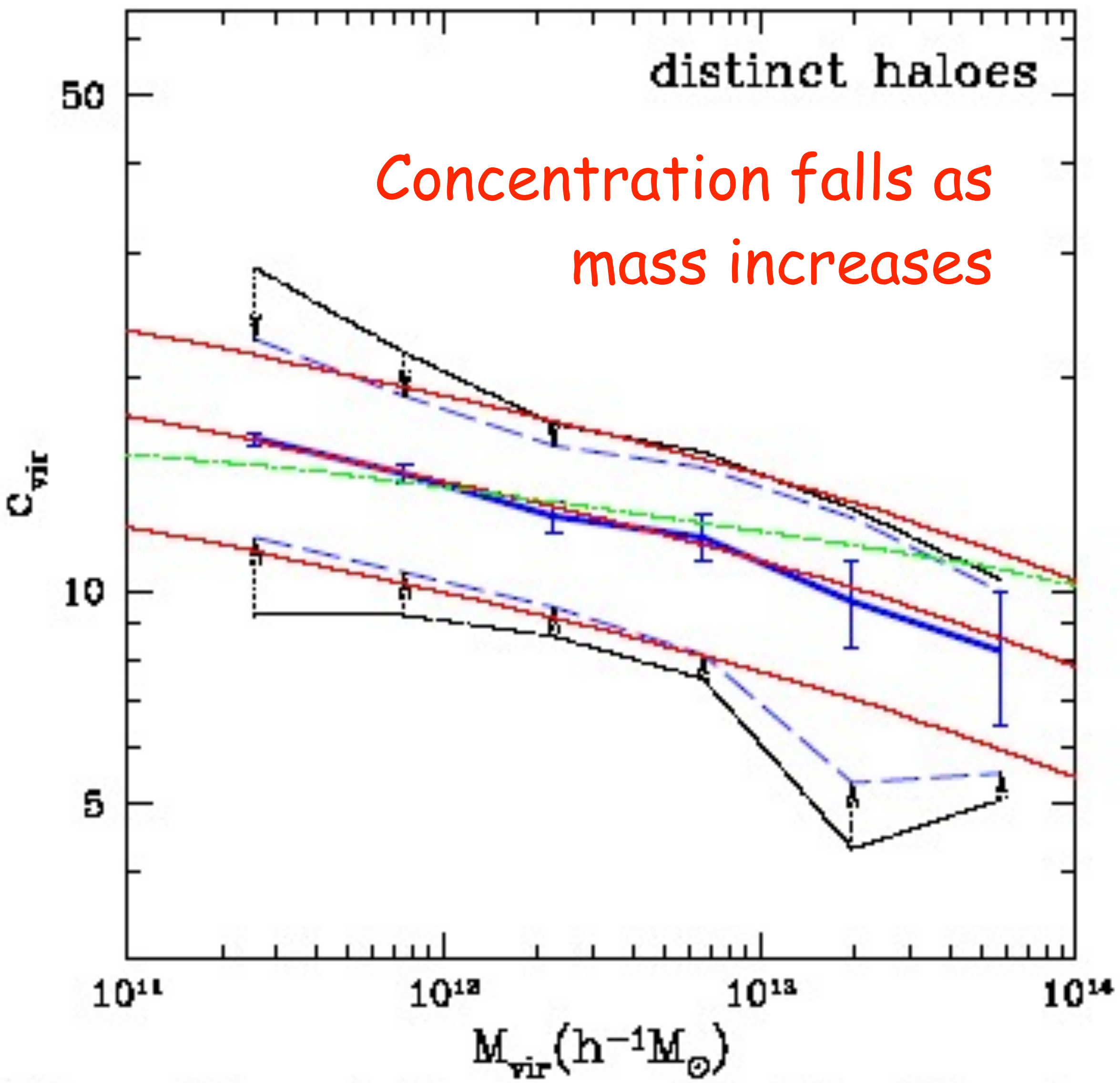

Figure 4. Concentration versus mass for distinct haloes at $z = 0$. The thick solid curve is the median at a given $M_{\rm vir}$. The error bars represent Poisson errors of the mean due to the sampling of a finite number of haloes per mass bin. The outer dot-dashed curves encompass 68% of the $c_{\rm vir}$ values as measured in the simulations. The inner dashed curves represent only the true, intrinsic scatter in $c_{\rm vir}$, after eliminating both the Poisson scatter and the scatter due to errors in the individual profile fits due, for example, to the finite number of particles per halo. The central and outer thin solid curves are the predictions for the median and 68% values by the toy model outlined in the text, for $F = 0.01$ and three different values of K. The thin dot-dashed line shows the prediction of the toy model of NFW97 for $f = 0.01$ and $k = 3.4 \times 10^3$.

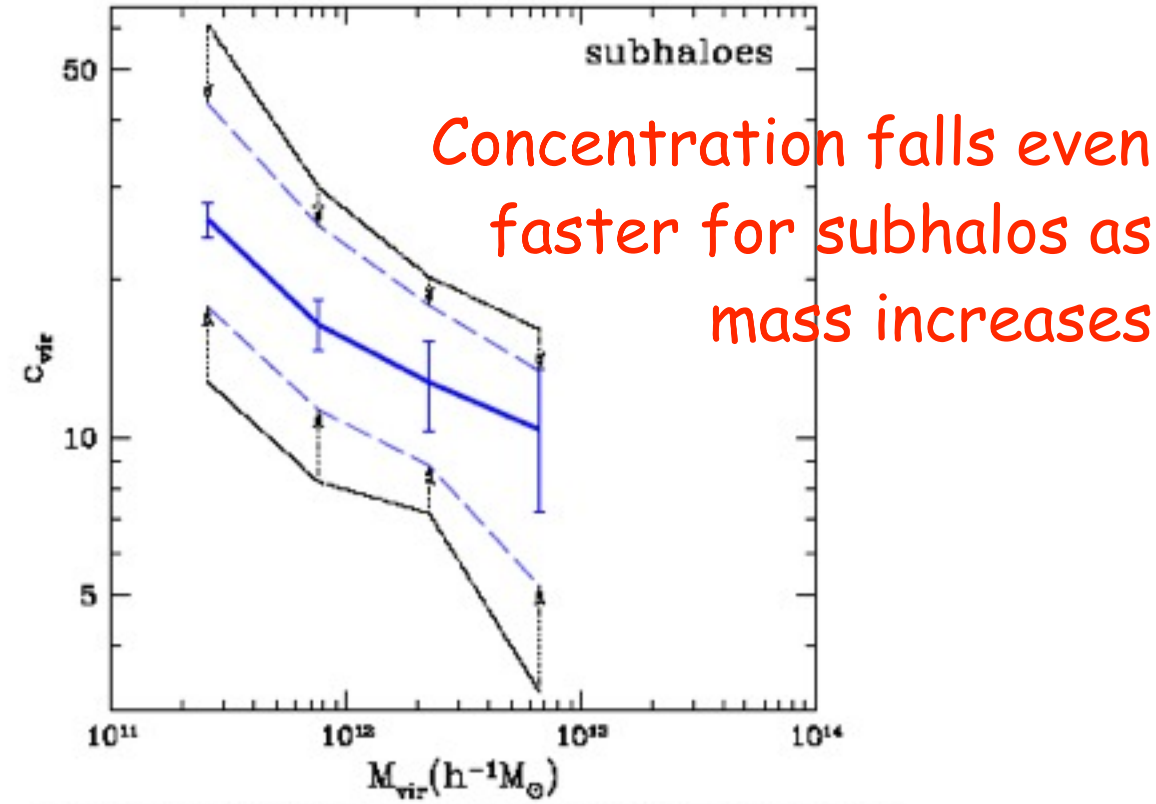

Figure 5. Concentration versus mass for subhaloes at $z = 0$. The curves and errors are the same as in Figure 4.

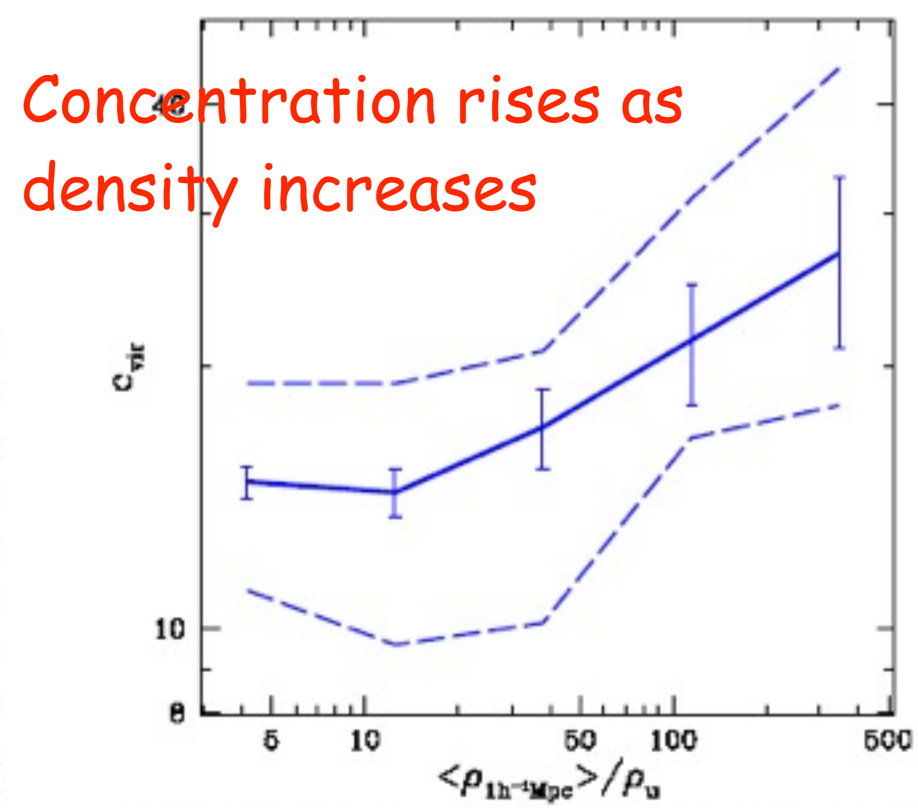

Figure 6. Concentrations versus environment. The concentration at $z = 0$ of all haloes in the mass range $0.5 - 1.0 \times 10^{12} h^{-1} M_\odot$ as a function of local density in units of the average density of the universe. The local density was determined within spheres of radius $1 h^{-1}$Mpc. The solid line represents the median $c_{\rm vir}$ value, the error bars are Poisson based on the number of haloes, and the dashed line indicates our best estimate of the intrinsic scatter.

Spread of Halo Concentrations

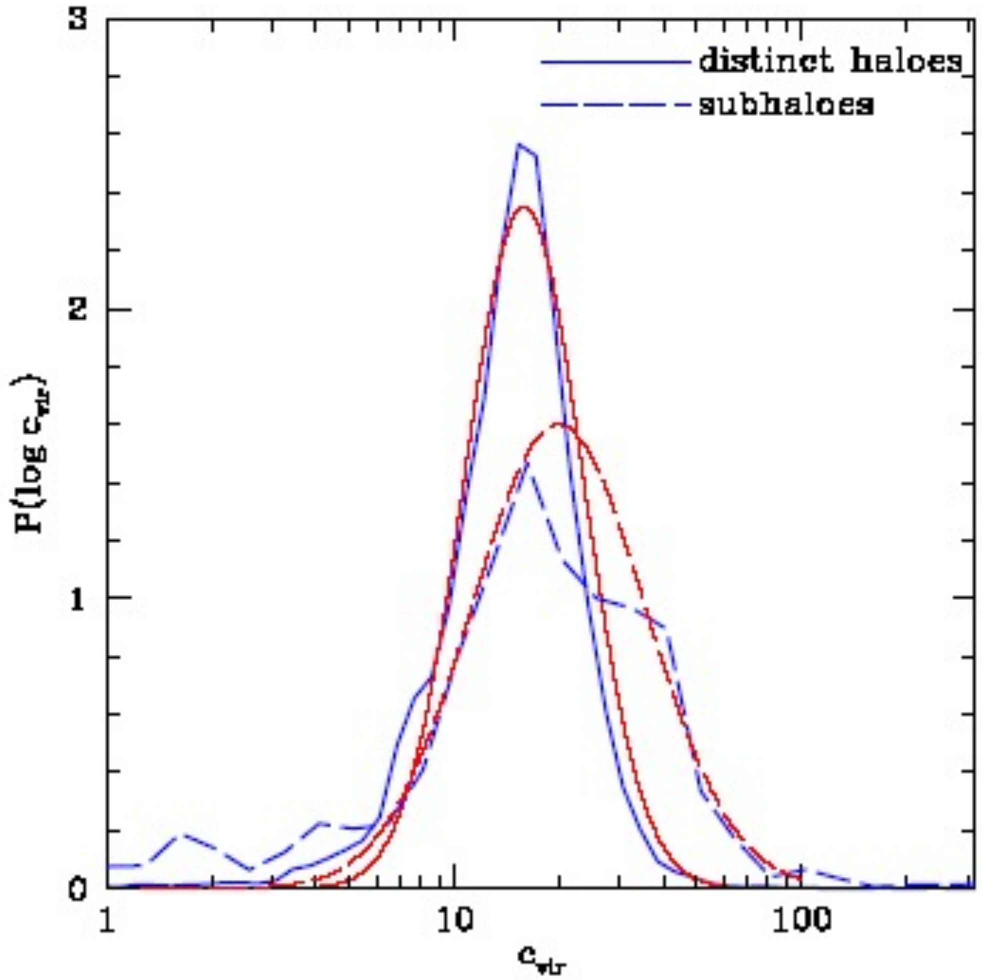

Figure 7. The probability distributions of distinct haloes (solid line) and subhaloes (dashed line) at $z = 0$ within the mass range $(0.5 - 1.0) \times 10^{12} h^{-1} M_{\odot}$. The simulated distributions (thick lines) include, the $\sim 2,000$ distinct haloes and ~ 200 subhaloes within this mass range. Log-normal distributions with the same median and standard deviation as the measured distributions are shown (thin lines). Subhaloes are, on average, more concentrated than distinct haloes and they show a larger spread.

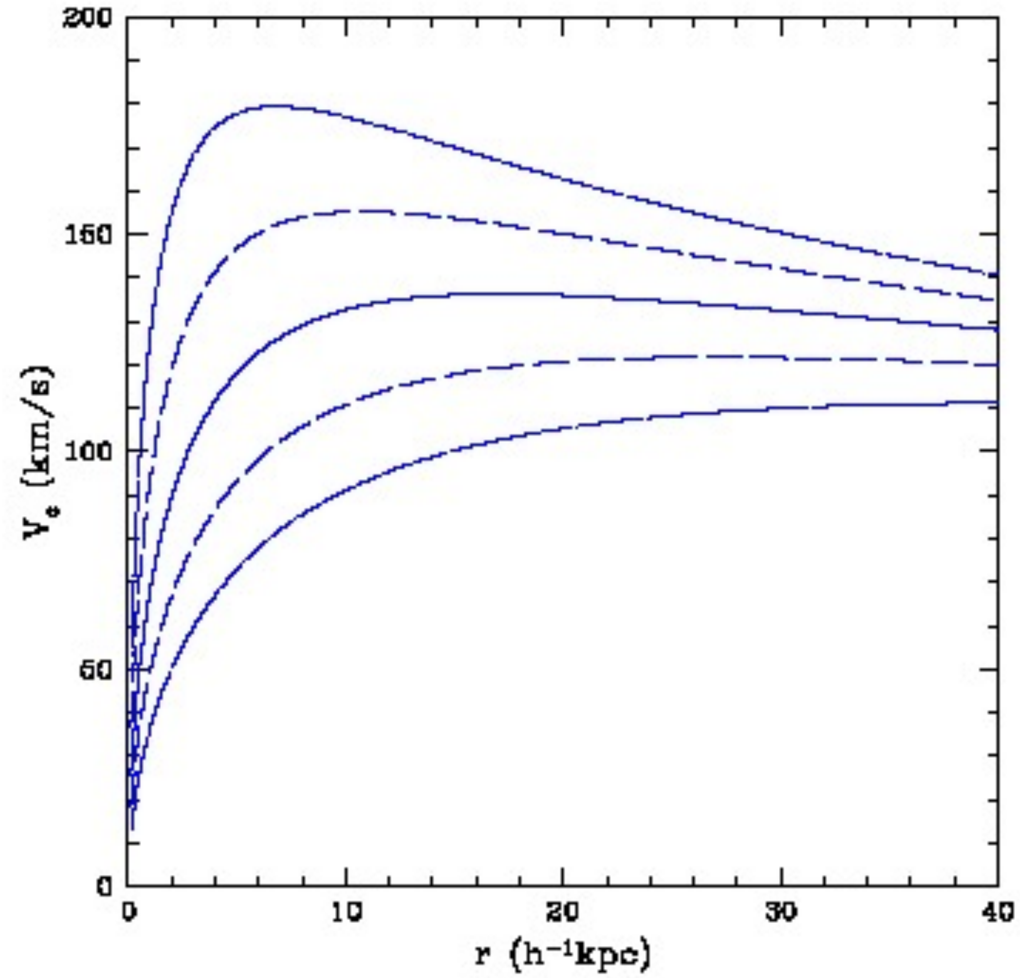

Figure 8. The spread in NFW rotation curves corresponding to the spread in concentration parameters for distinct haloes of $3 \times 10^{11} h^{-1} M_{\odot}$ at $z = 0$. Shown are the median (solid), $\pm 1\sigma$ (long dashed), and $\pm 2\sigma$ (dot-dashed) curves. The corresponding median rotation curve for subhaloes is comparable to the upper 1σ curve of distinct haloes.

Evolution of Halo Concentration with Redshift

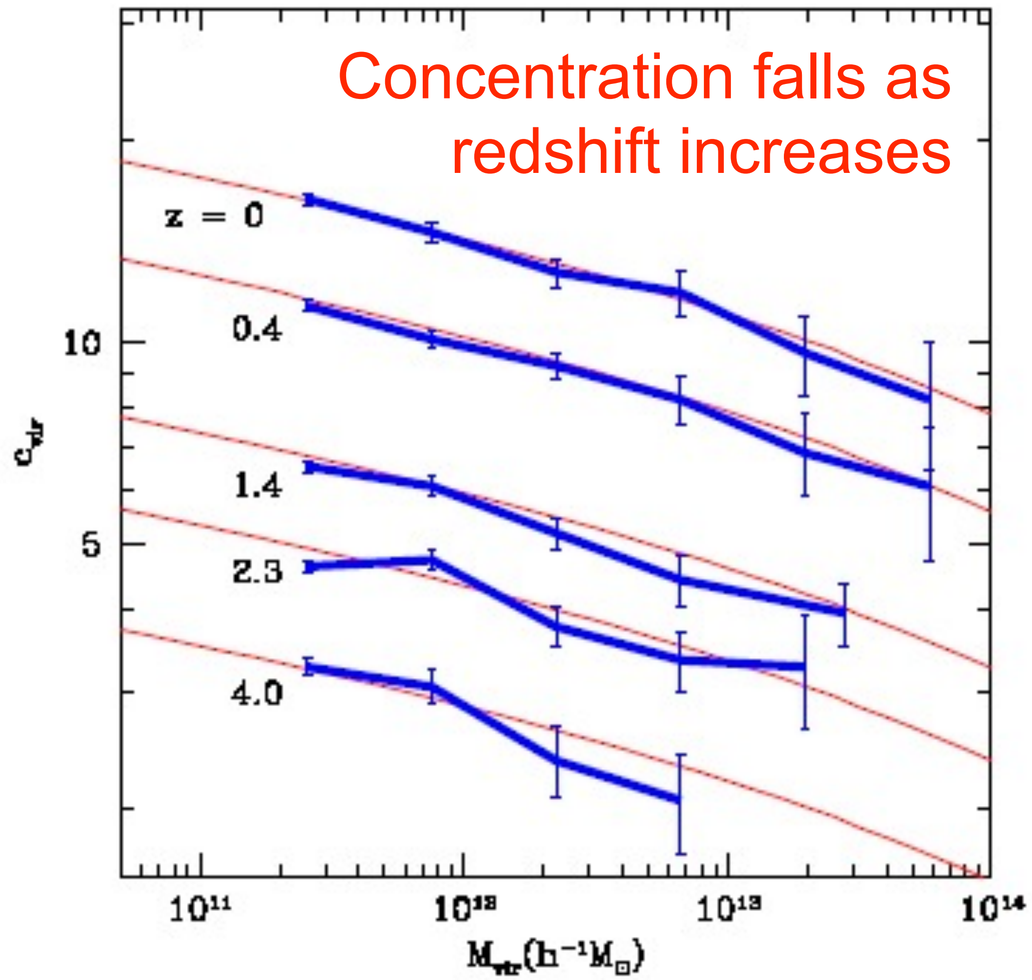

Figure 10. Median $c_{\rm vir}$ values as a function of $M_{\rm vir}$ for distinct haloes at various redshifts. The error bars are the Poisson errors due to the finite number of haloes in each mass bin. The thin solid lines show our toy model predictions.

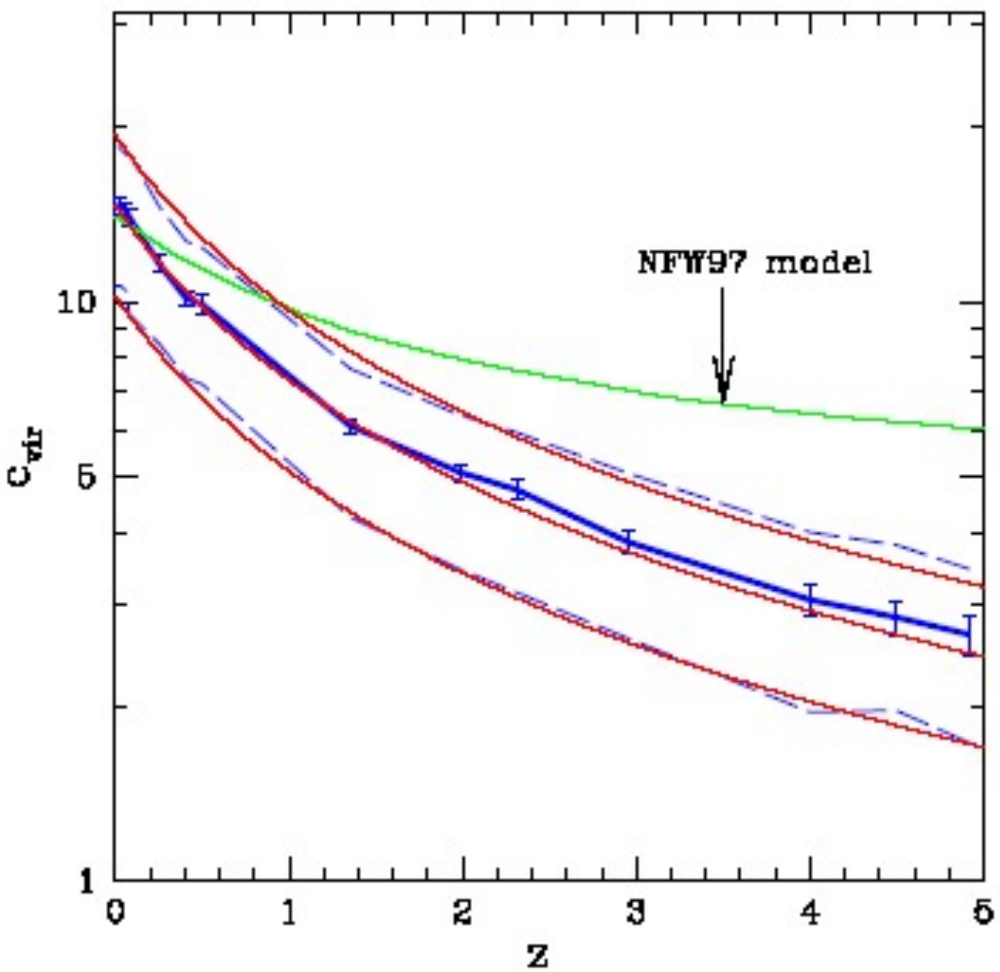

Figure 11. Concentration as a function of redshift for distinct haloes of a fixed mass, $M_{\rm vir} = 0.5 - 1.0 \times 10^{12} h^{-1} M_{\odot}$. The median (heavy solid line) and intrinsic 68% spread (dashed line) are shown. The behavior predicted by the NFW97 toy model is marked. Our revised toy model for the median and spread for $8 \times 10^{11} h^{-1} M_{\odot}$ haloes (thin solid lines) reproduces the observed behavior rather well.

$C_{vir} \propto 1/(1+z)$
at fixed mass

Merger Trees

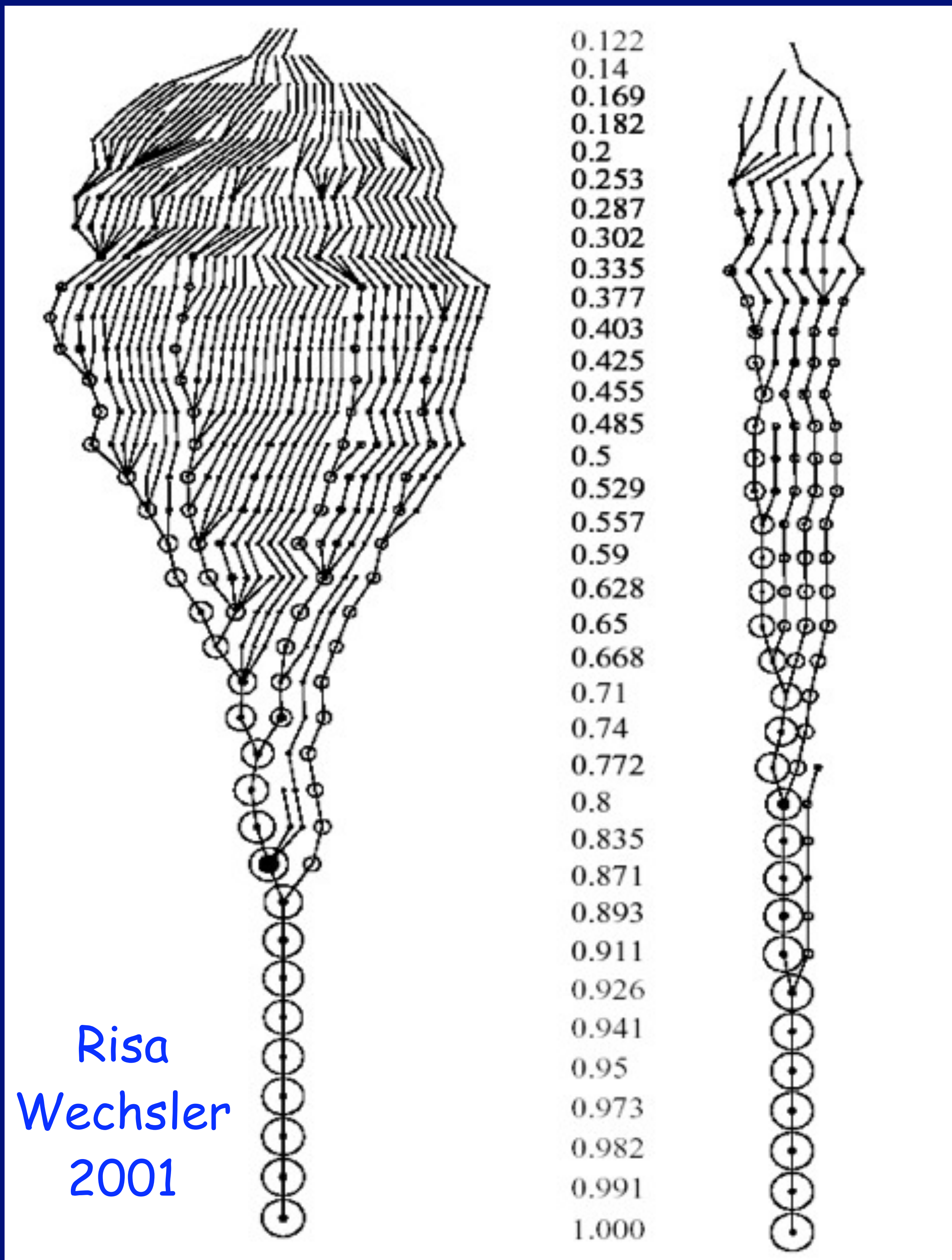

Risa Wechsler 2001

Based on our ART simulations, Wechsler created the first structural merger trees tracing the merging history of thousands of halos with structural information on their higher-redshift progenitors, including their radial profiles and spins. This led to the discovery that a halo's merging history can be characterized by a single parameter a_c which describes the scale factor at which the halo's mass accretion slows, and that this parameter correlates very well with the halo concentration, thus showing that the distribution of dark matter halo concentrations reflects mostly the distribution of their mass accretion rates. We found that the radius of the inner part of the halo, where the density profile is roughly 1/r, is established during the early, rapid-accretion phase of halo growth (a result subsequently confirmed and extended by other groups, e.g., Zhao et al. 2003, Reed et al. 2004).

CONCENTRATIONS OF DARK HALOS FROM THEIR ASSEMBLY HISTORIES

RISA H. WECHSLER[1], JAMES S. BULLOCK[2], JOEL R. PRIMACK[1], ANDREY V. KRAVTSOV[2,3], AVISHAI DEKEL[4], ApJ 568 (2002) 52-70

$$\rho_{\rm NFW}(r) = \frac{\rho_s}{(r/R_s)\,(1+r/R_s)^2}, \qquad (1)$$

where R_s is a characteristic "inner" radius, and ρ_s a corresponding inner density. One of the inner parameters can be replaced by a "virial" parameter, either the virial radius ($R_{\rm vir}$), mass ($M_{\rm vir}$), or velocity ($V_{\rm vir}$), defined such that the mean density inside the virial radius is $\Delta_{\rm vir}$ times the mean universal density ρ_u at that redshift:

$$M_{\rm vir} \equiv \frac{4\pi}{3}\Delta_{\rm vir}\rho_u {R_{\rm vir}}^3. \qquad (2)$$

The critical overdensity at virialization, $\Delta_{\rm vir}$, is motivated by the spherical collapse model; it has a value $\simeq 180$ for the Einstein-deSitter cosmology, and $\simeq 340$ for the ΛCDM cosmology assumed here. A useful alternative parameter for describing the shape of the profile is the concentration parameter $c_{\rm vir}$, defined as $c_{\rm vir} \equiv R_{\rm vir}/R_s$.

(Bryan & Norman 1998) $\Delta_{\rm vir} \simeq (18\pi^2 + 82x - 39x^2)/\Omega(z)$ where $x \equiv \Omega(z) - 1$

By examining a range of full mass assembly histories for our sample of halos, we have found a useful parameterized form that captures many essential aspects of halo growth over time. Remarkably, we find that both average mass accretion histories and mass accretion histories for individual halos, as observed at $z = 0$, can be characterized by a simple function:

$$M(a) = M_o e^{-\alpha z}, \quad a = (1+z)^{-1}. \qquad (3)$$

The single free parameter in the model, α, can be related to a characteristic epoch for formation, a_c, defined as the expansion scale factor a when the logarithmic slope of the accretion rate, $d\log M/d\log a$, falls below some specified value, S. The functional form defined in Eq. 3 implies $a_c = \alpha/S$. In what follows we have chosen $S = 2$.

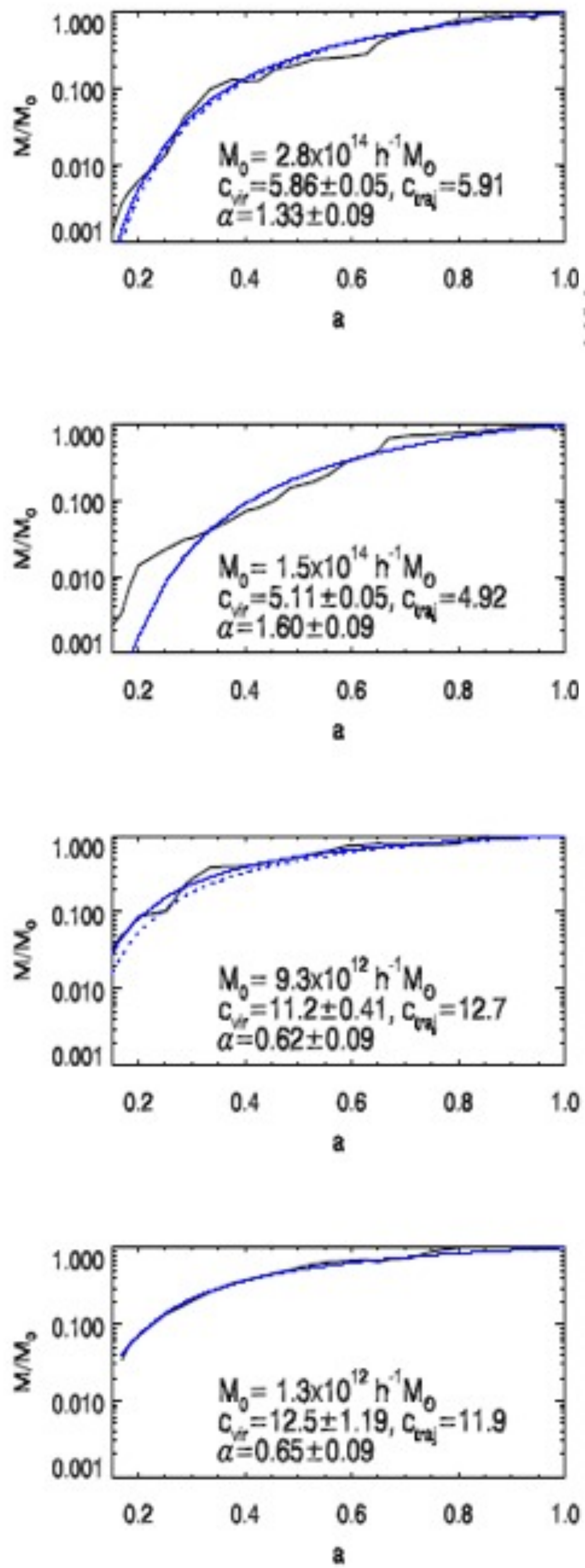

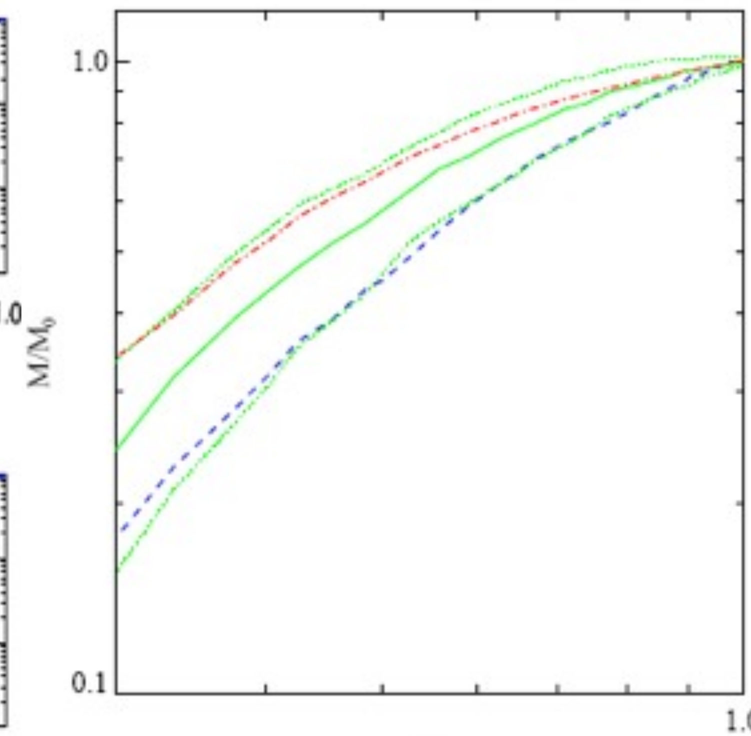

Average mass accretion histories, normalized at a = 1. The three green curves connect the averages of $M(a)/M_0$ at each output time. The pair of dotted lines shows the 68% spread about the middle case. Red dot-dashed lines correspond to early formers (typically low mass halos), blue dashed lines to late formers (typically higher mass halos). We see that massive halos tend to form later than lower mass halos, whose mass accretion rate peaks at an earlier time.

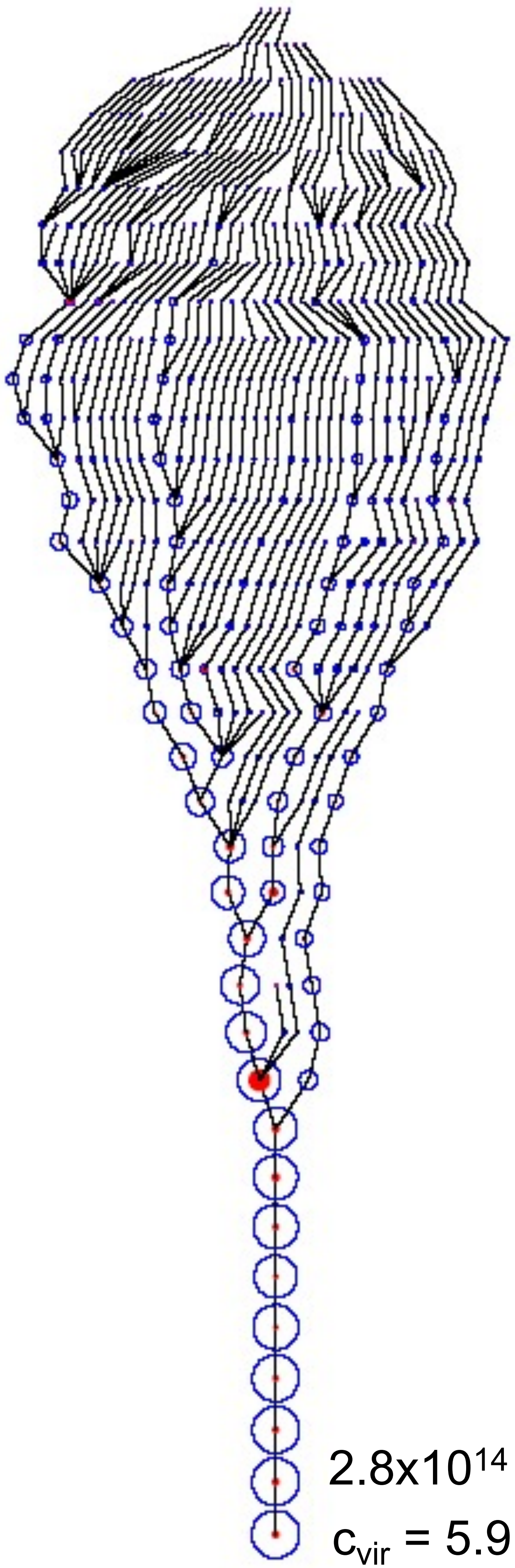

Structural merger trees for two halos. The radii of the outer and inner (filled) circles are proportional to the virial and inner NFW radii, Rvir and Rs, respectively, scaled such that the two halos have equal sizes at a = 1. Lines connect halos with their progenitor halos.

2.8×10^{14} M_{sun}/h

$c_{vir} = 5.9$

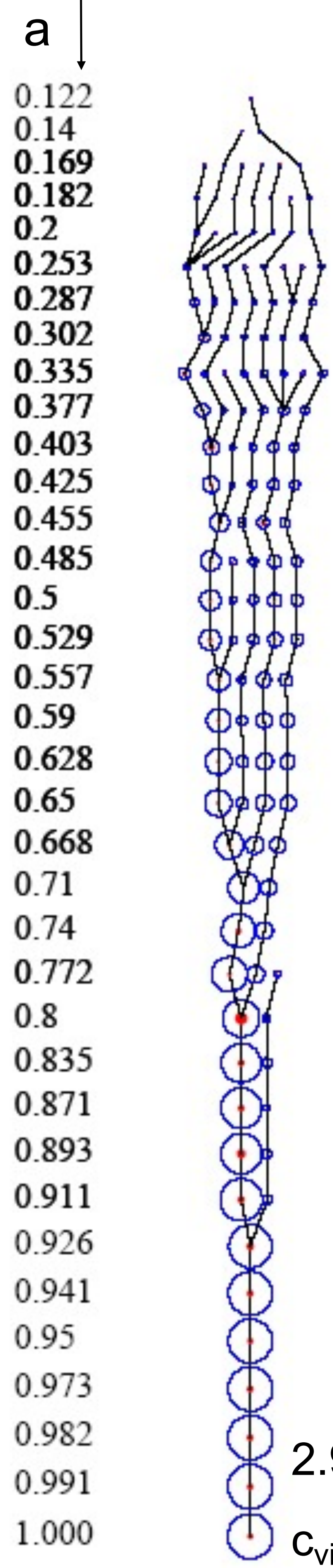

2.9×10^{12} M_{sun}/h

$c_{vir} = 12.5$

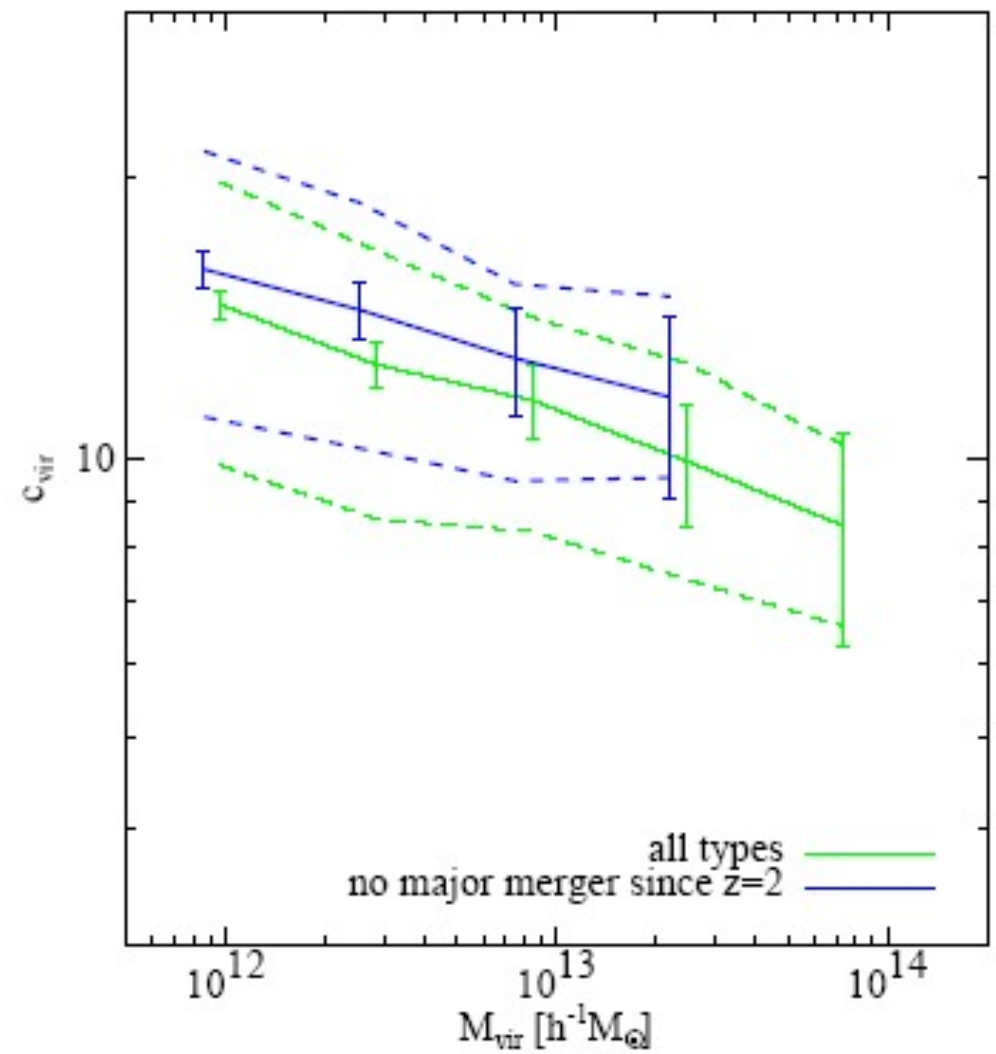

For halos without recent mergers, c_{vir} is higher and the scatter is reduced to log c_{vir} ≈ 0.10.

Wechsler et al. 2002

Halo Shapes

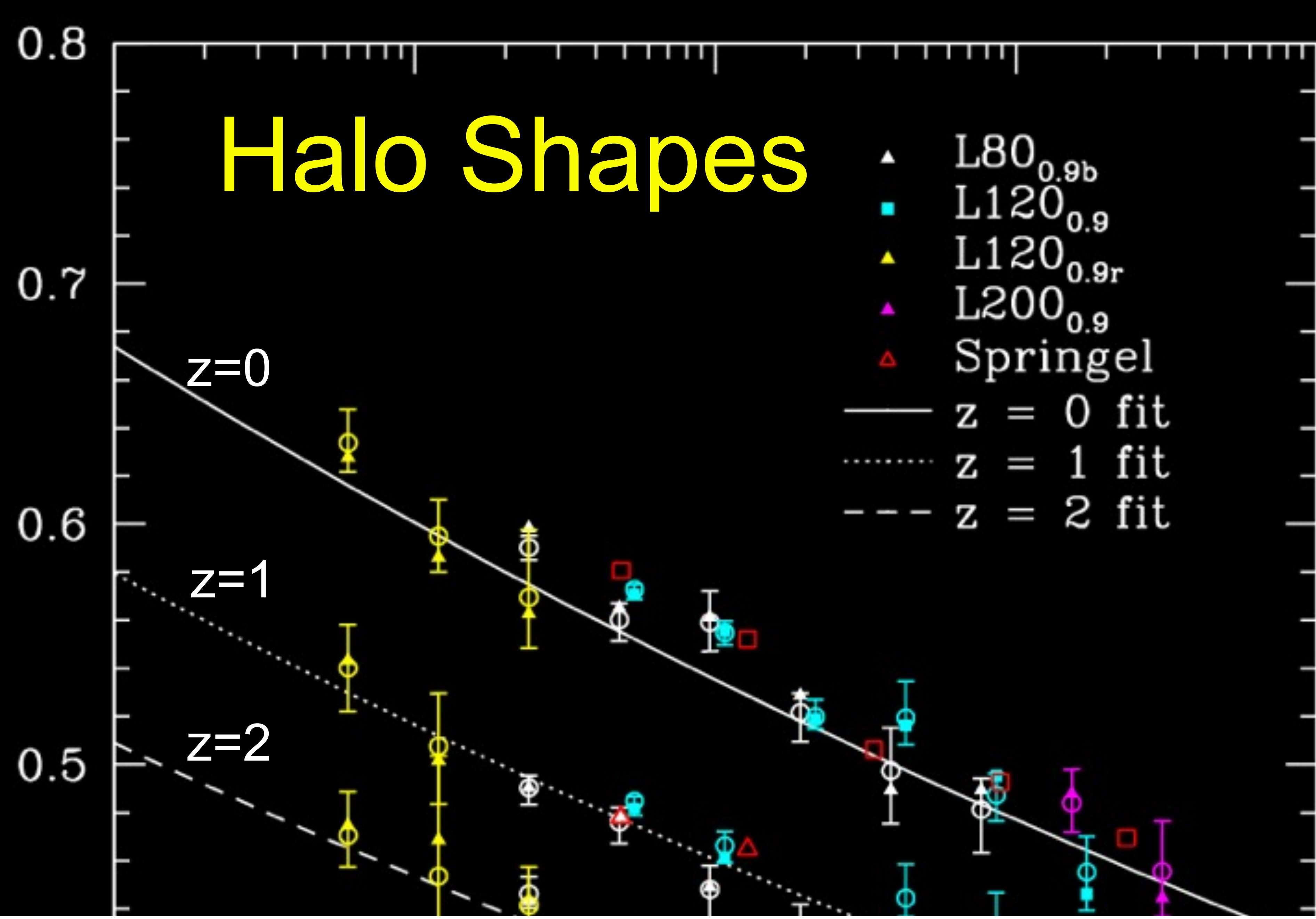

A simple formula describes these results, as well dependence on epoch and cosmological parameter σ_8 :

$$\langle s \rangle (M_{\rm vir}, z=0) = \alpha \left(\frac{M_{\rm vir}}{M_*} \right)^{\beta}$$

with best fit values

$$\alpha = 0.54 \pm 0.03, \ \beta = -0.050 \pm 0.003.$$

<s> = short / long axis of dark halos vs. mass and redshift. Dark halos are more elongated the more massive they are and the earlier they form. We found that the halo <s> scales as a power-law in Mhalo/M*. Halo shape is also related to the Wechsler halo formation scale factor ac.

Allgood et al. 2006

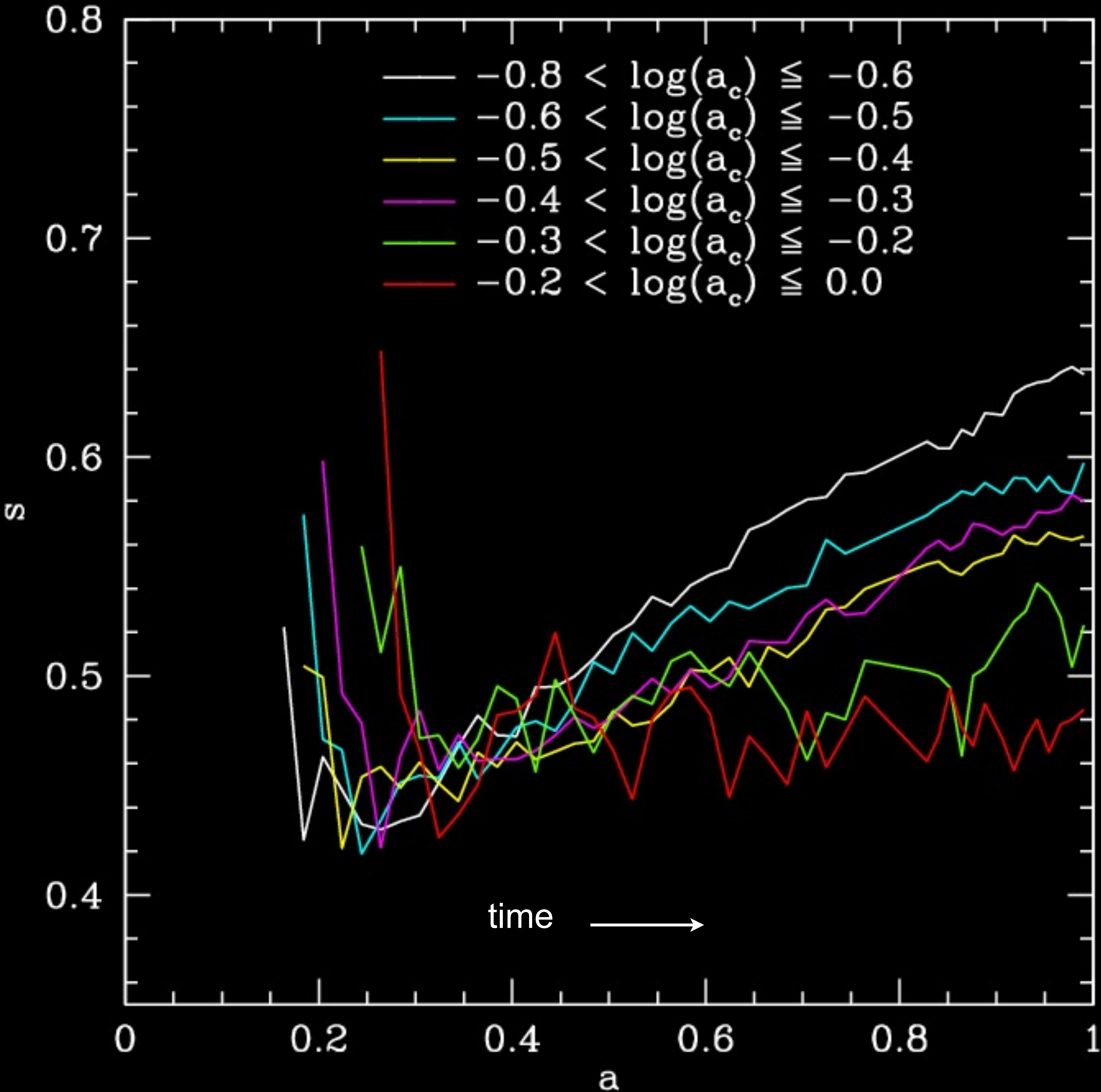

Halo shape $s = c / a$ vs. scale factor $a=1/(1+\text{redshift})$ for halos of mass between 3.2 and 6.4 x 10^{12} M_{sun} that form at different scale factors a_c. Halos become more spherical after they form, and those that form earlier (at lower a_c) become more spherical faster.

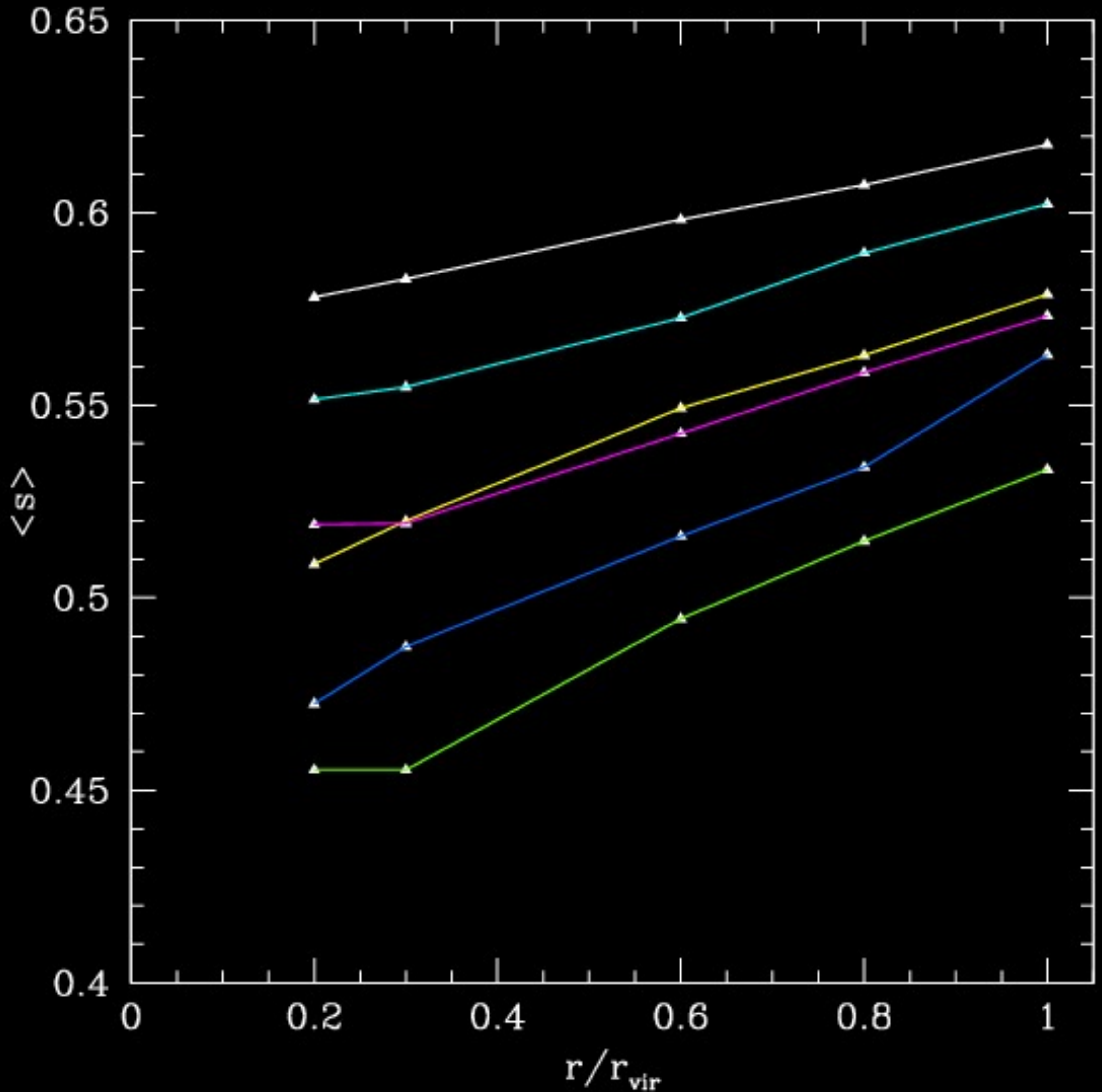

FIG. 7.— $\langle s \rangle$ with radius at $z = 0$. black: $1.6 \times 10^{12} < M < 3.2 \times 10^{12}$, red: $3.2 \times 10^{12} < M < 6.4 \times 10^{12}$, blue: $6.4 \times 10^{12} < M < 1.28 \times 10^{13}$, green: $1.28 \times 10^{13} < M < 2.56 \times 10^{13}$, orange: $2.56 \times 10^{13} < M < 5.12 \times 10^{13}$, violet: $5.12 \times 10^{13} < M$. These are the same mass bins as in Figure 3.

Halos become more spherical at larger radius and smaller mass. As before, s = short / long axis. These predictions can be tested against cluster X-ray data and galaxy weak lensing data.

[These figures are from Brandon Allgood's PhD dissertation.]

Recent Progress in Simulations

Improvements in resolution in DM simulations Diemand, Madau, Zemp; Springel, Aquarius simulations, ...

Stream-fed galaxies form most of the stars in the universe Birnboim & Dekel 03+, Keres+05, Dekel+08

Improvements in resolution and feedback treatment leading to formation of more realistic disk galaxies Fabio Governato's group, Klypin & Ceverino, ...

Predict appearance of interacting galaxies, AGN formation, and properties of merger remnants TJ Cox04, Cox+06,+08, Patrik Jonsson04,06, Hernquist's group+05++, Jonsson +06, Greg Novak+06,08, Matt Covington08,+08, ...

Statistically compare to observations (GOODS and AEGIS) Jennifer Lotz, Madau, & Primack 04; Lotz et al. 05, 06, 08; Cristy Pierce+06,... Nandra+06, Georgakakis+08, Pierce+08

At High z, in Massive Halos: Cold Streams in Hot Halos

in $M>M_{shock}$

Totally hot at z<1

Cold streams at z>2

Dekel & Birnboim 2006

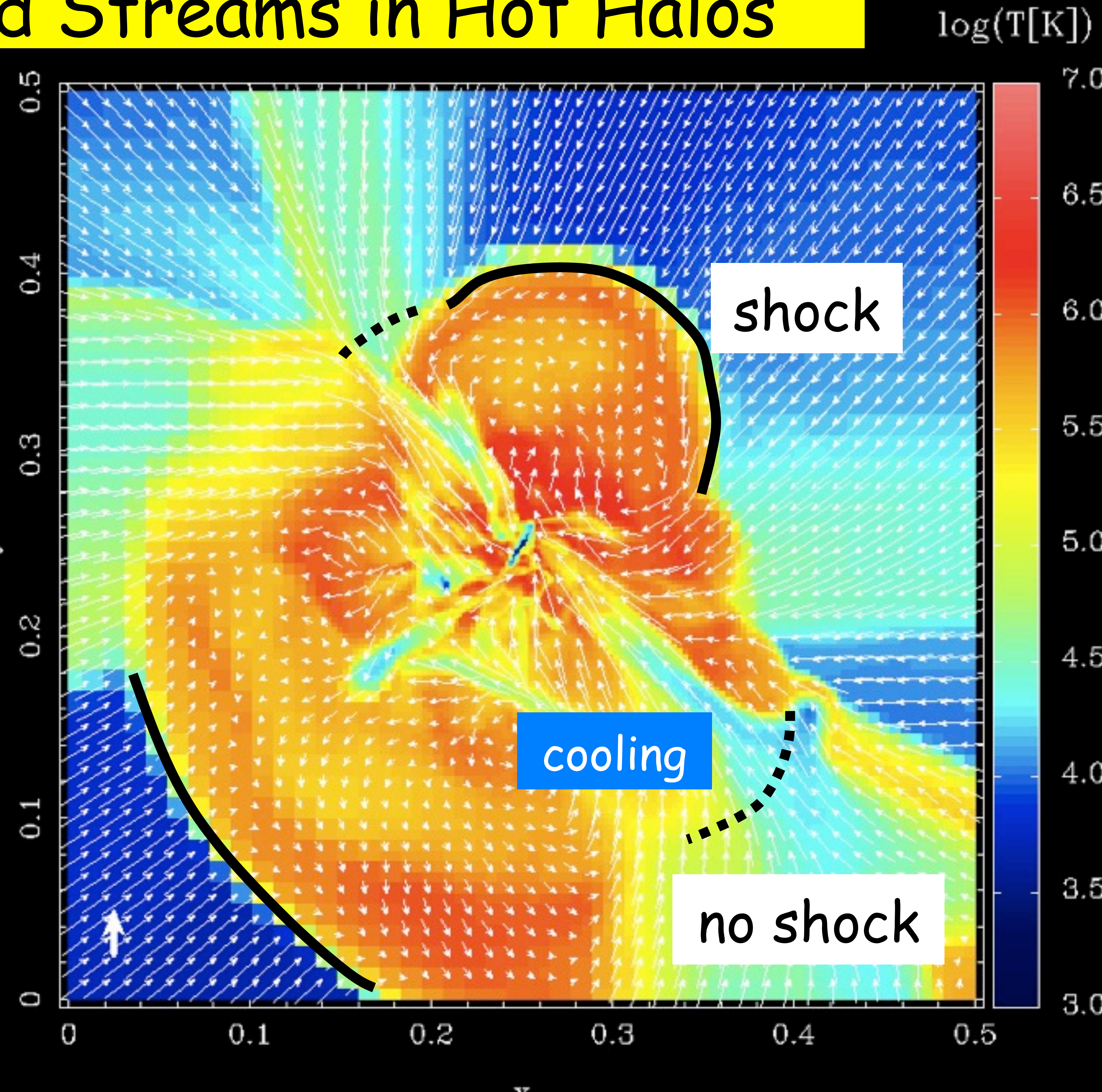

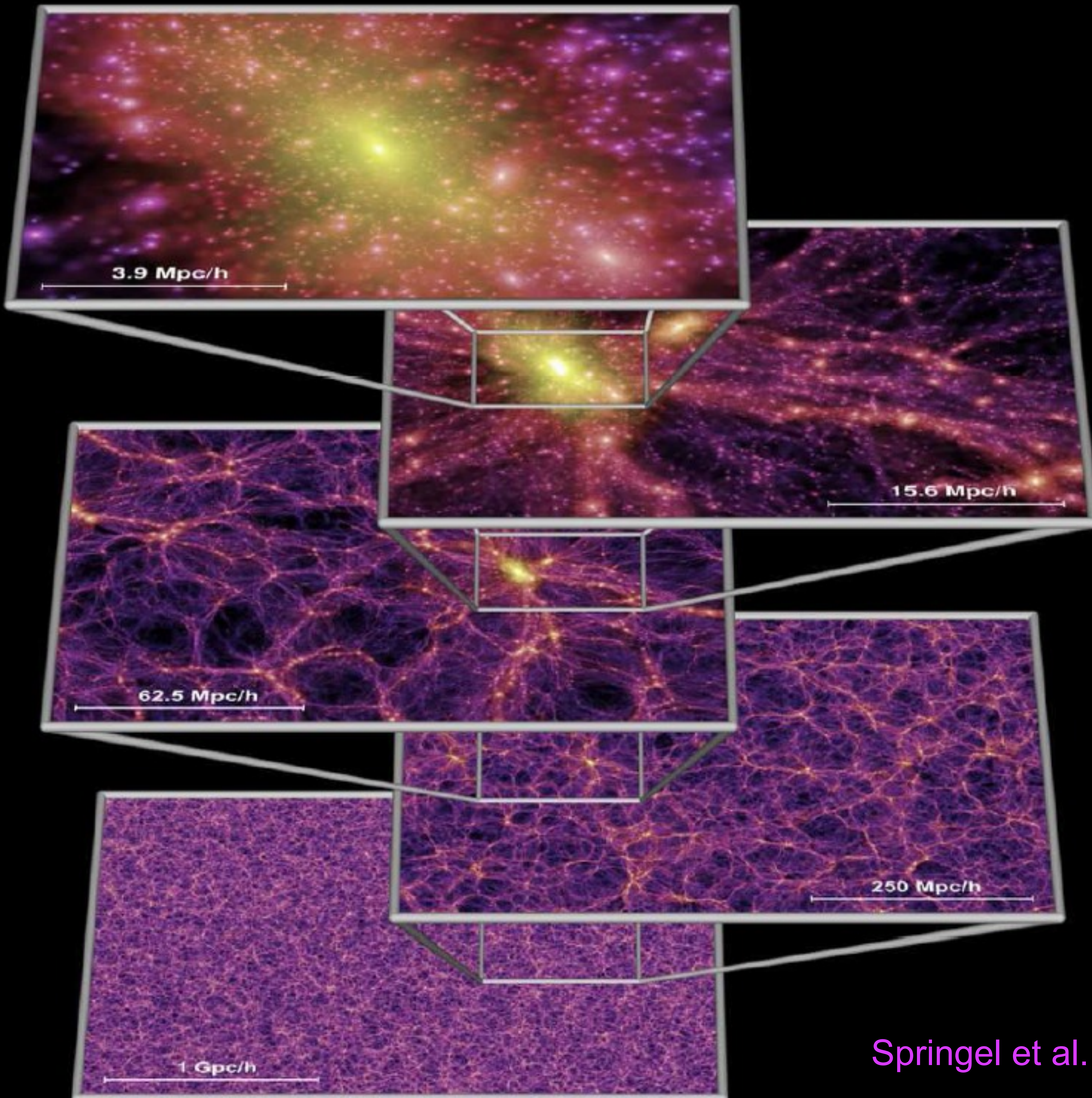

Springel et al. 2005

Particle number in cosmological N-body simulations vs. pub date

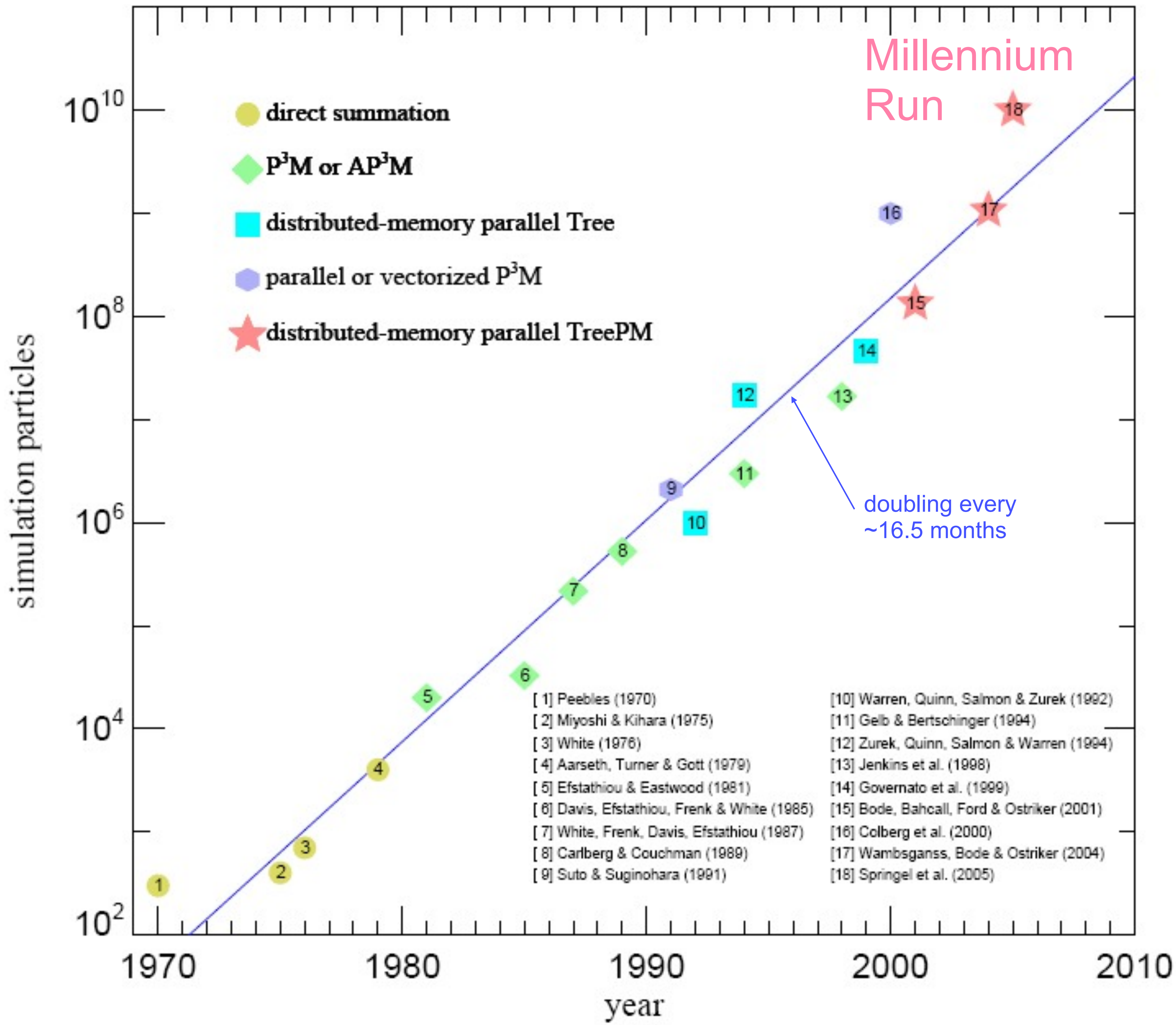

UNDERSTANDING GALAXY CORRELATIONS

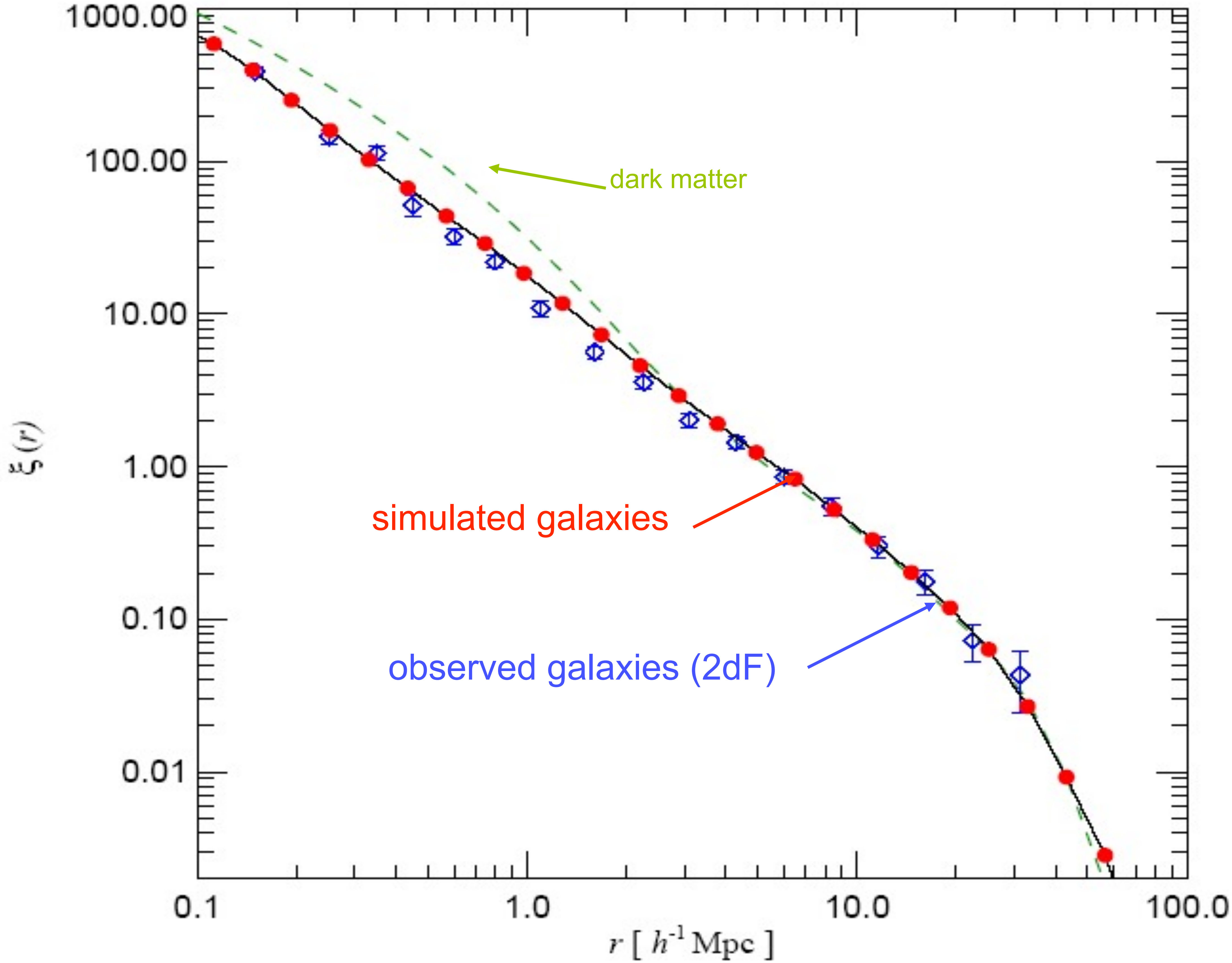

Galaxy 2-point correlation function at the present epoch.

Springel et al. 2005

Galaxy type correlated with large scale structure

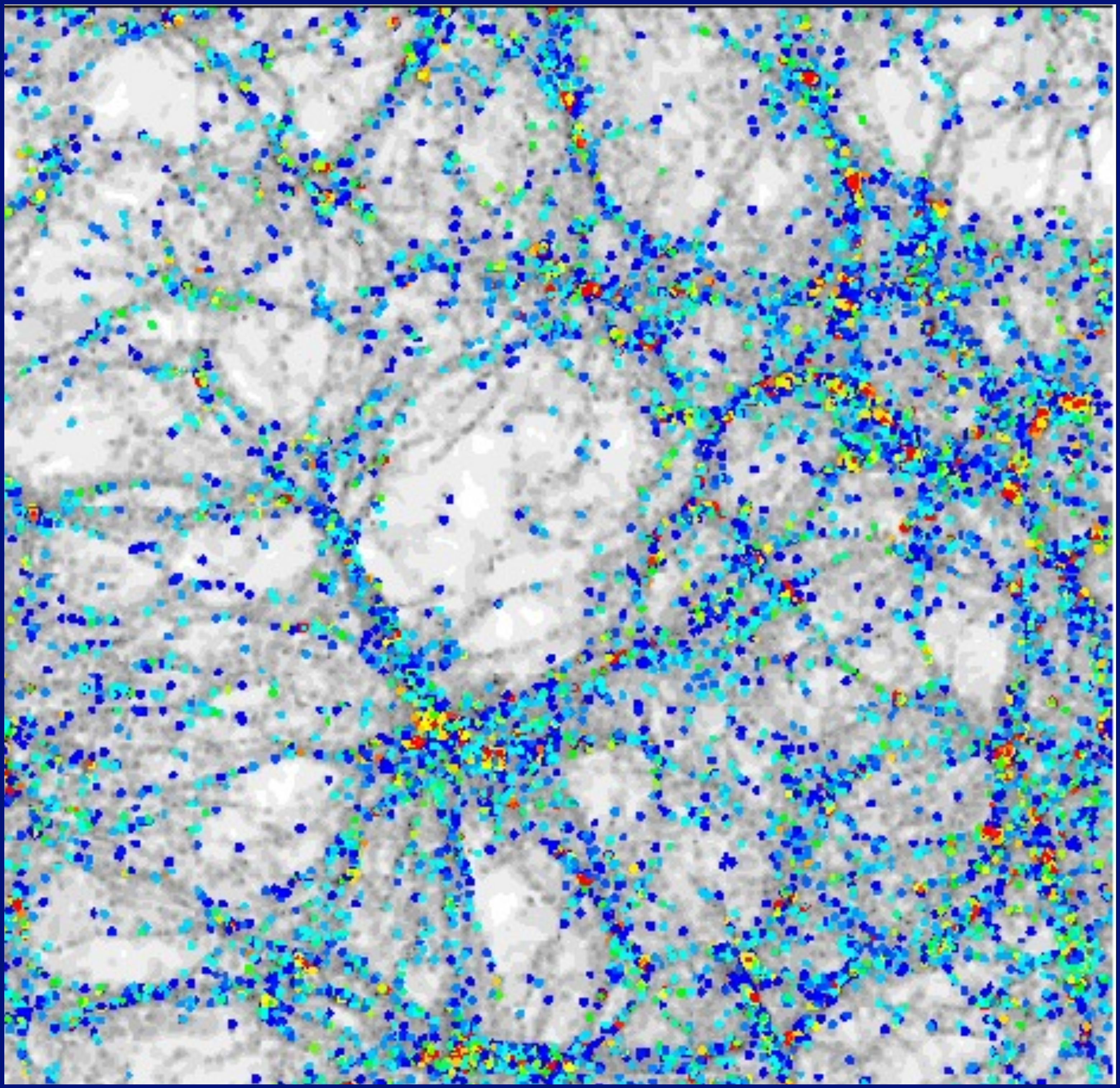

elliptical

elliptical

bulge+disk

disk

Semi-Analytic Modeling

Kauffmann et al.

Elliptical galaxies in clusters in the local universe

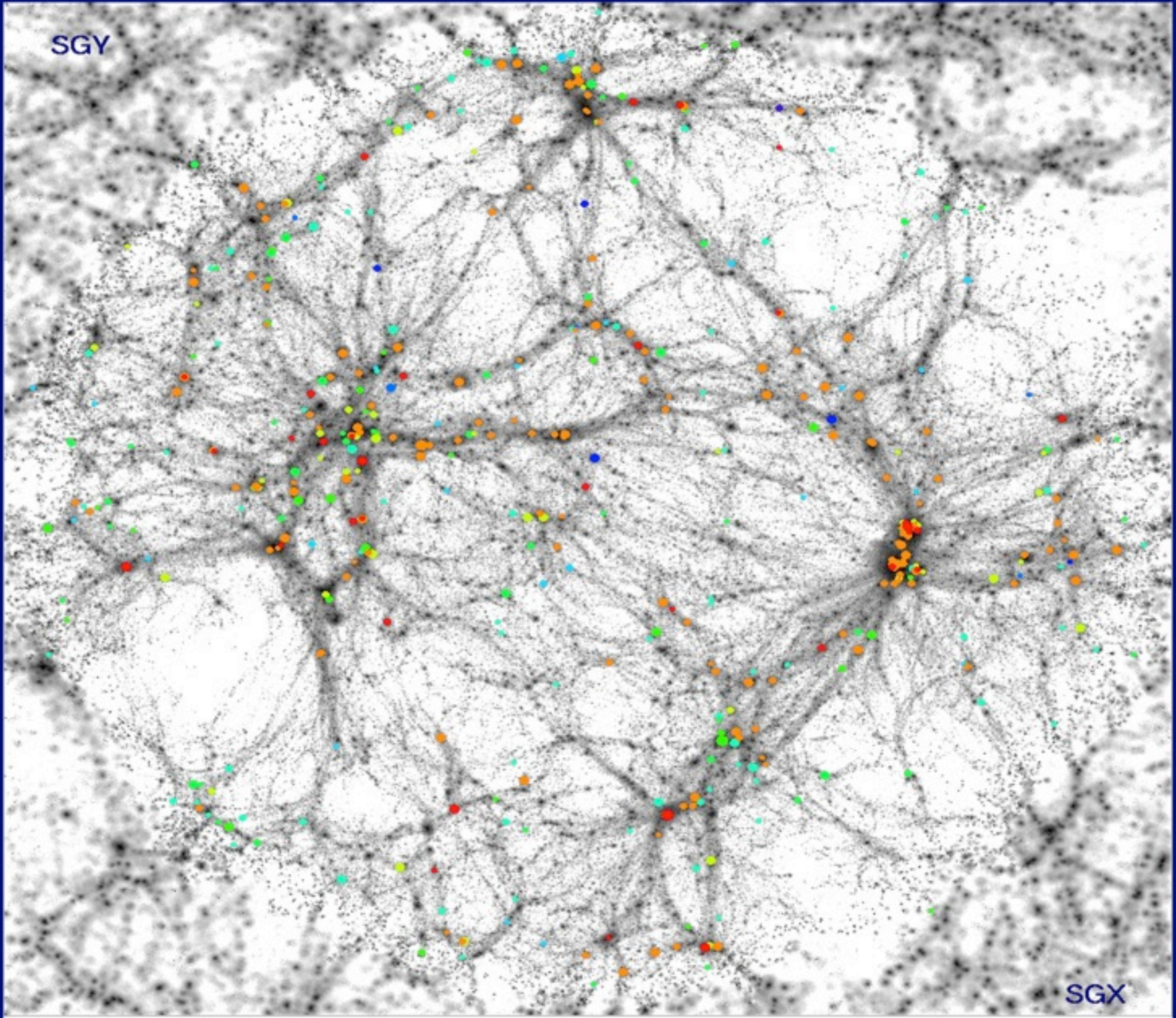

ΛCDM CR : E and S0 galaxies
Credits : Mathis, Lemson, Springel, Kauffmann, White and Dekel.

Formation of galaxies in a cluster

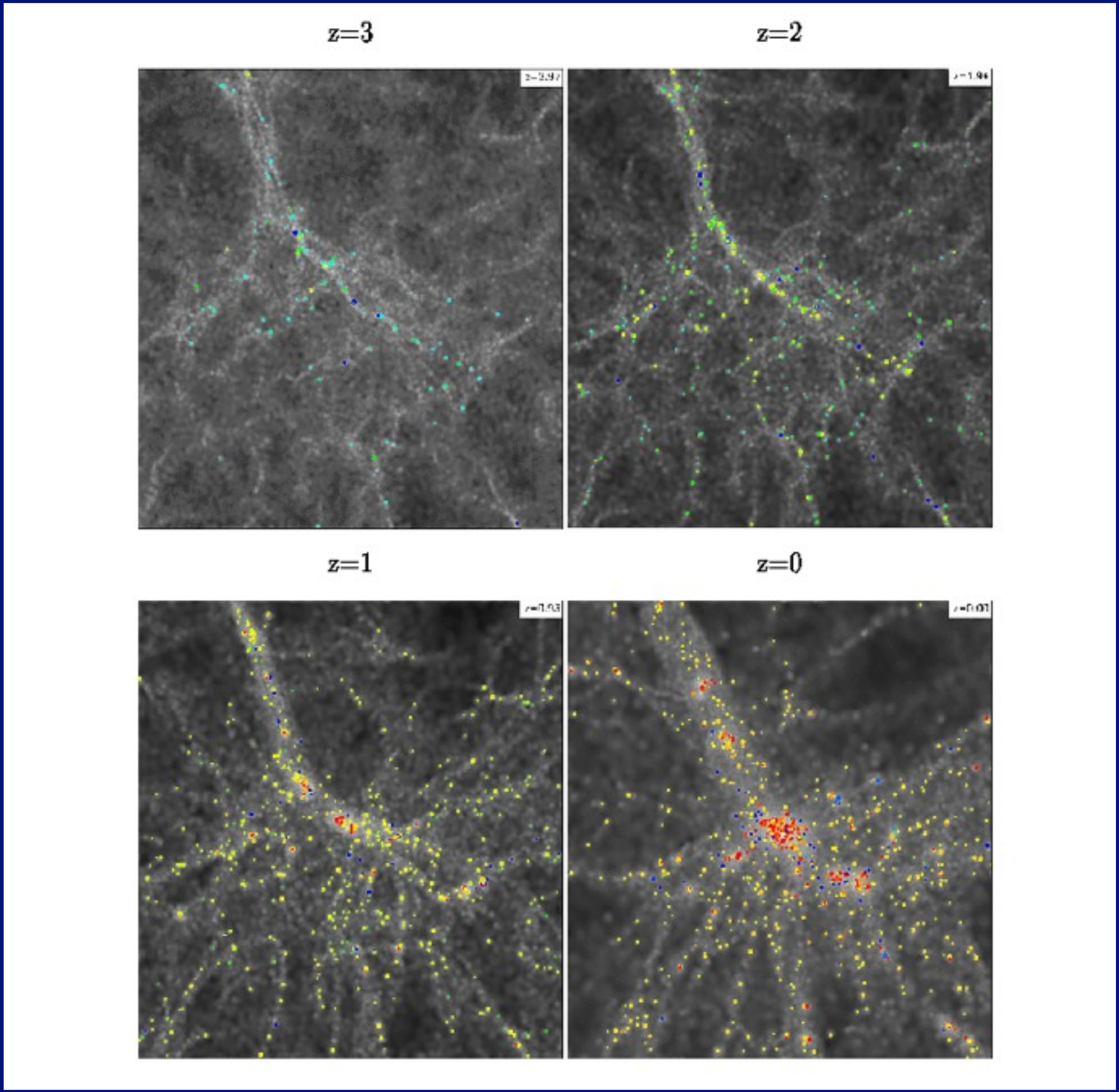

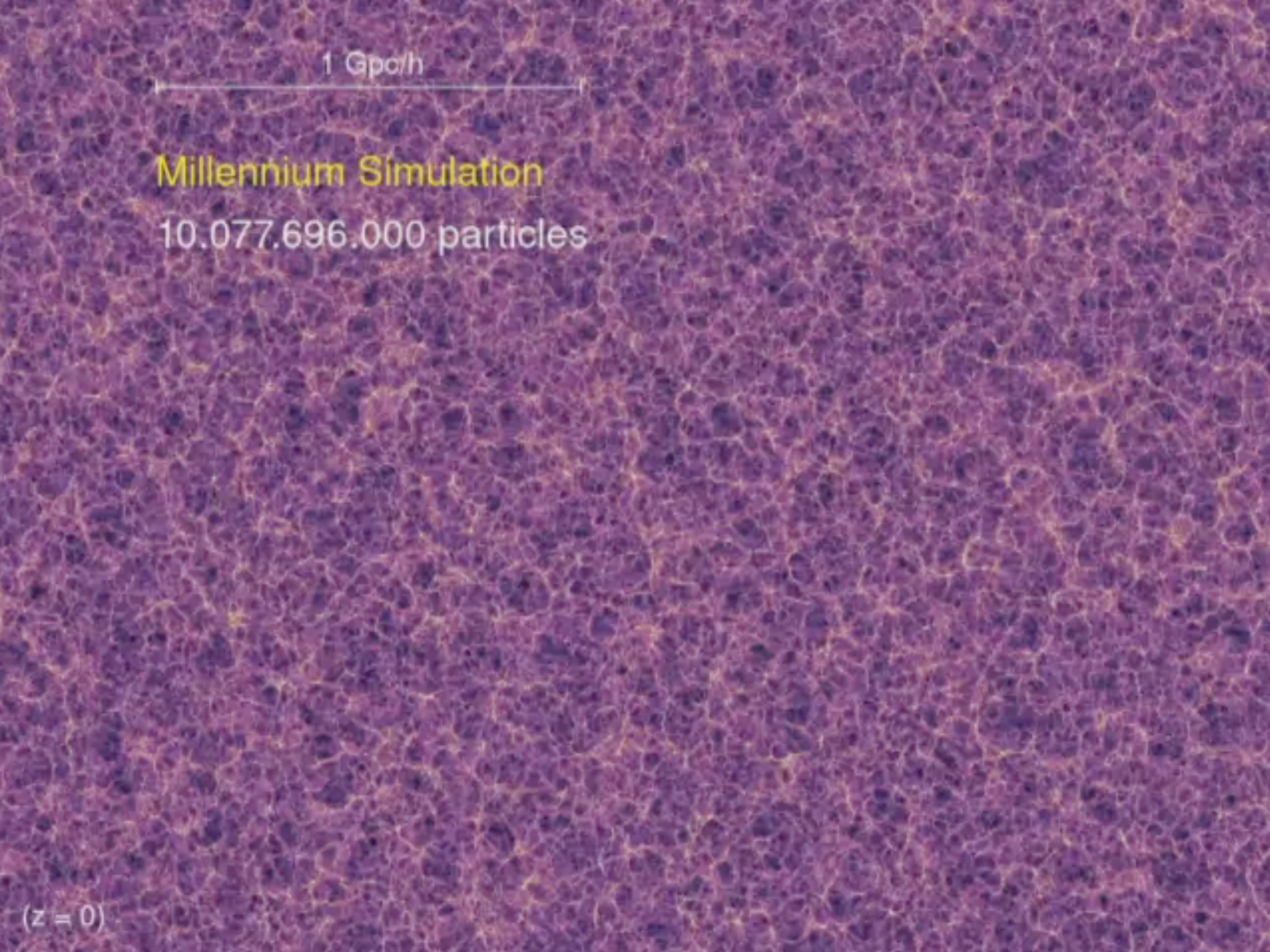
1 Gpc/h
Millennium Simulation
10.077.696.000 particles
(z = 0)

The Millennium Run

• **properties of halos** (radial profile, concentration, shapes)
• **evolution of the number density of halos**, essential for normalization of Press-Schechter-type models
• **evolution of the distribution and clustering of halos** in real and redshift space, for comparison with observations
• **accretion history of halos**, assembly bias (variation of large-scale clustering with as- sembly history), and correlation with halo properties including angular momenta and shapes
• **halo statistics** including the mass and velocity functions, angular momentum and shapes, subhalo numbers and distribution, and correlation with environment

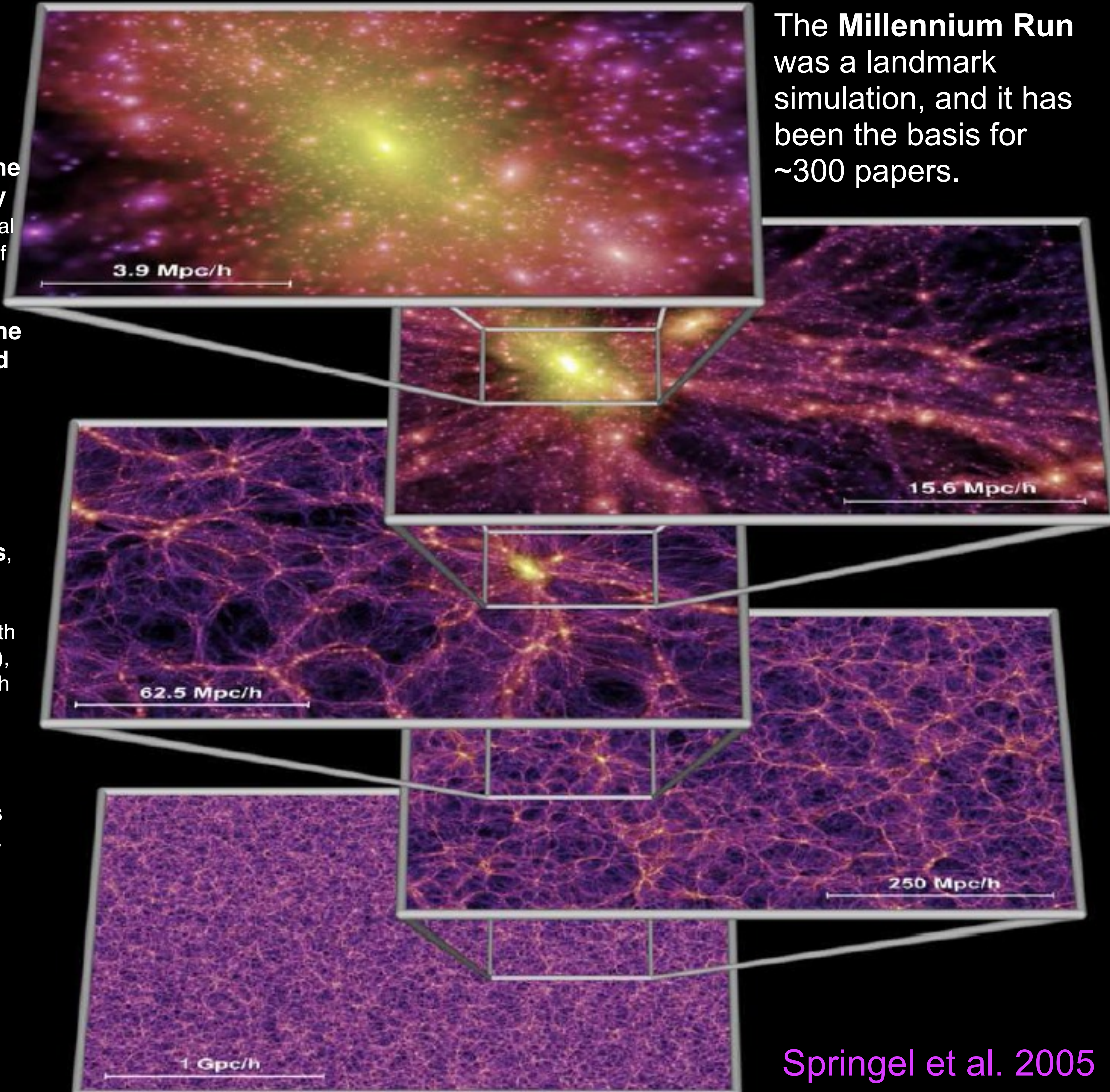

The **Millennium Run** was a landmark simulation, and it has been the basis for ~300 papers.

Springel et al. 2005

• **void statistics**, including sizes and shapes and their evolution, and the orientation of halo spins around voids
• quantitative descriptions of the evolving **cosmic web**, including applications to weak gravitational lensing
• preparation of **mock catalogs**, essential for analyzing SDSS and other survey data, and for preparing for new large surveys for dark energy etc.
• **merger trees**, essential for **semi-analytic modeling** of the evolving galaxy population, including models for the galaxy merger rate, the history of star formation and galaxy colors and morphology, the evolving AGN luminosity function, stellar and AGN feedback, recycling of gas and metals, etc.

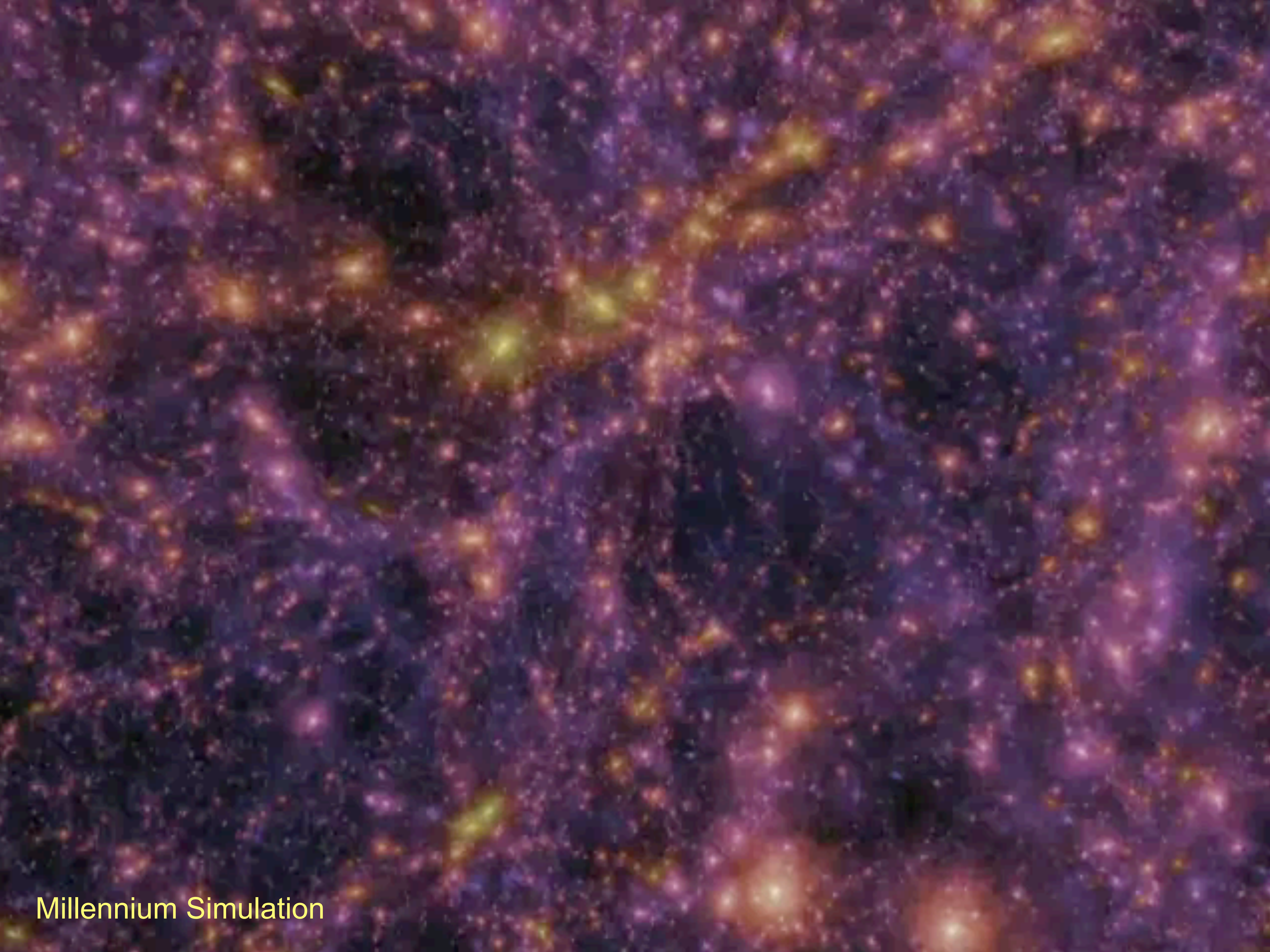
Millennium Simulation

Environment of a ‘first quasar candidate’ at high and low redshifts. The two panels on the left show the projected dark matter distribution in a cube of comoving sidelength $10h^{-1}$ Mpc, colourcoded
according to density and local dark matter velocity dispersion. The panels on the right show the galaxies of the semi-analytic model overlayed on a gray-scale image of the dark matter density. The volume of the sphere representing each galaxy is proportional to its stellar mass, and the chosen colours encode the restframe stellar $B-V$ colour index. While at $z = 6.2$ (top) all galaxies appear blue due to ongoing star formation, many of the galaxies that have fallen into the rich cluster at $z = 0$ (bottom) have turned red.

Springel et al. 2005

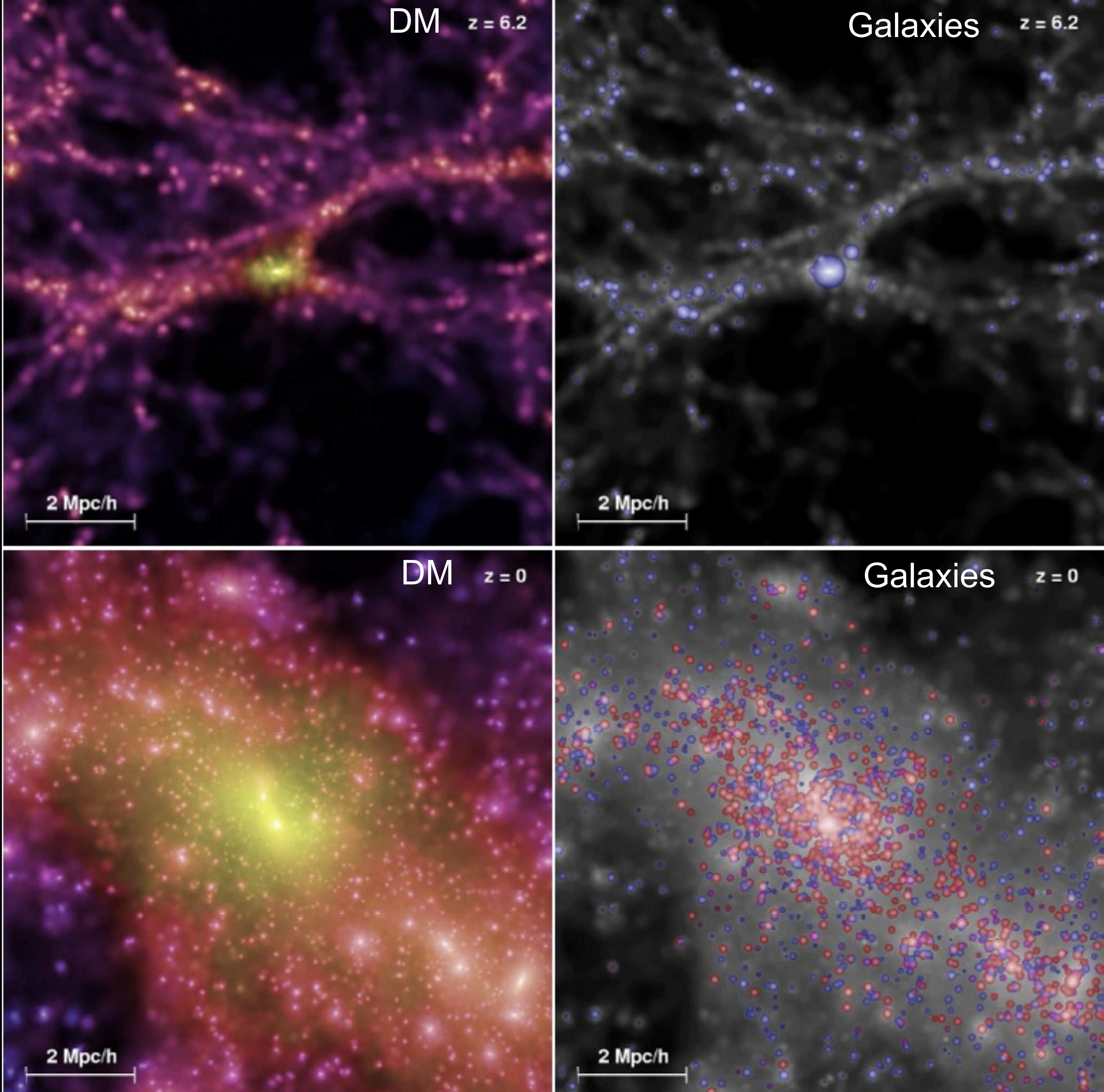

The Bolshoi simulation

ART code

250Mpc/h Box
LCDM
s8 = 0.83
h = 0.73
8G particles
1kpc/h force resolution
1e8 Msun/h mass res

dynamical range 262,000
time-steps = 400,000

NASA AMES
supercomputing center
Pleiades computer
13824 cores
12TB RAM
75TB disk storage
6M cpu hrs
18 days wall-clock time

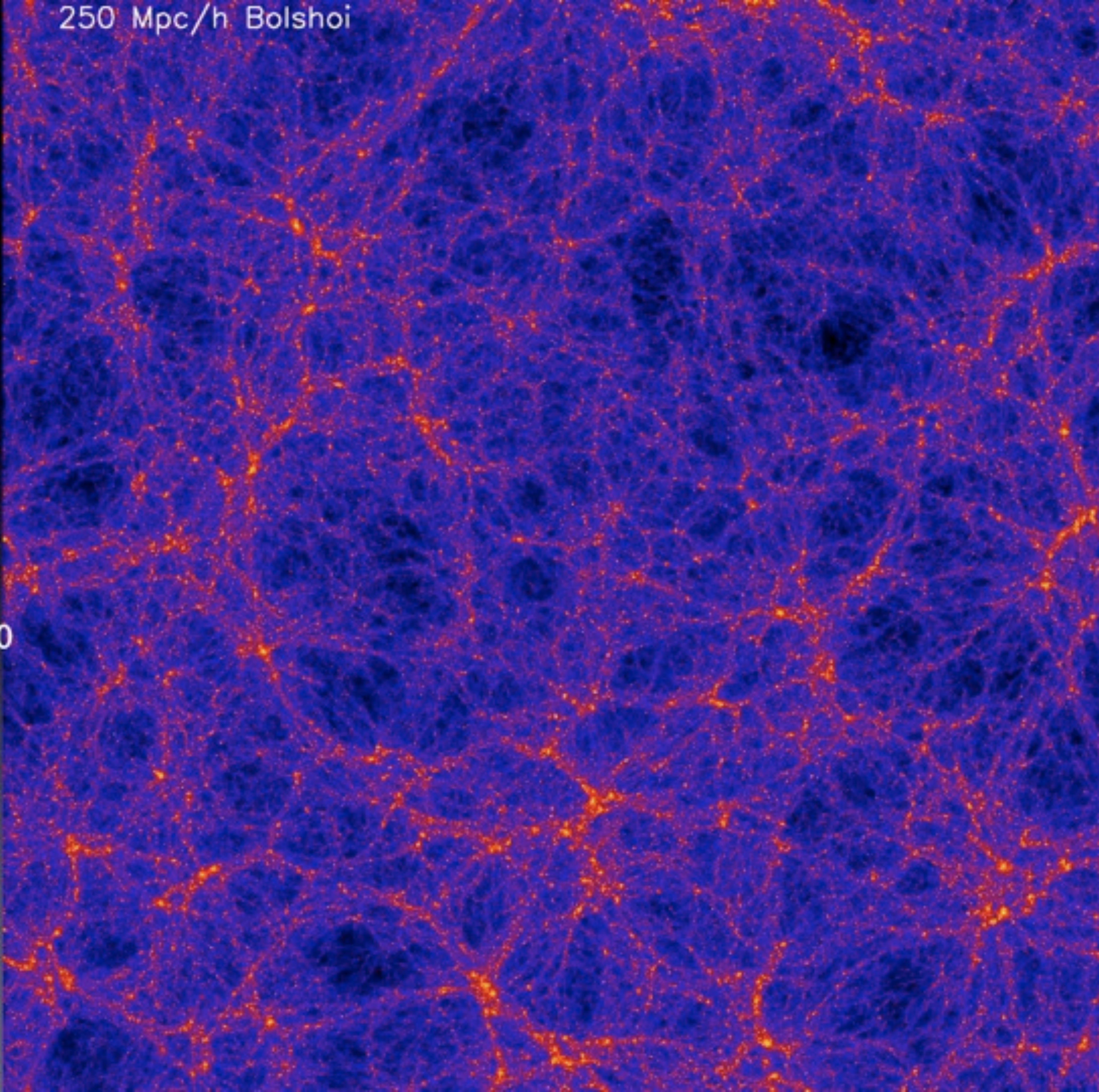

BOLSHOI SIMULATION ZOOM-IN

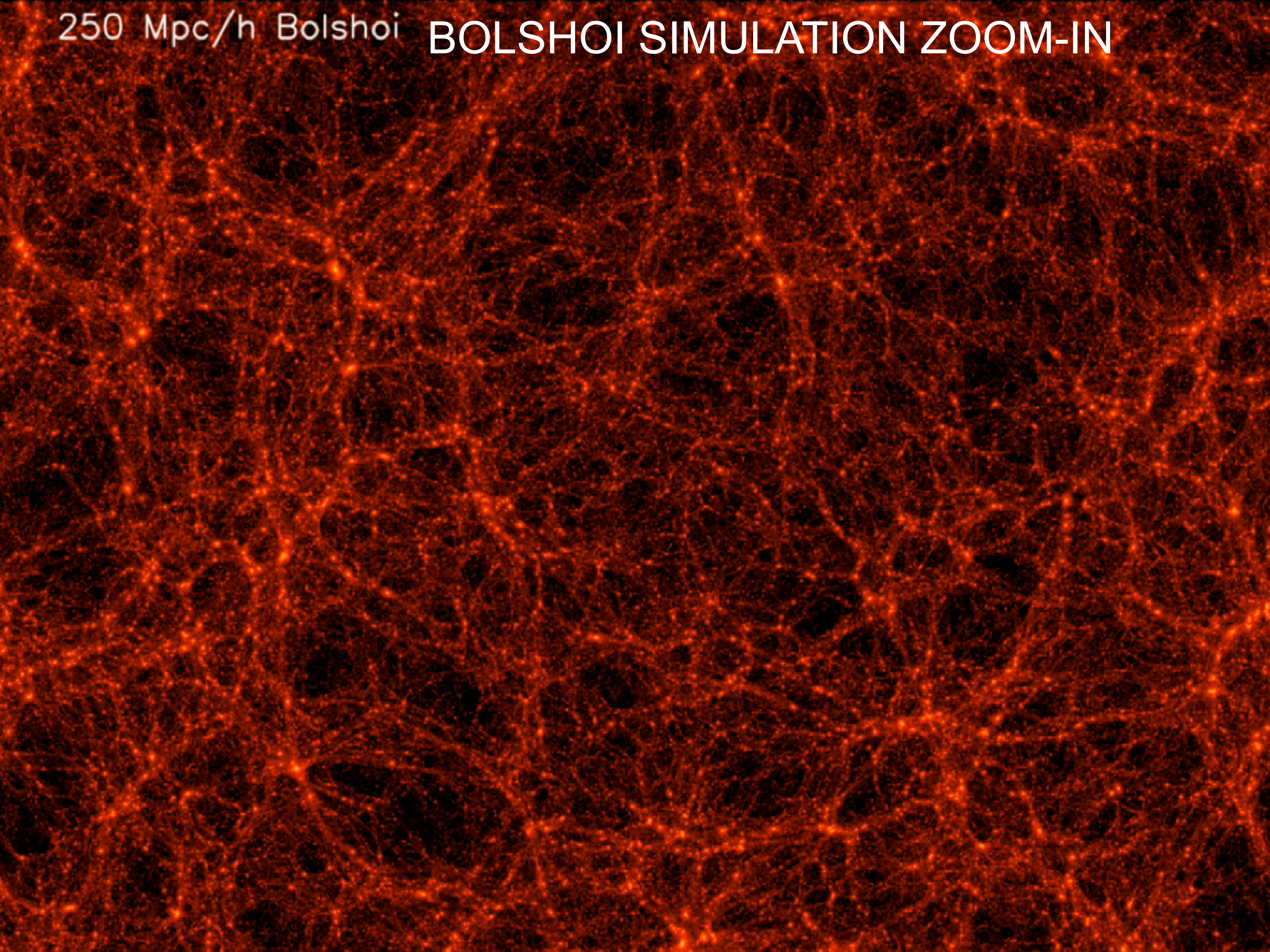

Bolshoi - biggest and best cosmological simulation yet
1 Billion Light Years across

$<10^{-3}$
of the
Bolshoi
Simulation
Volume

100 Million Light Years

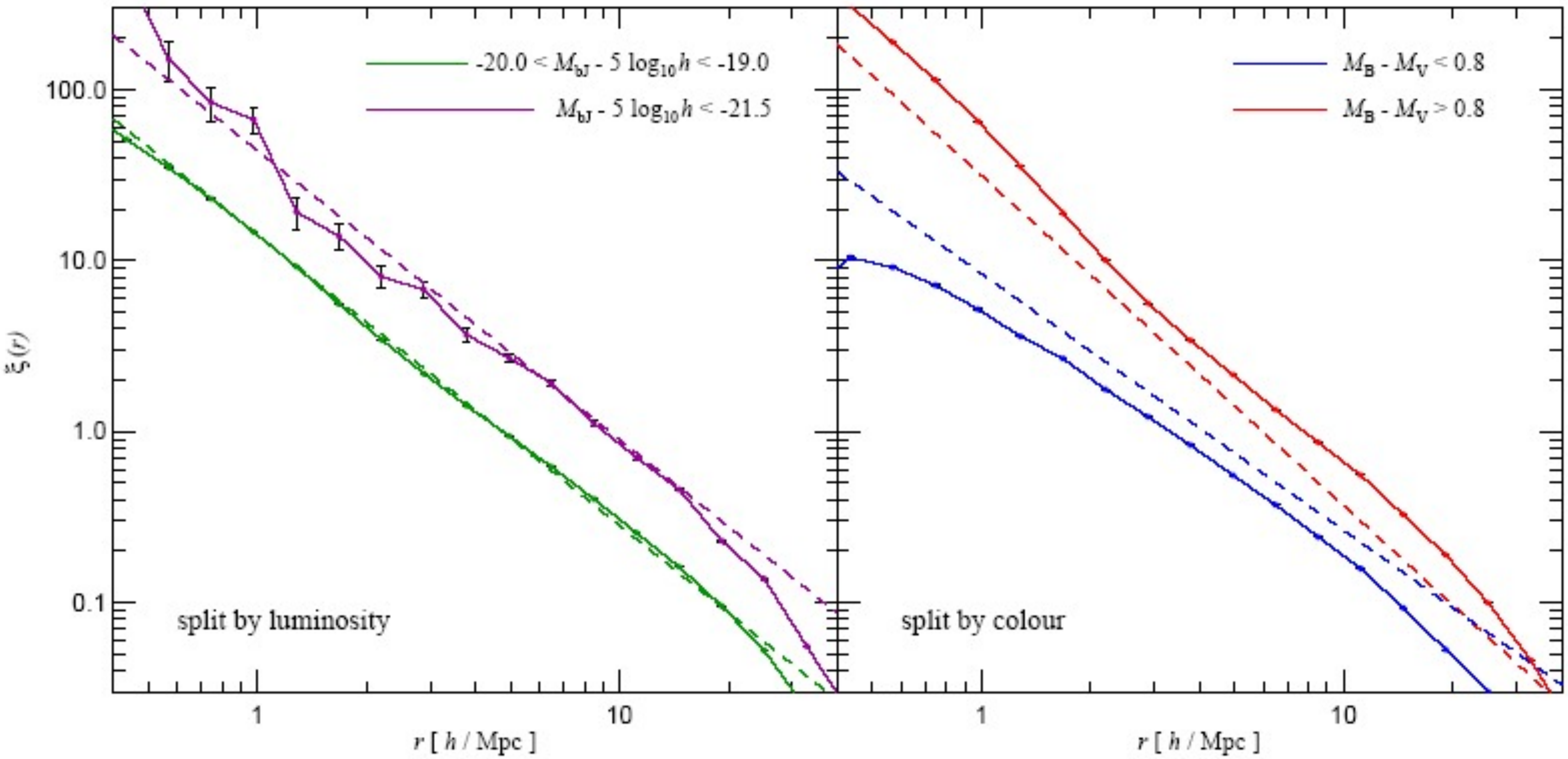

Figure 5: Galaxy clustering as a function of luminosity and colour. In the panel on the left, we show the 2-point correlation function of our galaxy catalogue at $z = 0$ split by luminosity in the bJ-band (symbols). Brighter galaxies are more strongly clustered, in quantitative agreement with observations[33] (dashed lines). Splitting galaxies according to colour (right panel), we find that red galaxies are more strongly clustered with a steeper correlation slope than blue galaxies. Observations[35] (dashed lines) show a similar trend, although the difference in clustering amplitude is smaller than in this particular semi-analytic model.

Springel et al. 2005

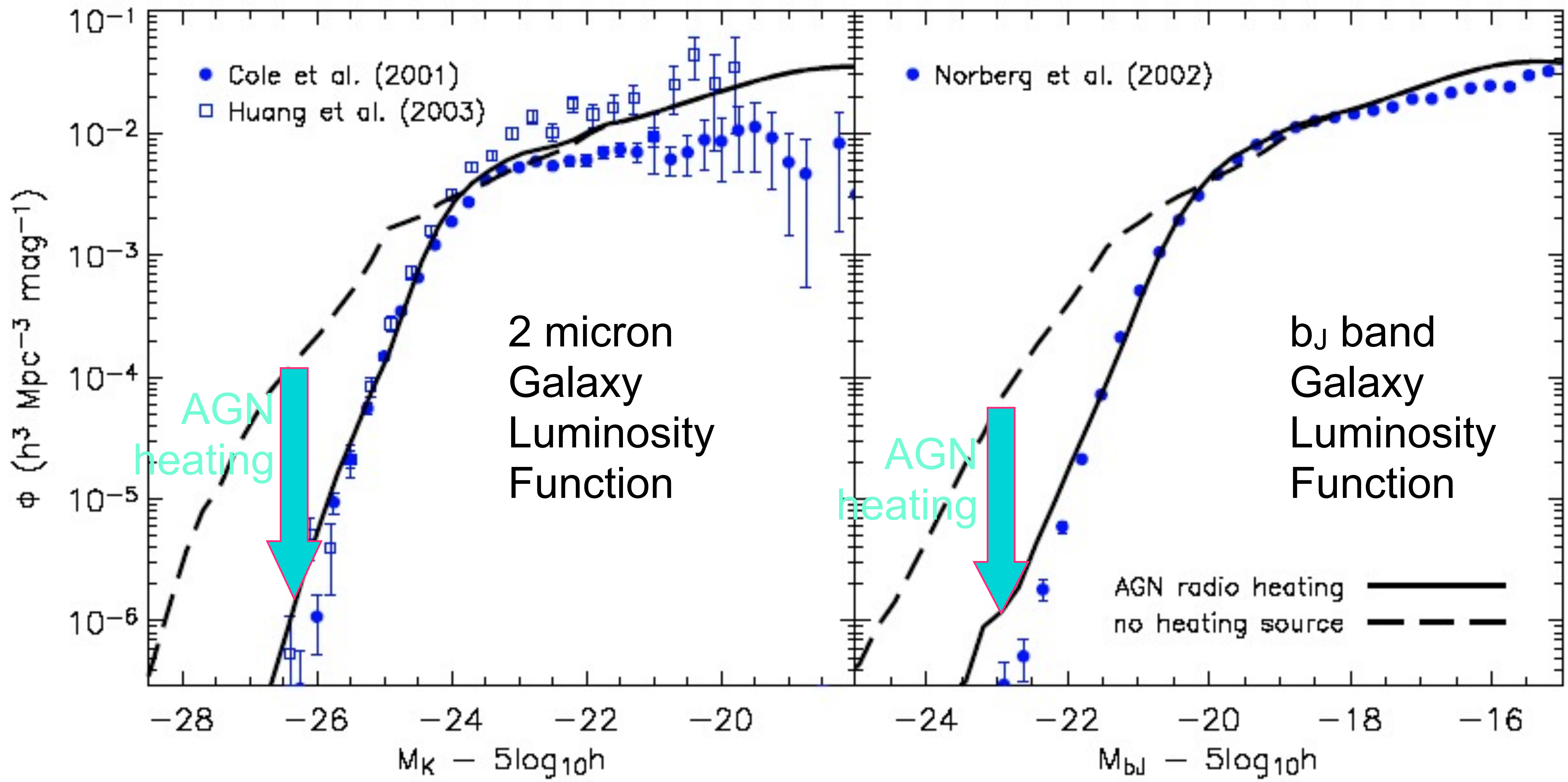

Figure 8. Galaxy luminosity functions in the K (left) and b_J (right) photometric bands, plotted with and without 'radio mode' feedback (solid and long dashed lines respectively – see Section 3.4). Symbols indicate observational results as listed in each panel. As can be seen, the inclusion of AGN heating produces a good fit to the data in both colours. Without this heating source our model overpredicts the luminosities of massive galaxies by about two magnitudes and fails to reproduce the sharp bright end cut-offs in the observed luminosity functions.

Croton et al. 2006

Color Magnitude Diagram

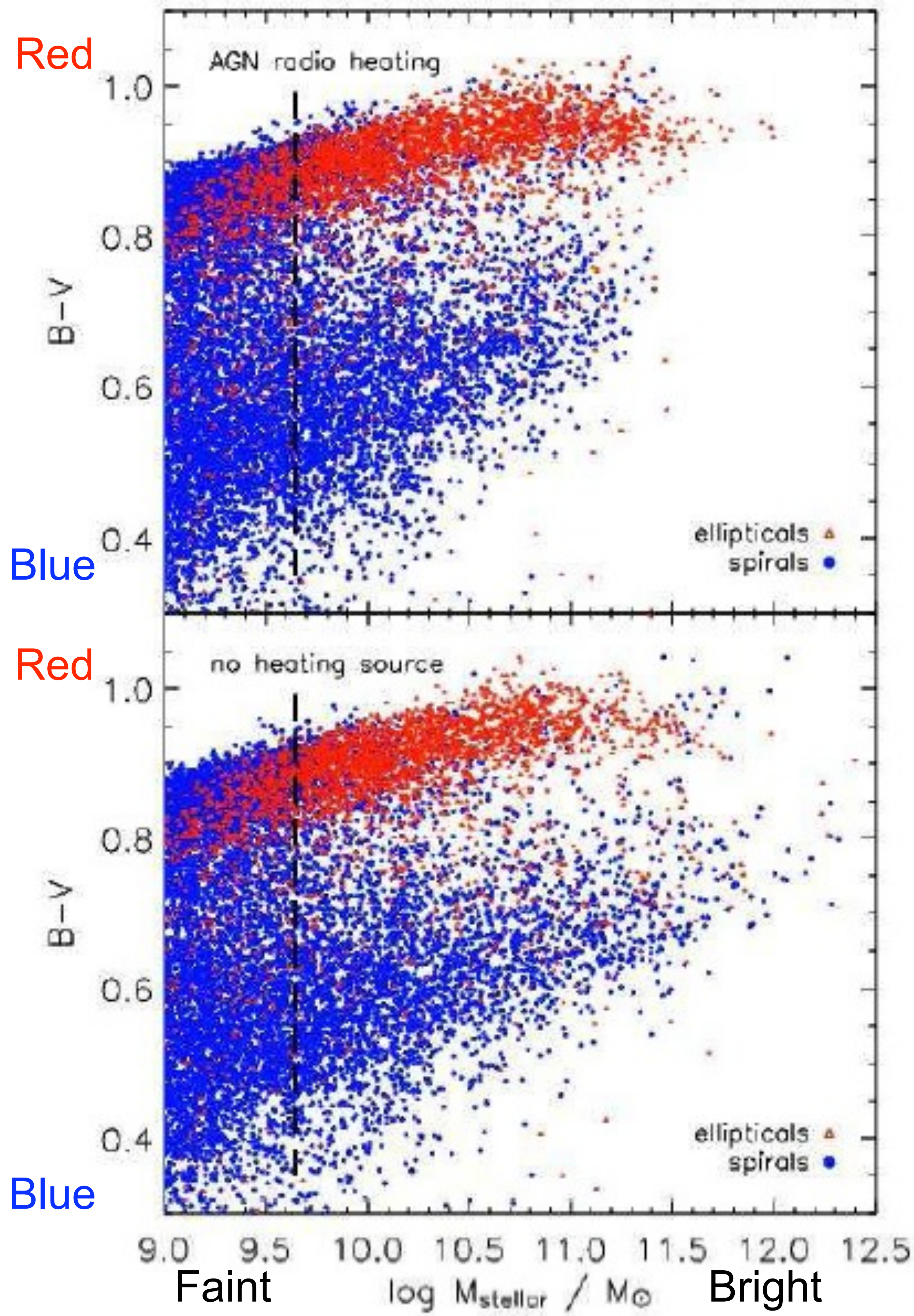

With AGN heating – brightest galaxies are red, as observed

Without heating – brightest galaxies are blue

Croton et al. 2006

(see also Cattaneo et al. 2006)

Semi-Analytic Models of Galaxy Formation

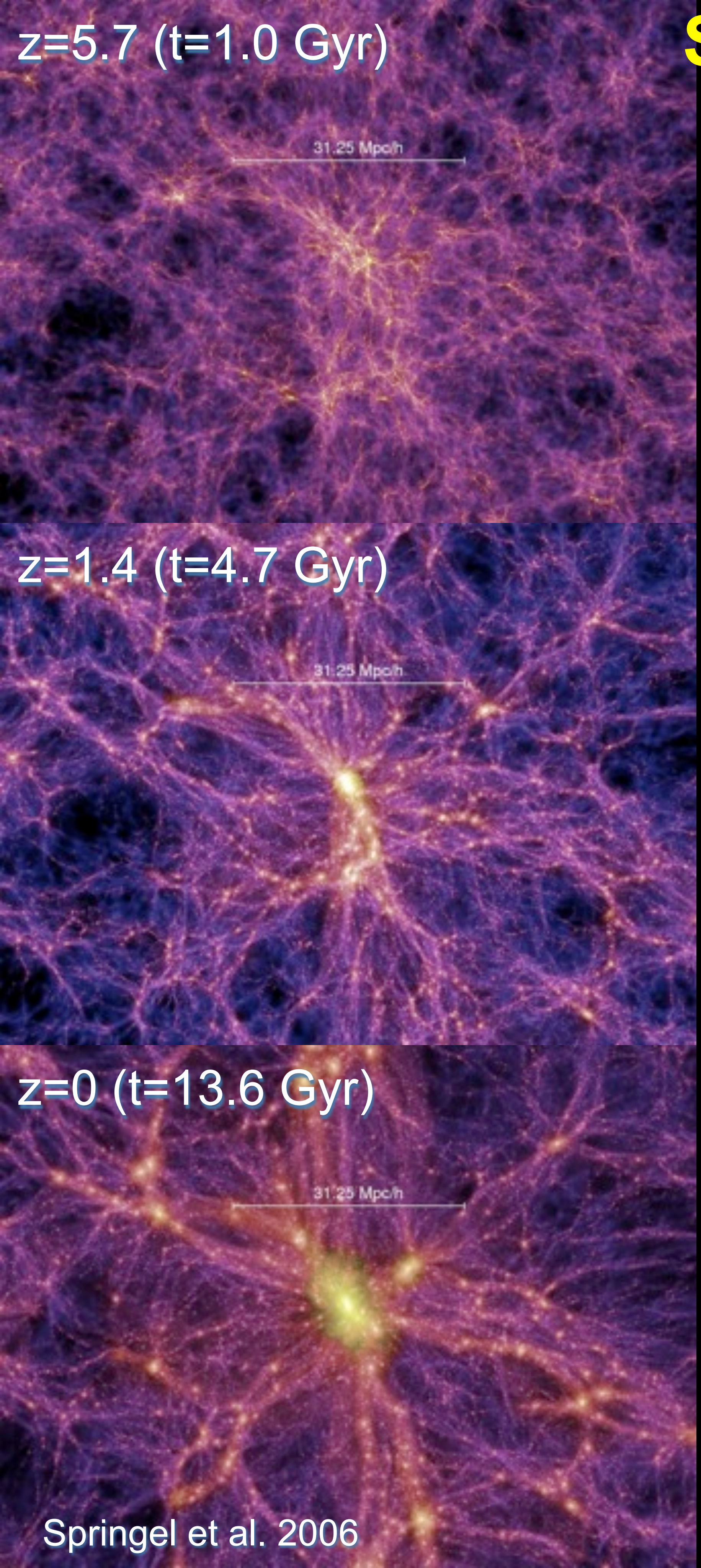

Springel et al. 2006

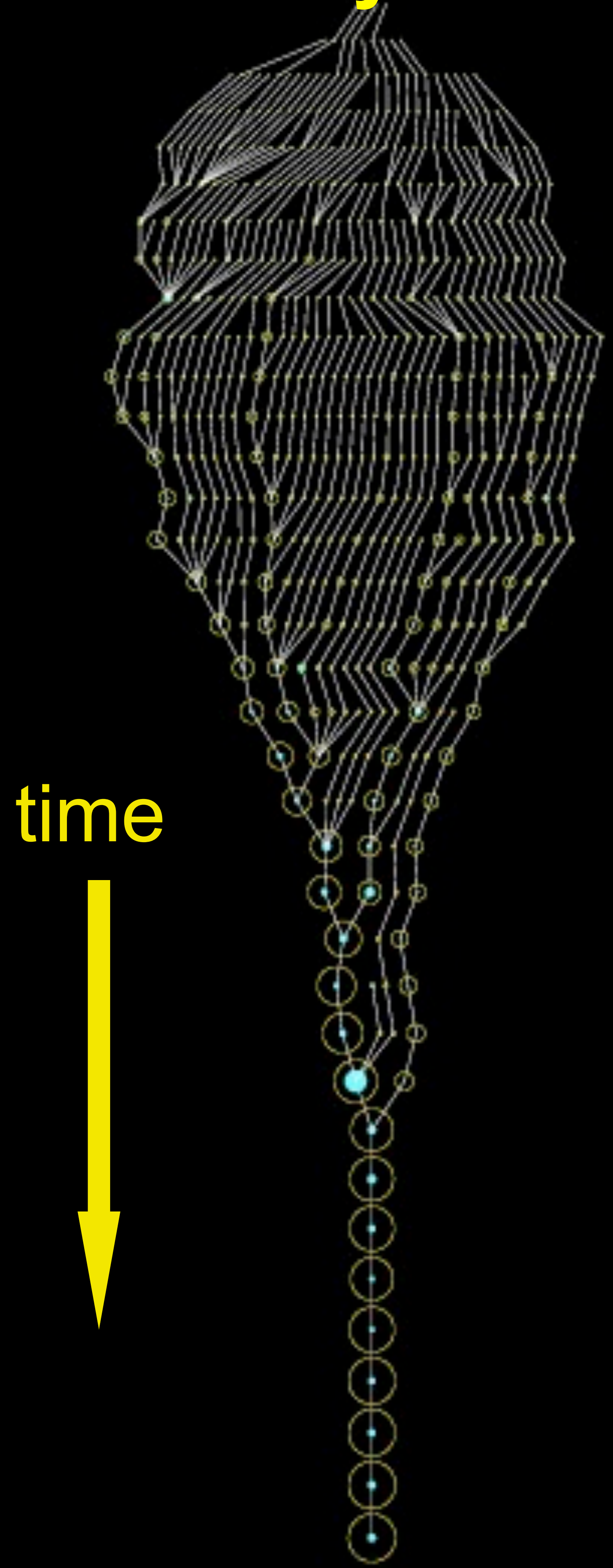

Wechsler et al. 2002

Present status of ΛCDM "Double Dark" theory:

- cosmological parameters are now well constrained by observations
- structure formation in dominant dark matter component accurately quantified
- mass accretion history of dark matter halos is represented by 'merger trees' like the one at left

Semi-Analytic Models of Galaxy Formation

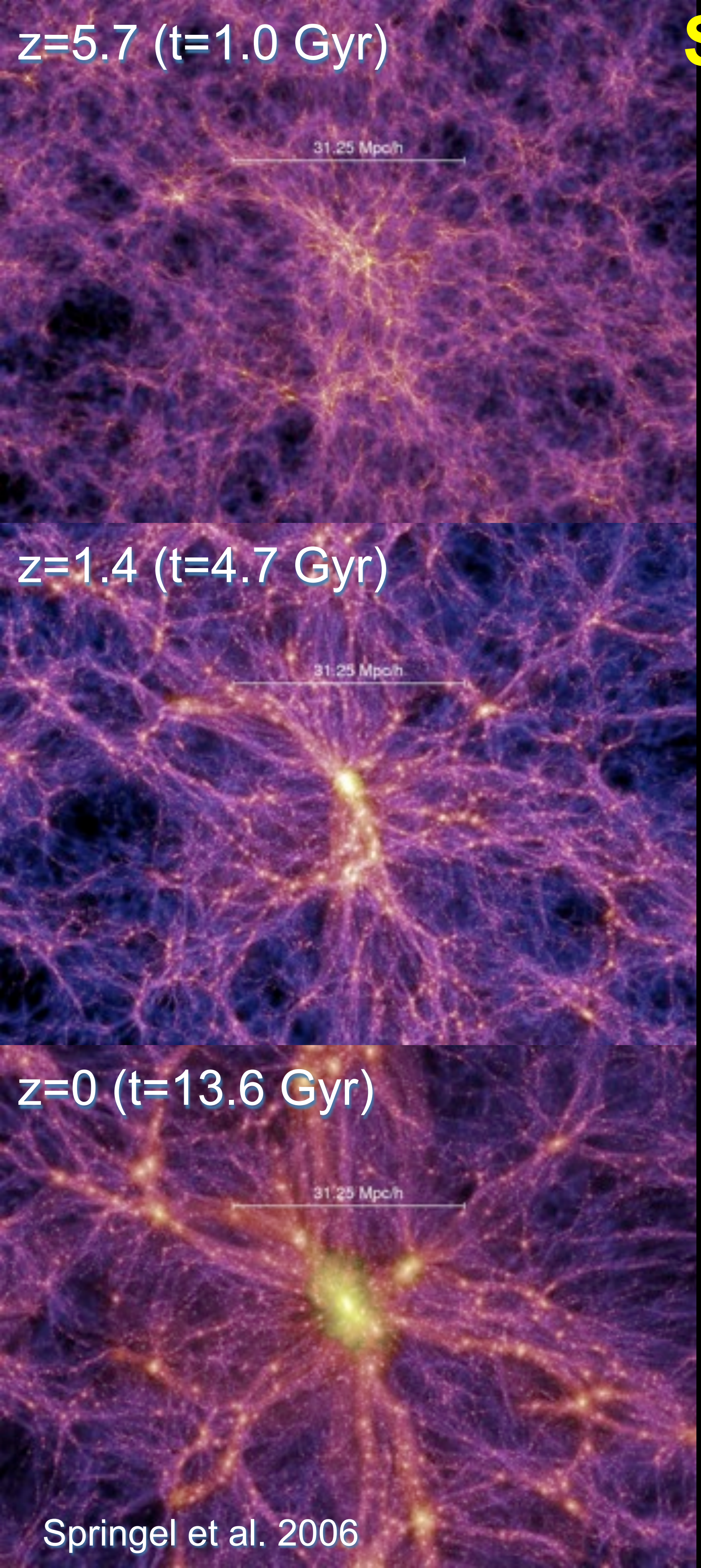

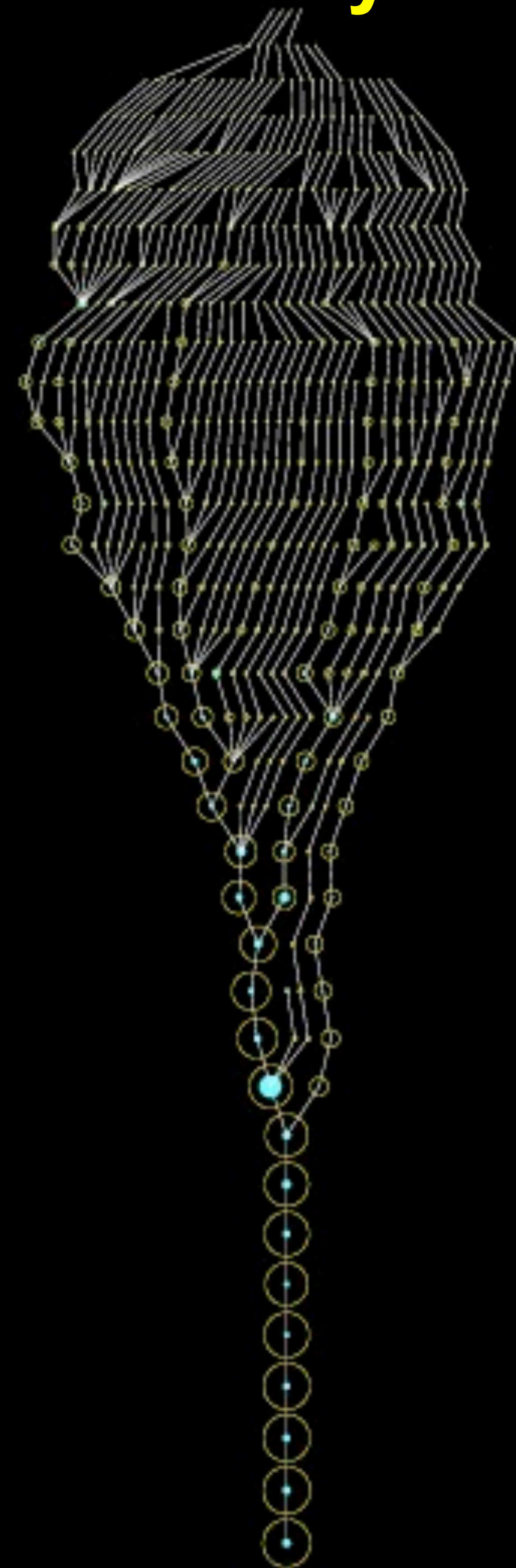

Astrophysical processes modeled:

- shock heating & radiative cooling
- photoionization squelching
- merging
- star formation (quiescent & burst)
- SN heating & SN-driven winds
- AGN accretion and feedback
- chemical evolution
- stellar populations & dust

Semi-Analytic Models of Galaxy Formation

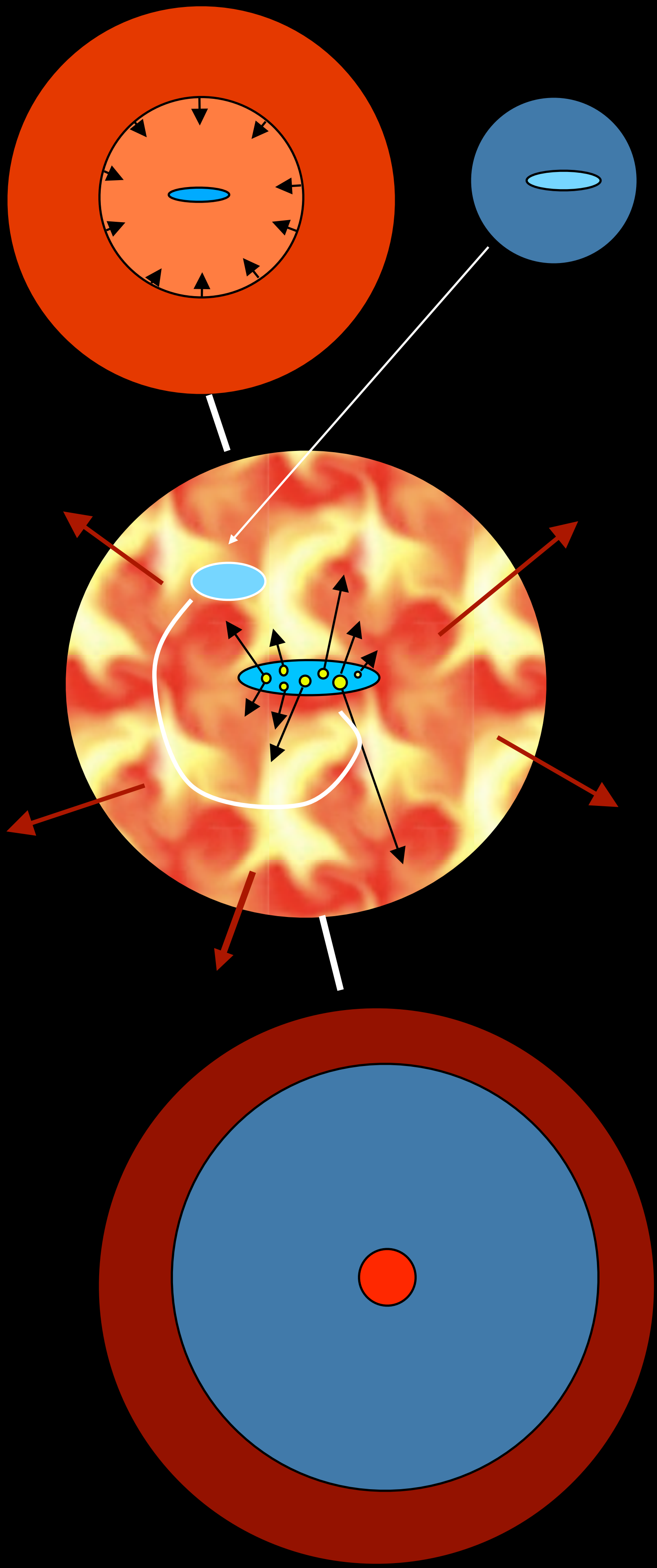

- gas is collisionally heated when perturbations 'turn around' and collapse to form gravitationally bound structures
- gas in halos cools via atomic line transitions (depends on density, temperature, and metallicity)
- cooled gas collapses to form a rotationally supported disk
- cold gas forms stars, with efficiency a function of gas density (e.g. Schmidt-Kennicutt Law)
- massive stars and SNae reheat (and expel?) cold gas and some metals
- galaxy mergers trigger bursts of star formation; 'major' mergers transform disks into spheroids

White & Frenk 1991; Kauffmann et al. 93; Cole et al. 94; Somerville & Primack 99; Cole et al. 2000; Somerville, Primack, & Faber 01; Croton et al. 06; De Lucia & Blaizot 06; Cattaneo et al. 07; Somerville et al. 08, 10

New Improved Semi-Analytic Models Work!

- Earlier CDM-based galaxy formation models suffered from a set of interlinked problems
  - overcooling/cooling flow problems in galaxies and clusters
  - failure to produce observed color bimodality
- 'Bright mode' AGN feedback may regulate BH formation & temporarily quench star formation, but is not a viable 'maintenance' mechanism
- Low-accretion rate 'radio mode' feedback is a promising mechanism for counteracting cooling flows over long time scales
- New self-consistent 'hybrid' models based on physical scaling from numerical simulations and calibrated against empirical constraints now enable us to predict/ interpret the relationship between galaxies, BH, and AGN across cosmic history

-- Rachel Somerville

Baryons in Dark Matter Halos

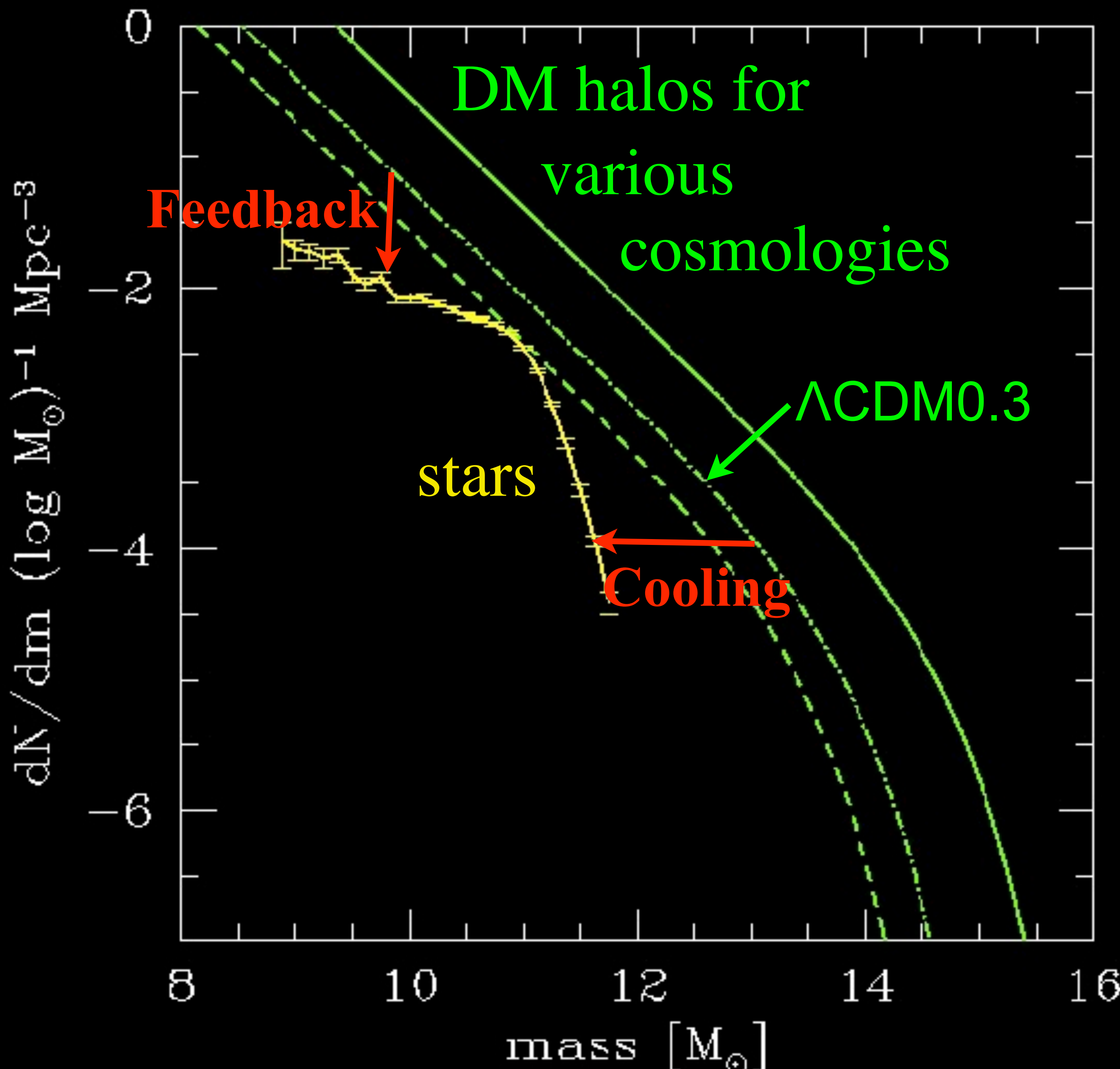

- in order to reconcile CDM (sub)halo mass function with galaxy LF or stellar MF, cooling/star formation must be inefficient overall, most efficient at $M_{halo} \sim 10^{11}$ M_{sun}
- baryon/DM ratio must be a strongly non-linear (& non-monotonic) function of halo mass

Somerville & Primack 1999; cf. Benson et al. 2003

Dark halo mass growth vs. time: 4 clusters

GALics DM halos by Cattaneo et al. 2006

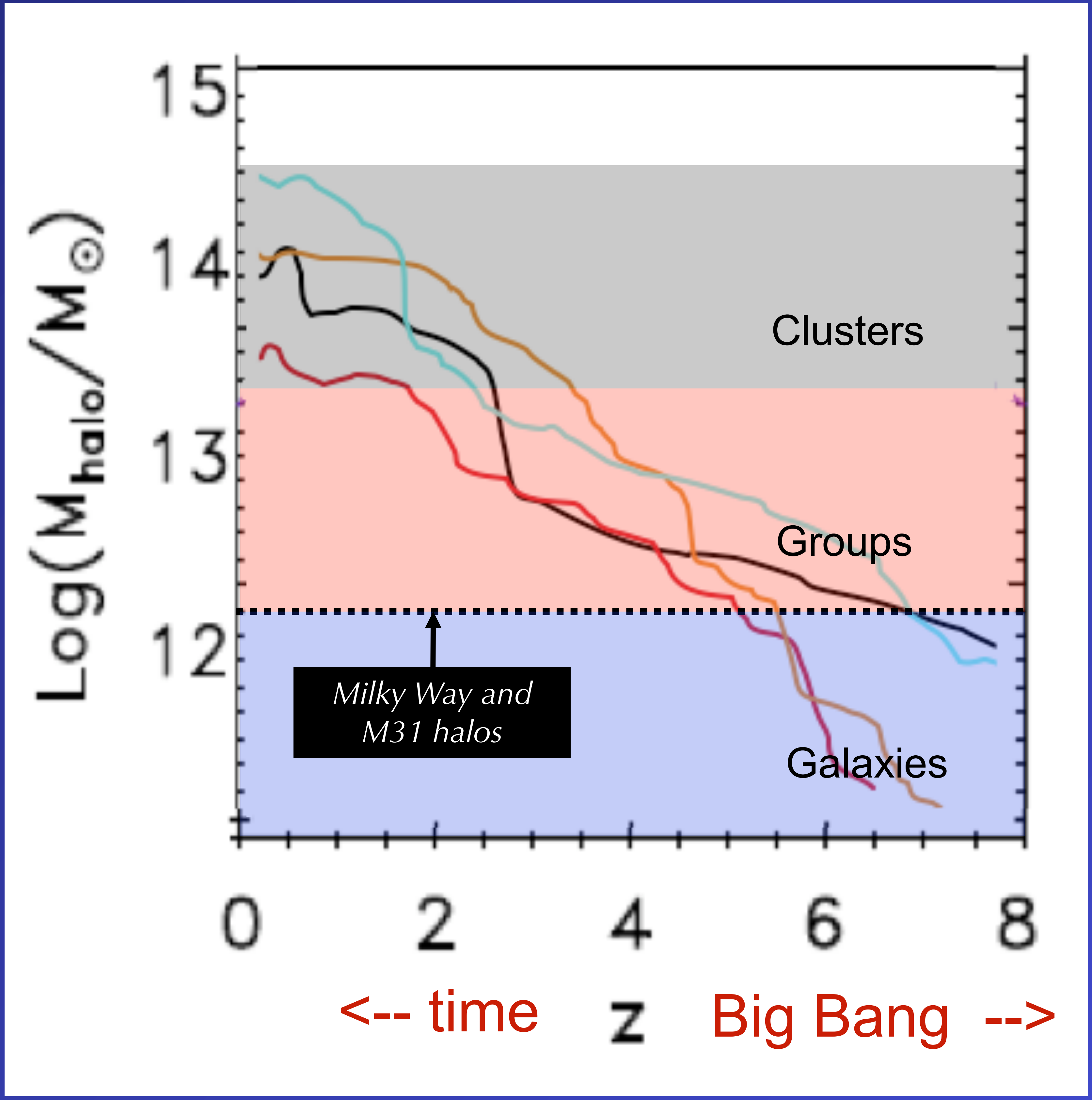

Dark halos of progressively smaller mass

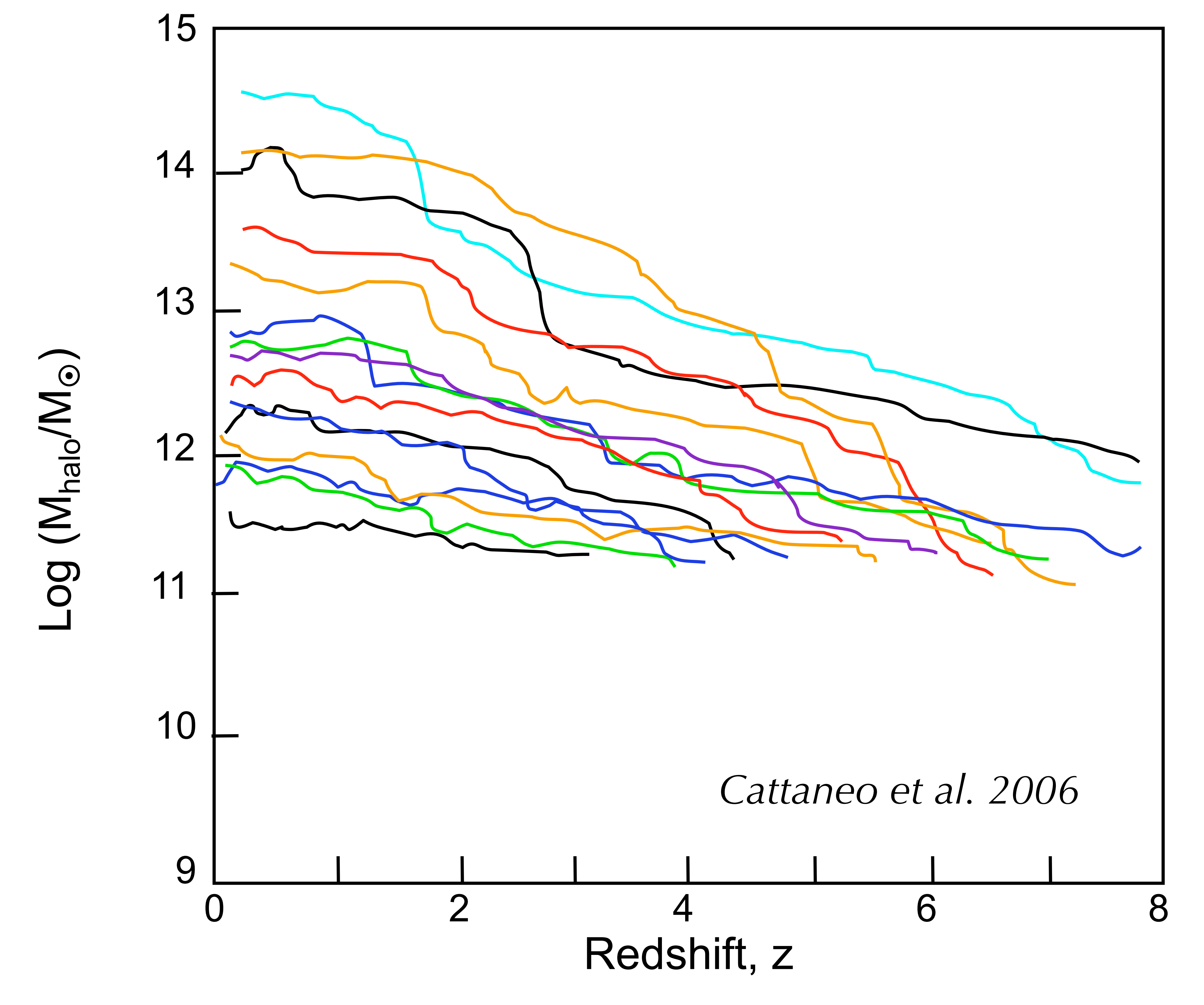

A schematic model of average halo mass growth

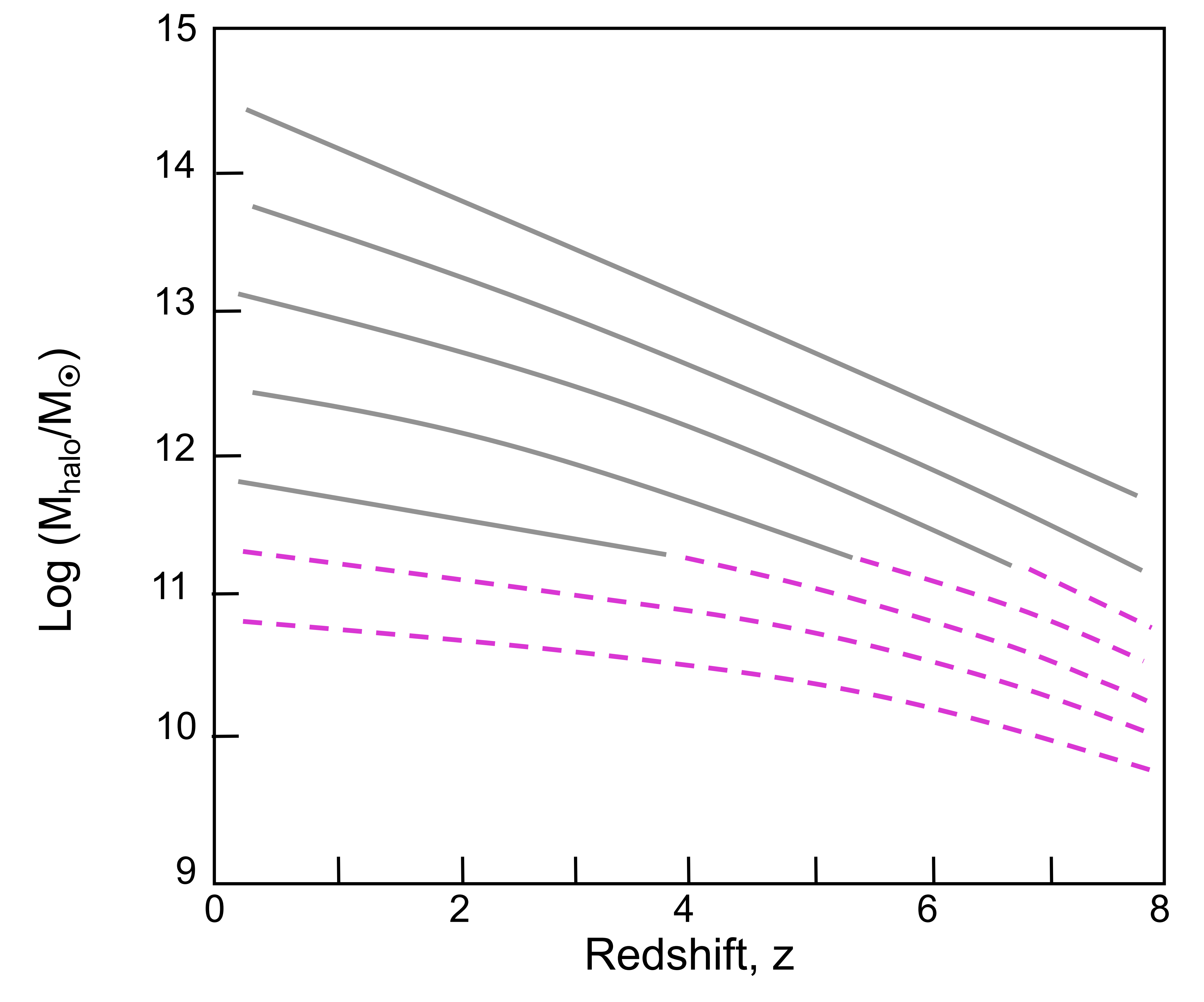

Key assumption: ***star-forming band*** in dark-halo mass

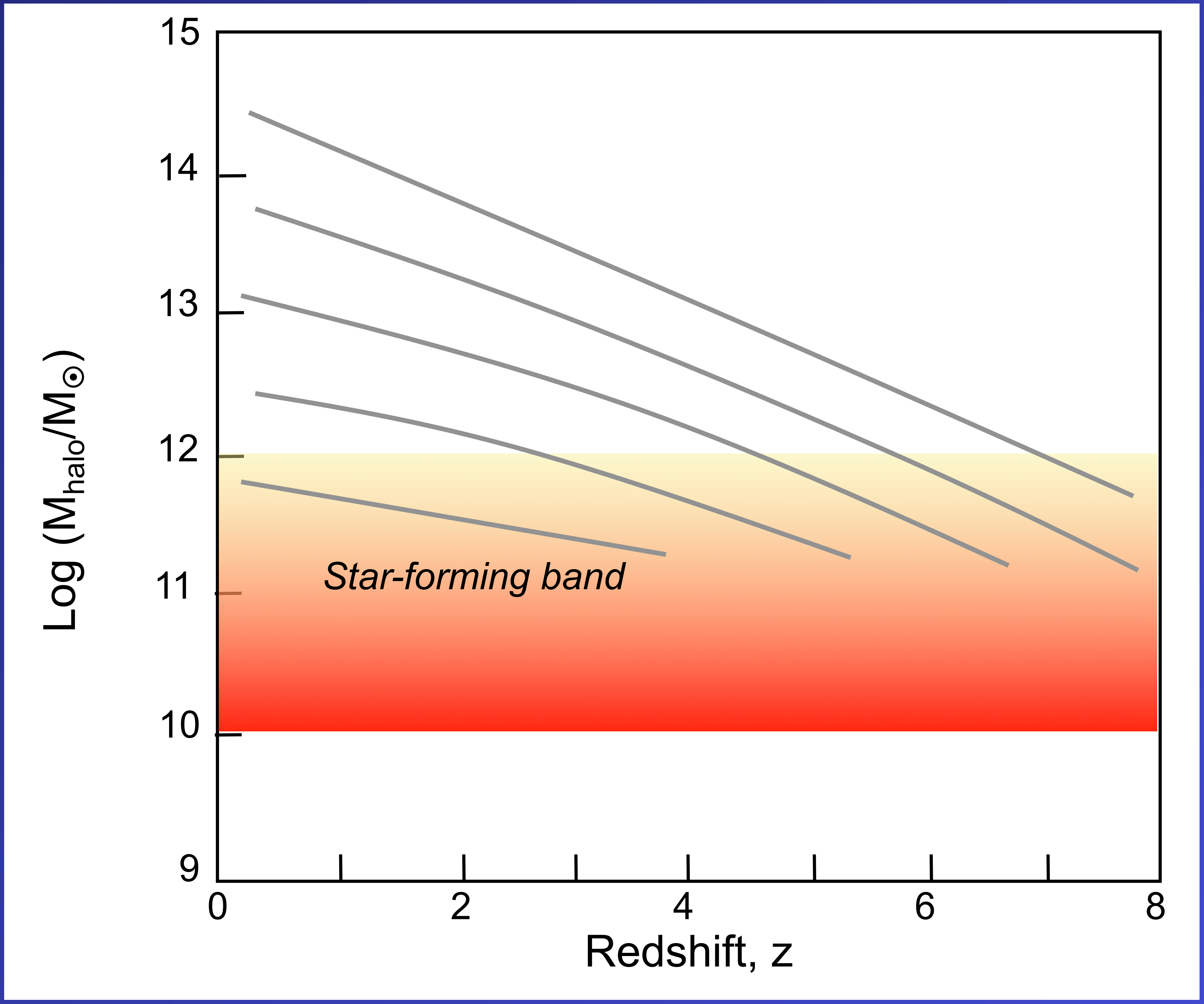

Key assumption: ***star-forming band*** in dark-halo mass

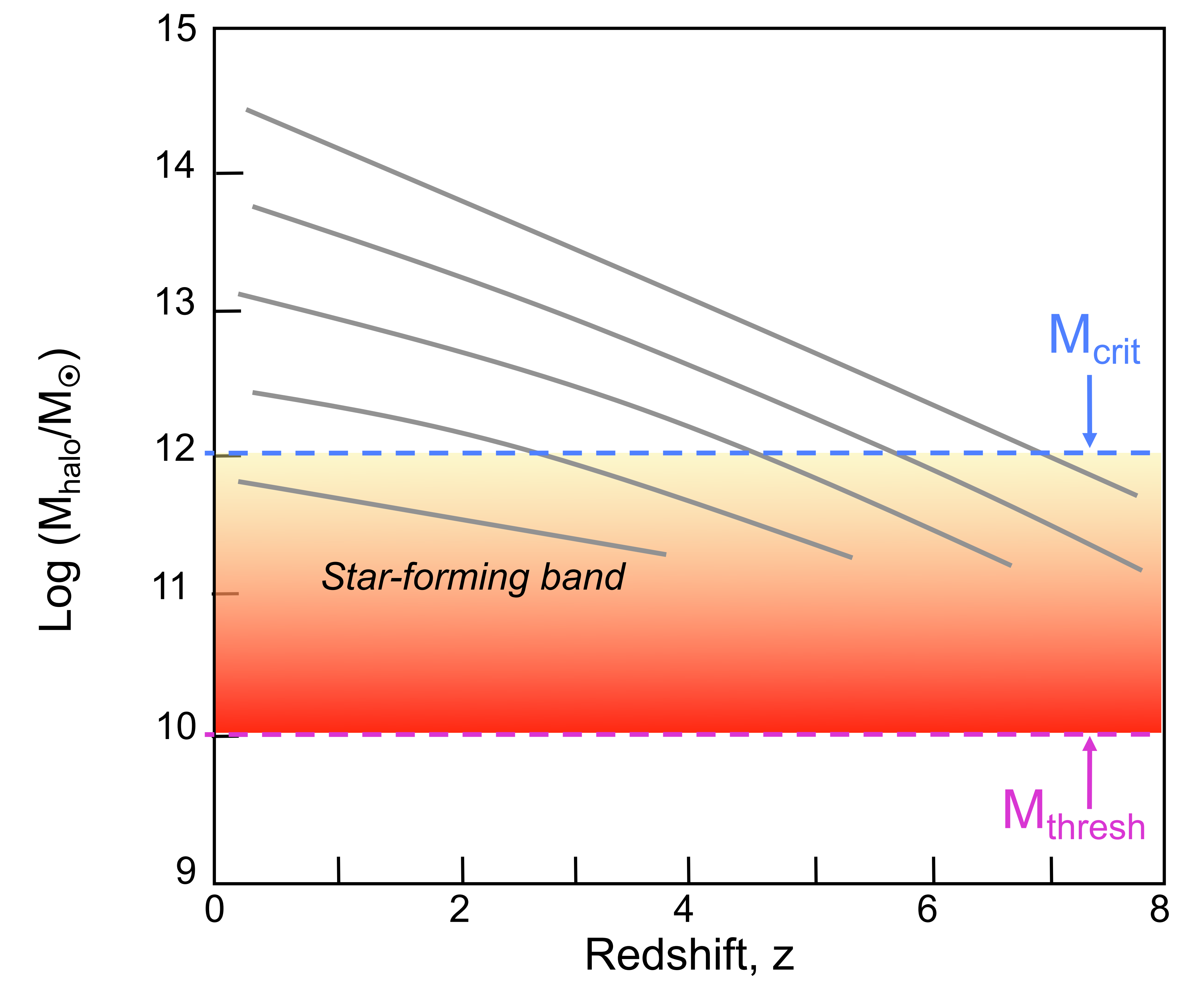

Key assumption: ***star-forming band*** in dark-halo mass

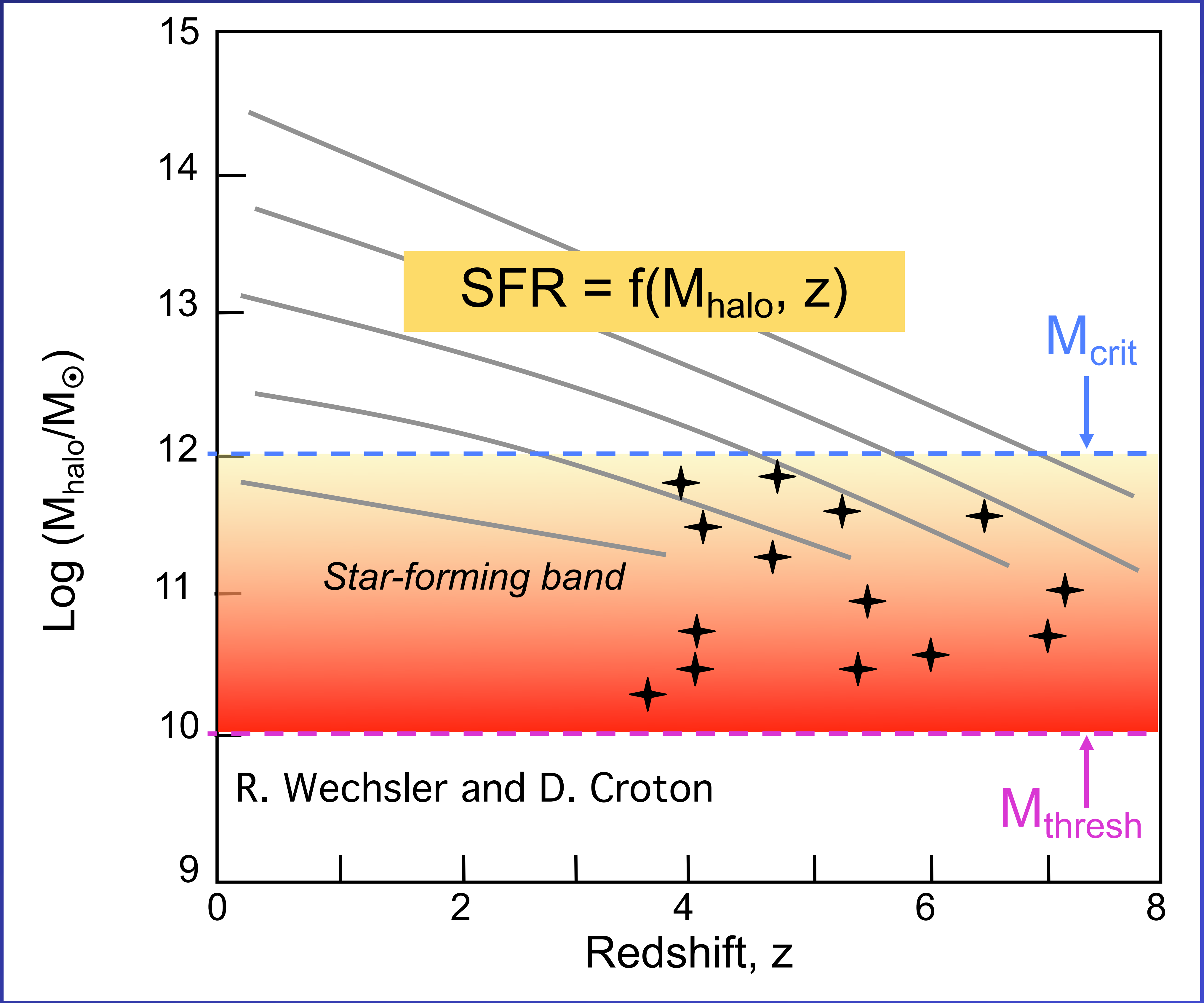

Implications and Predictions of the Model

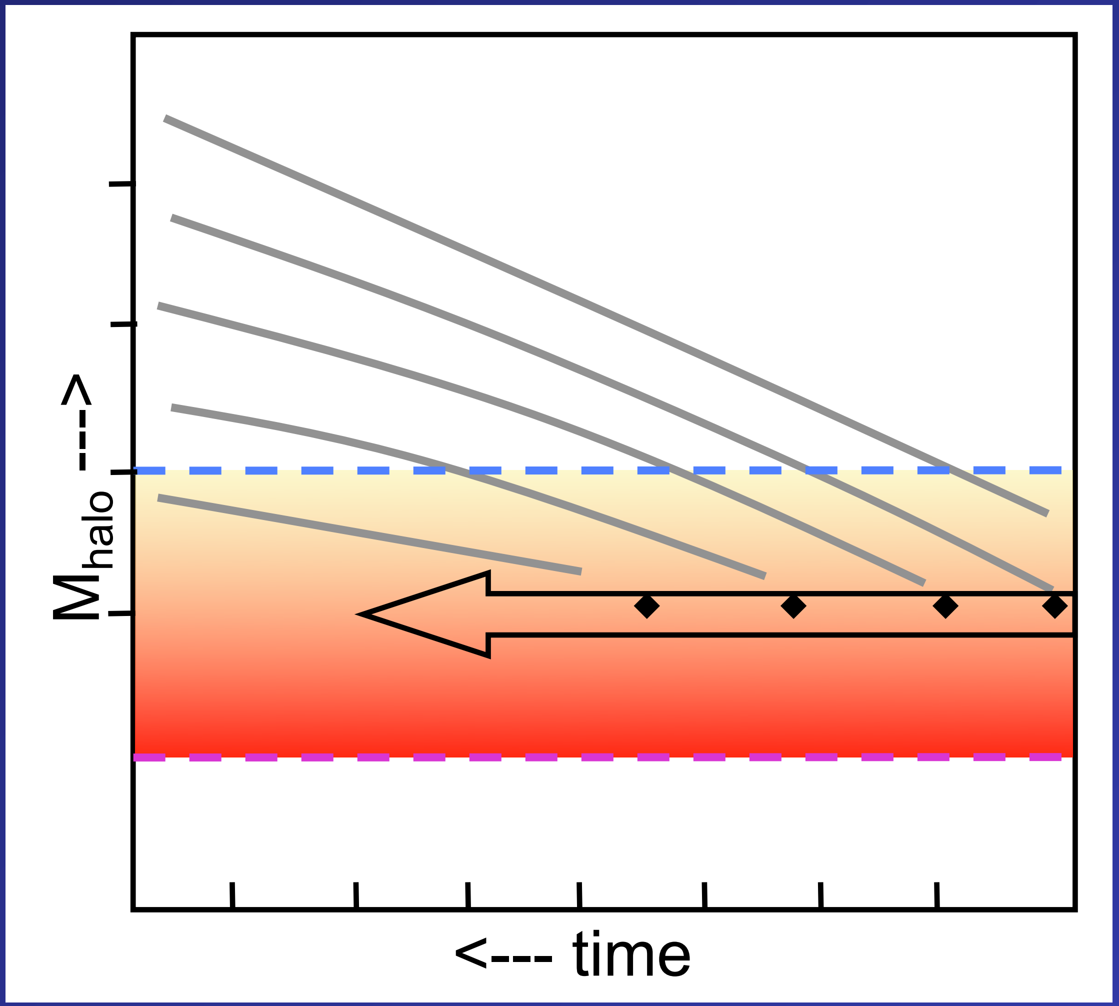

1) Each halo has a unique dark-matter growth path and associated stellar mass growth path.

2) Stellar mass follows halo mass until M_{halo} crosses M_{crit}.

SAMs: $M_{star} < 0.05\ M_{halo}$

3) A ***mass sequence*** comes from the fact that different halo masses enter the star-forming band at different times. A galaxy's position is determined by its ***entry redshift*** into the band. More massive galaxies enter earlier. Thus:

z_{entry} <--> M_{halo} <--> M_{star}

Implications and Predictions of the Model

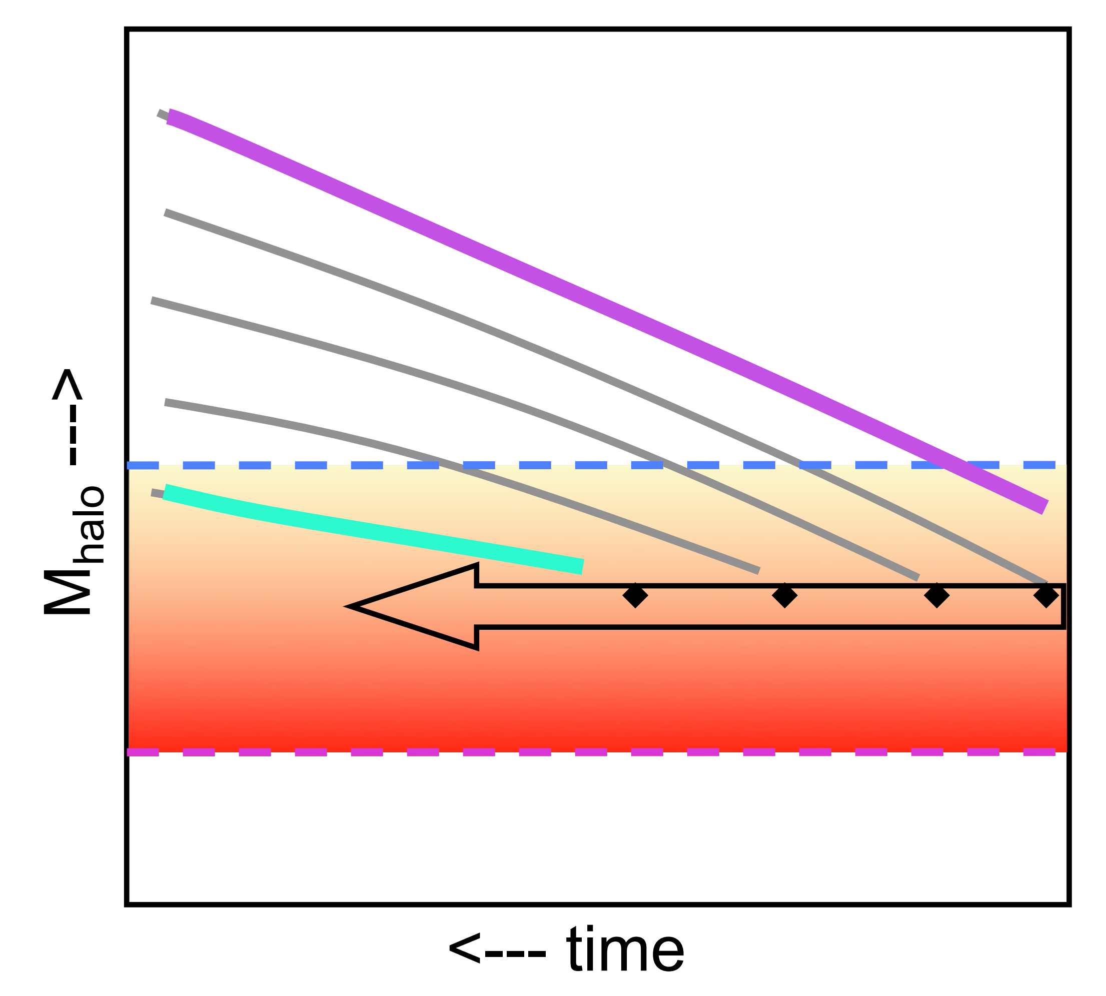

Massive galaxies:

- Started forming stars early.
- Shut down early.
- Are red today.
- Populate dark halos that are much more massive than their stellar mass.

Small galaxies:

- Started forming stars late.
- Are still making stars today.
- Are blue today.
- Populate dark halos that match their stellar mass.

"Downsizing"

Star formation is a wave that started in the largest galaxies and swept down to smaller masses later (Cowie et al. 1996).

Theories for the ***lower*** halo star-formation boundary

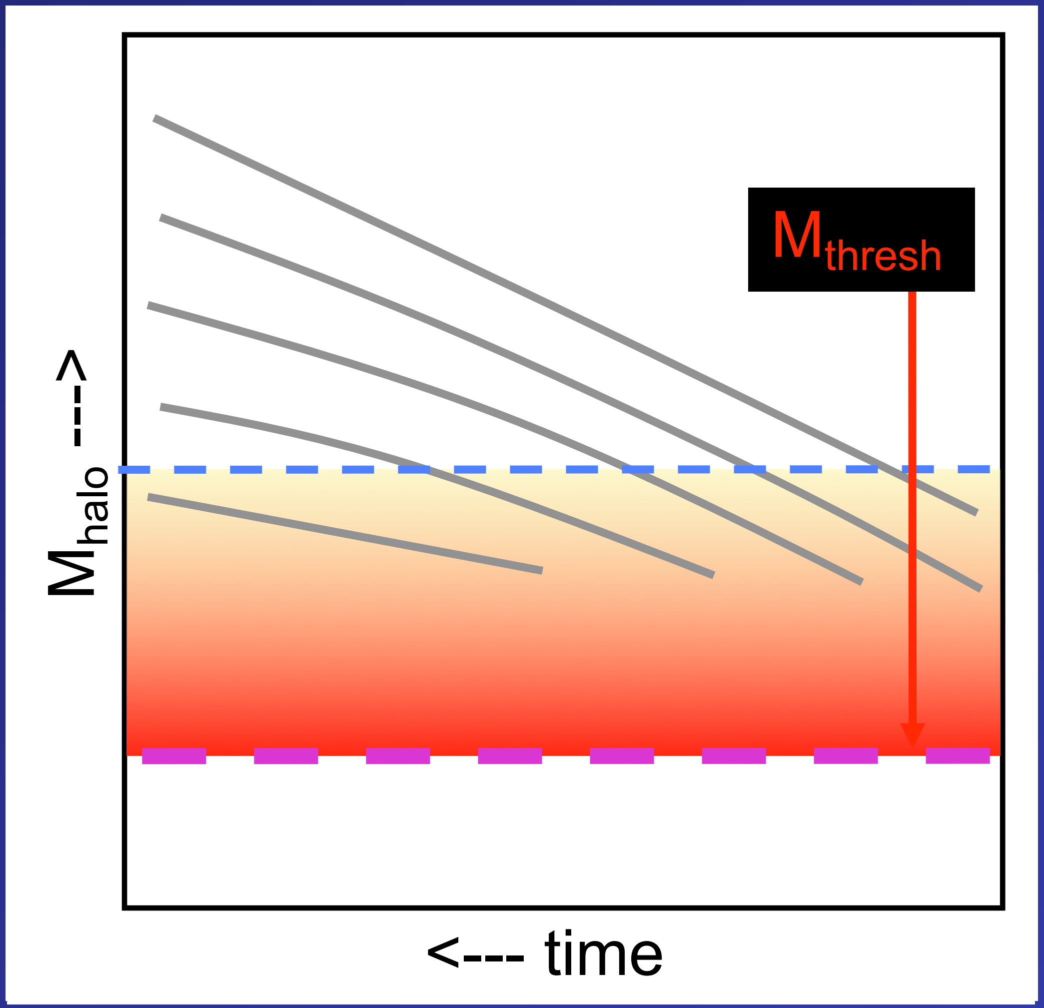

M_{thresh} is the halo mass at the LOWER edge of the star-formation band, roughly 10^{10} $M_{\odot}$.

Not yet well understood

1. Supernova feedback (Dekel & Silk 1985):

   $v_{lim} < 100$ km/sec

2. Early Universe reionization (e.g., Somerville 2002):

   $v_{lim} < 30$ km/sec

3. Plus tidal destruction!

Theories for the ***upper*** halo star-formation boundary

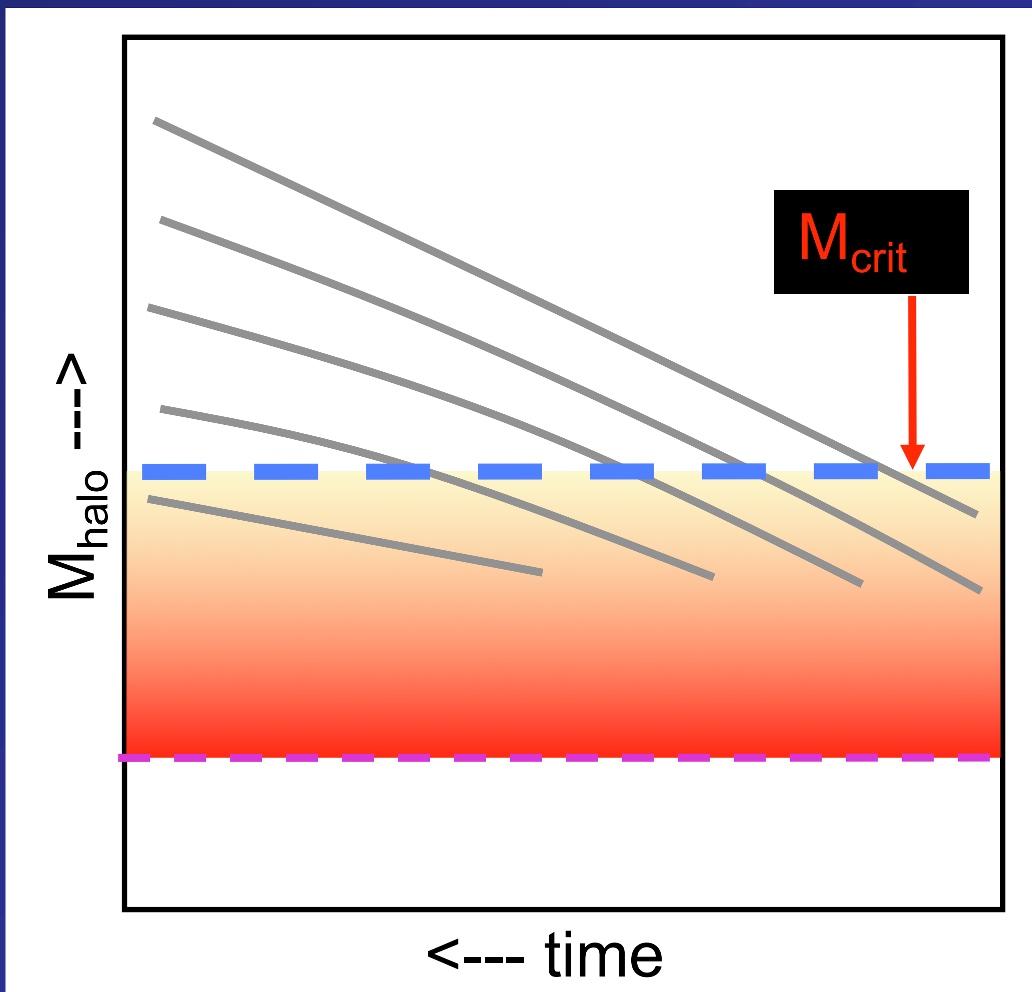

M_{crit} is the halo mass at the UPPER edge of the star-formation band, roughly $10^{12}\ M_{¤}$.

1 Gas in halos above the critical halo mass $M_{crit} \sim 10^{12}\ M_{\odot}$ cannot cool (Ostriker & Rees 1978, Blumenthal et al. 1984, Dekel & Birnboim 2007).

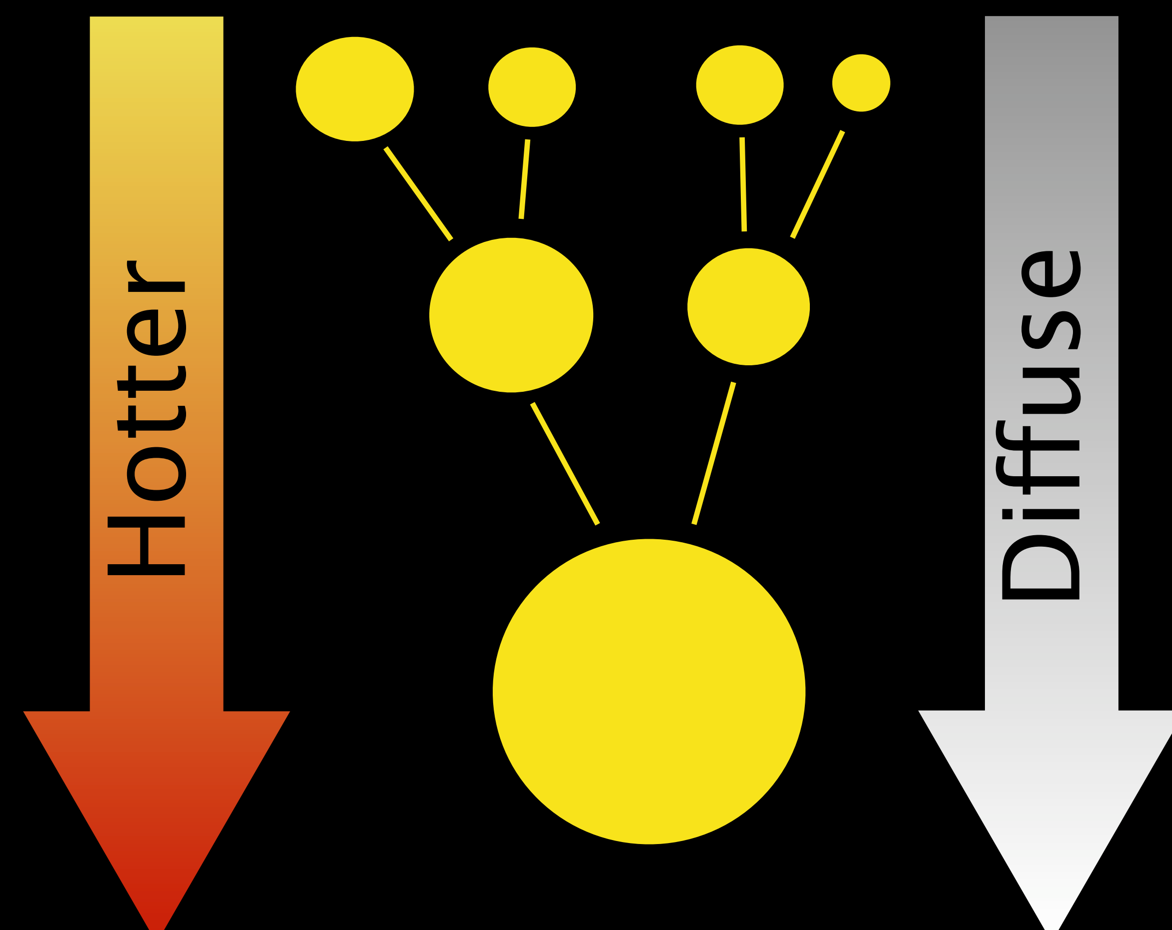

More realistic model of halo-cooling boundary

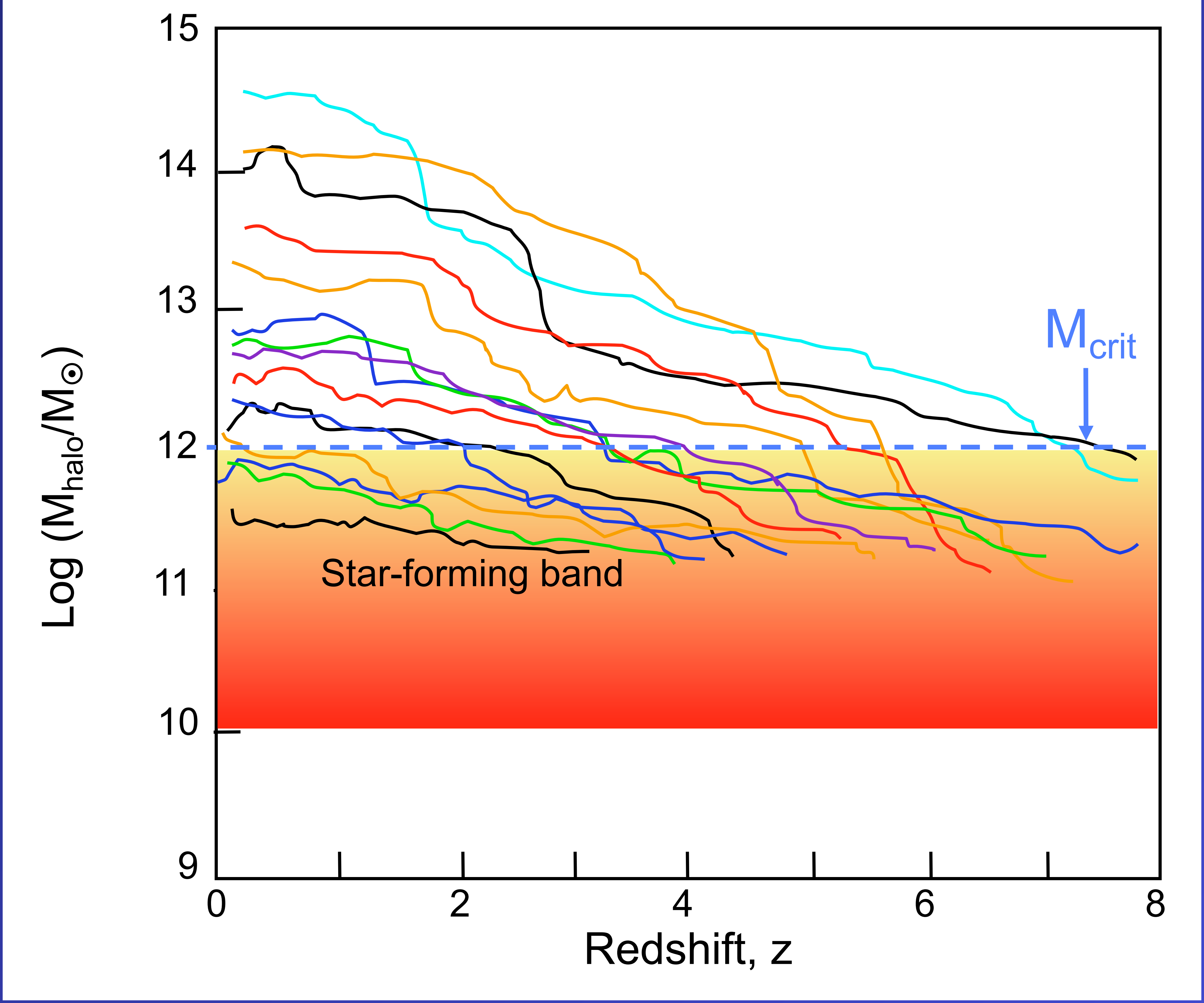

More realistic model of halo-cooling boundary

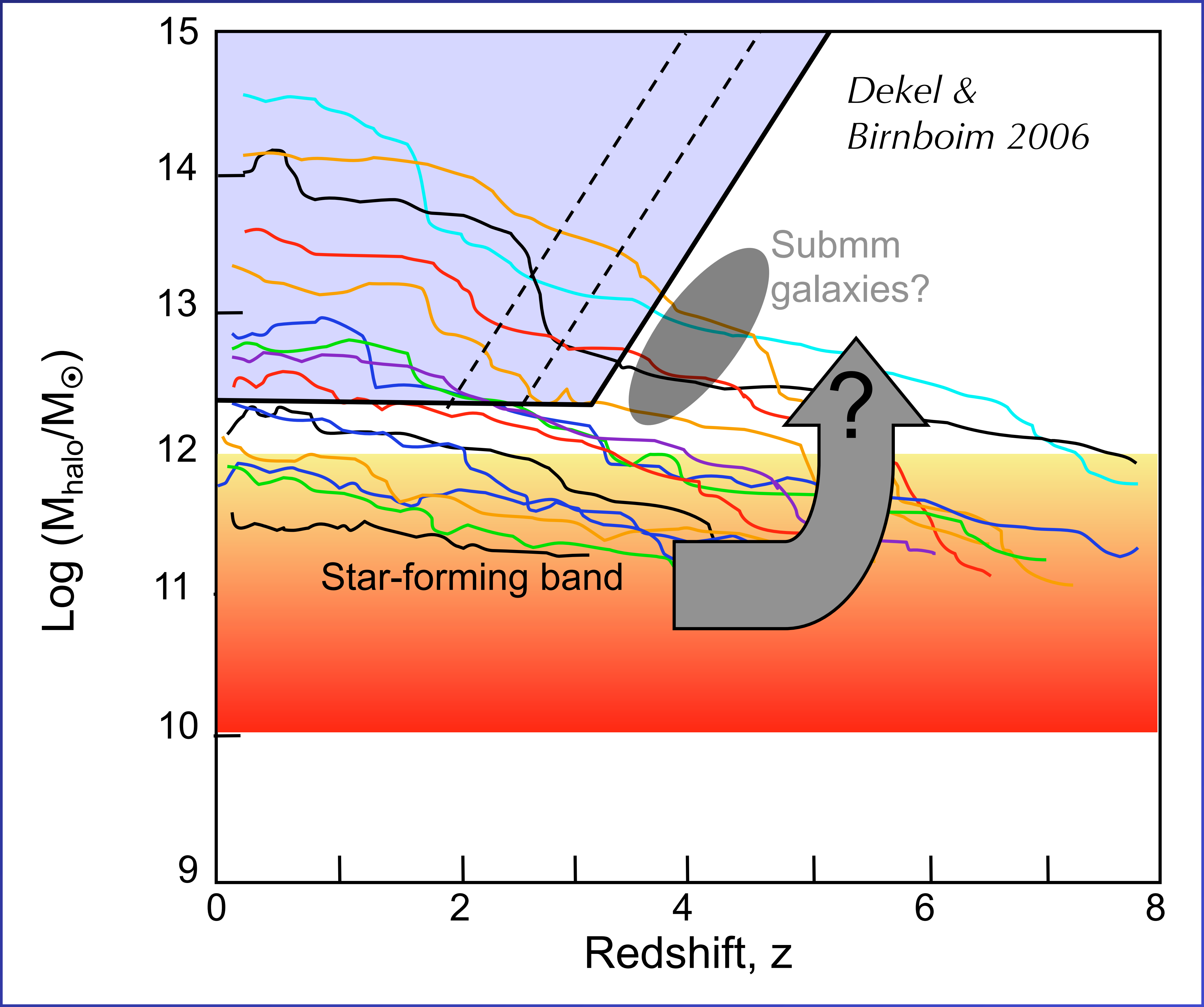

Theories for the ***upper*** halo star-formation boundary

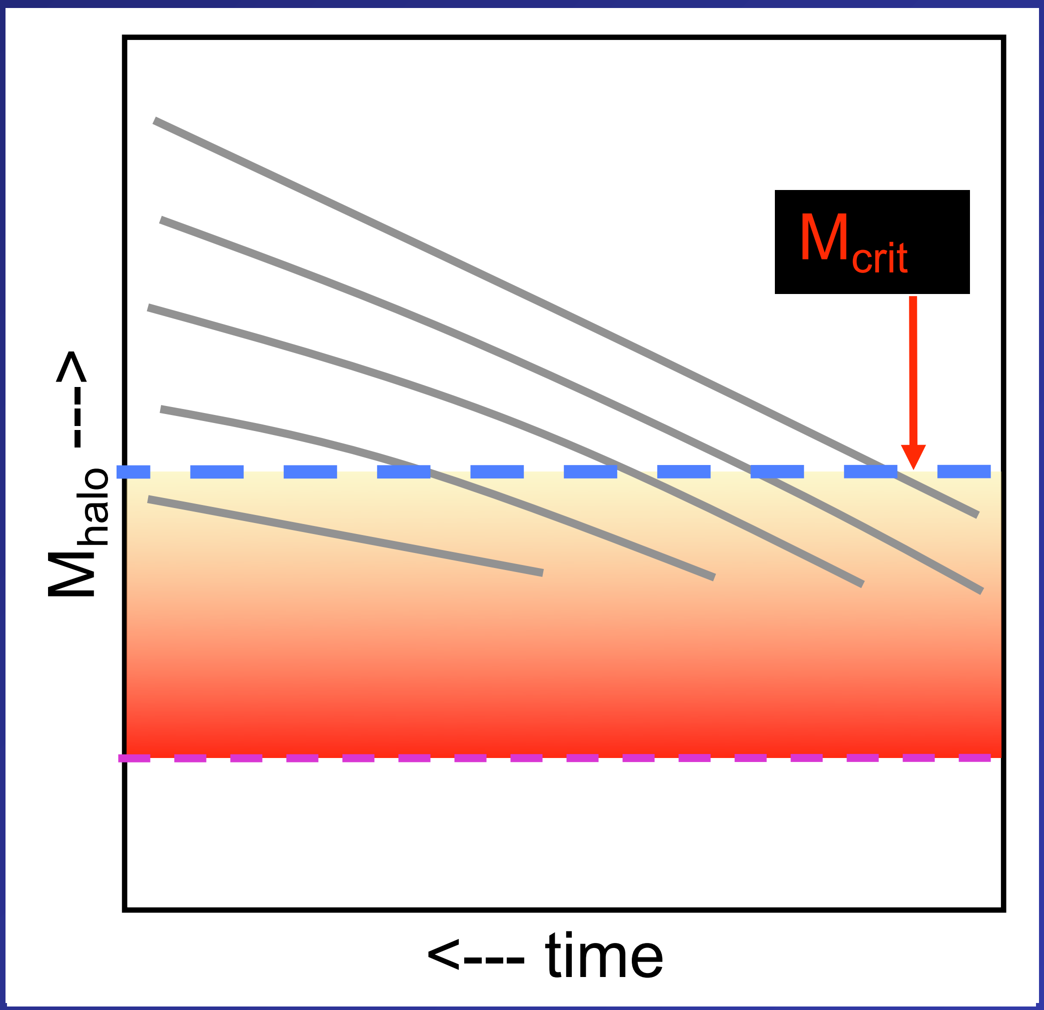

M_{crit} is the halo mass at the UPPER edge of the star-formation band, roughly 10^{12} $M_{\odot}$.

2 Merging galaxies trigger BH growth. AGN feedback drives out galaxy gas (Hopkins et al 2006).

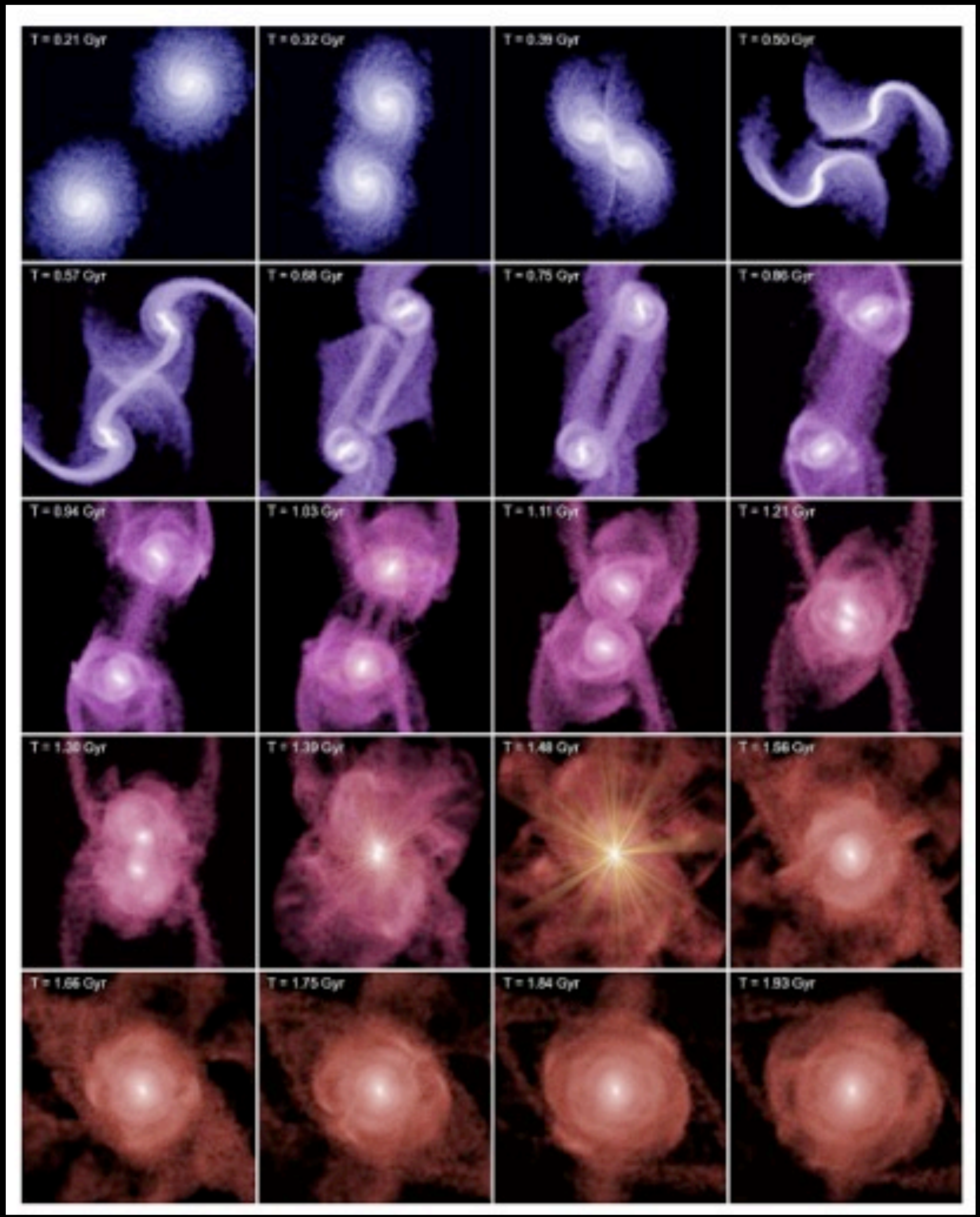

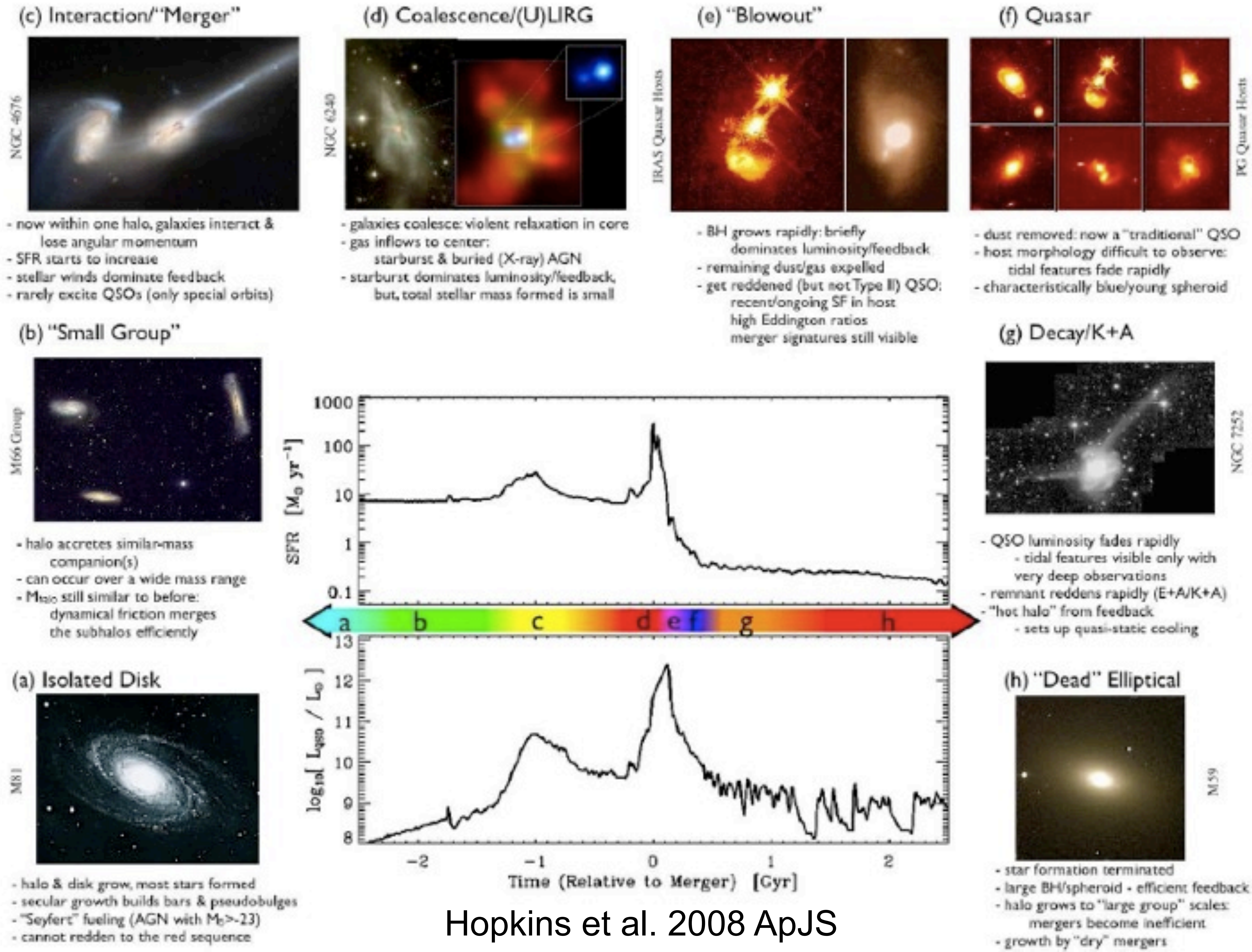

Hopkins et al. 2008 ApJS

Why AGN Feedback Can Make Massive Galaxies Red/Dead

- Need mechanism to
  - quench star formation in massive galaxies
  - stop cooling in clusters
- SN feedback inadequate: not enough energy, little star formation in red galaxies
- BH mass closely connected with host galaxy's spheroid mass
- Bigger BH ⇒ more energy
  ($L_{max} \sim L_{Edd} \sim M_{BH}$)

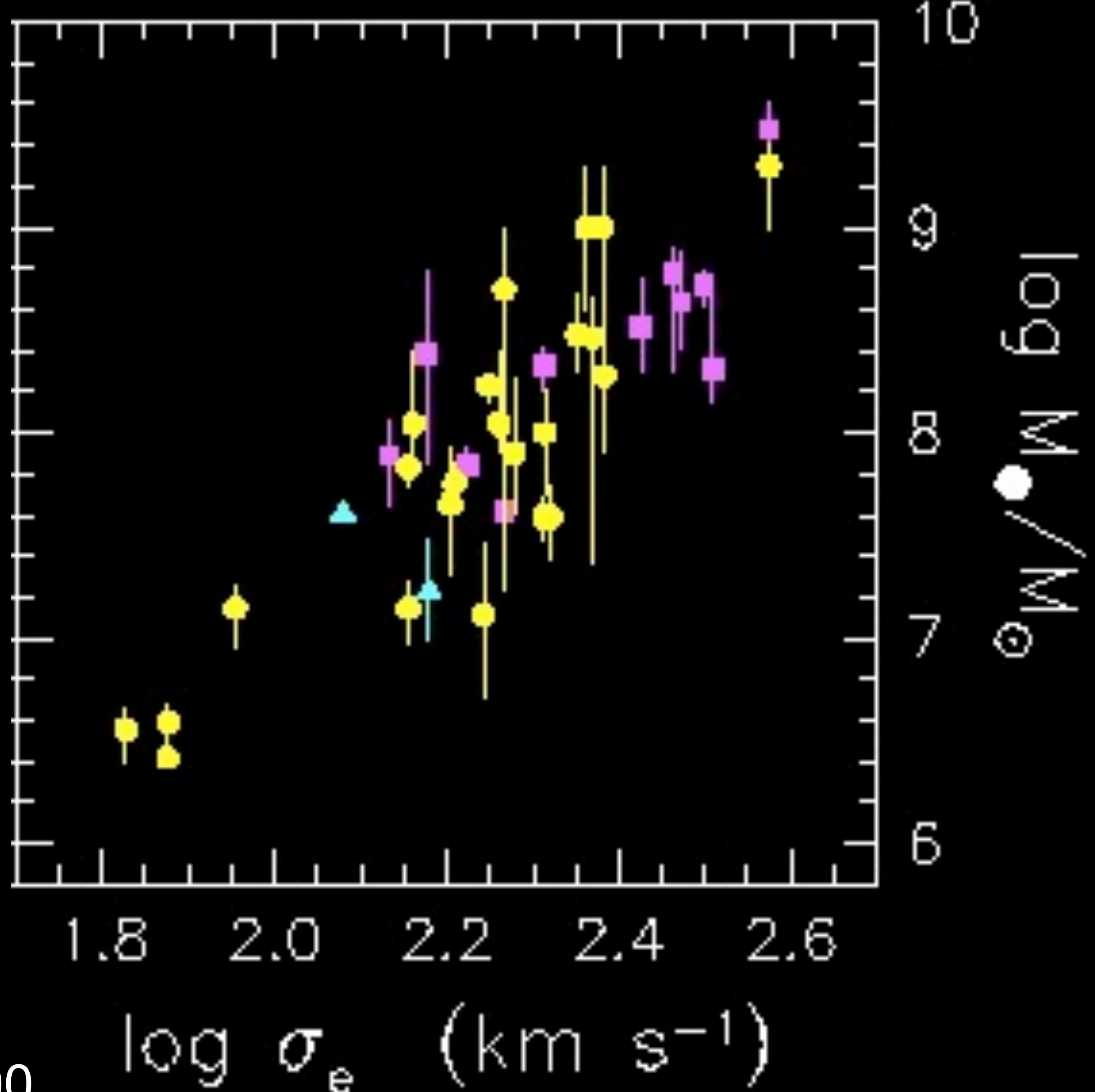

Magorrian et al. 1998;
Gebhardt et al. 2000,
Ferrarese & Merritt 2000

The challenge of simulating BH growth and AGN FB in a cosmological context

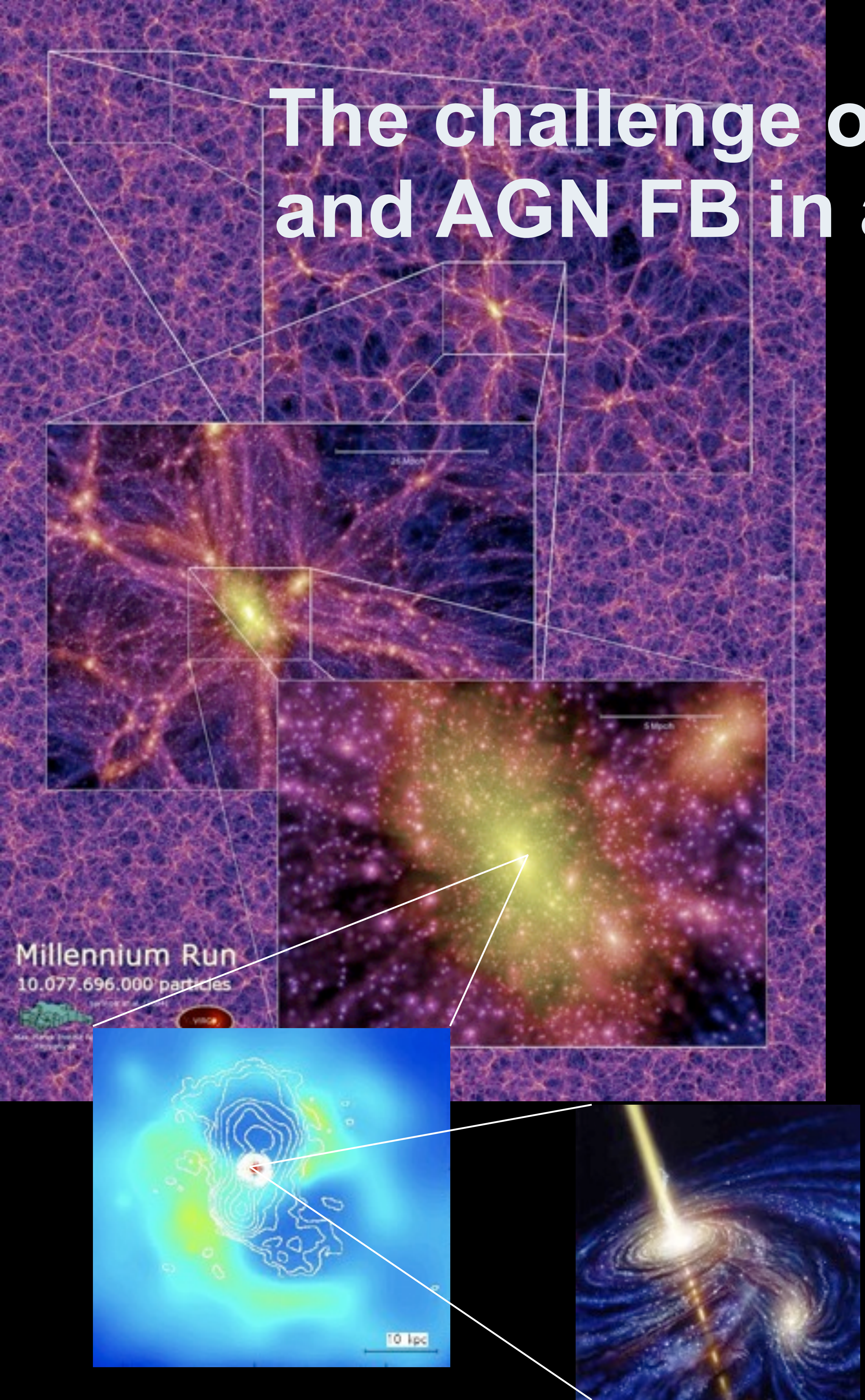

- dynamic range:
  - Gpc (luminous QSO)
  - few 100 Mpc (LSS)
  - 10’s of kpc (ICM, jets)
  - sub-kpc (star formation, stellar FB)
  - few 100 pc (nuclear gas inflows, starbursts, AGN feeding, winds)
  - pc & sub-pc (accretion disk, BH mergers, etc)
- poorly understood physics (B-fields, conduction, cosmic ray pressure, turbulence, feeding problem, ...)

AGN feedback 1: bright mode

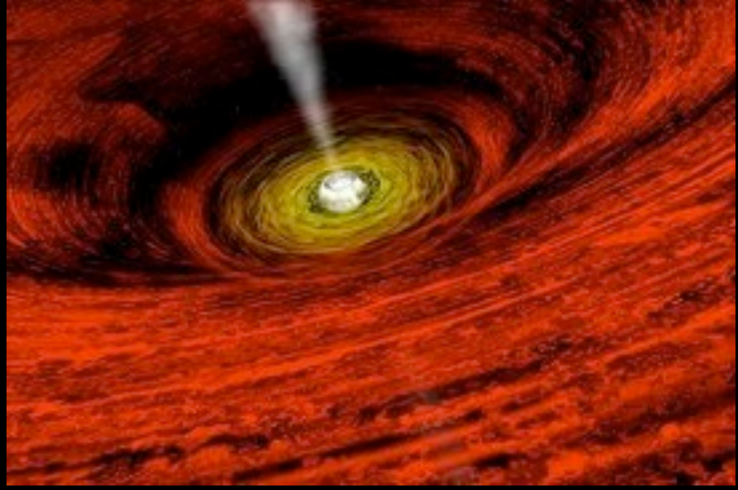

- optical/X-ray luminous AGN/QSO, produced during periods of efficient feeding (mergers?)
- high accretion rates (0.1-1 L_{Edd}), fueled by cold gas via thin accretion disk --> BH grows rapidly
- rare-->duty cycle short
- thermal coupling of AGN energy with ISM is probably fairly weak (<5%)

Di Matteo, Springel & Hernquist 2005

Hydrodynamic simulations of galaxy mergers including black hole growth and feedback

- self-regulated BH growth, reproducing M_{BH}-σ relation (di Matteo et al. 2004)
- AGN-driven wind removes residual cold gas at the end of the merger, leading to lower SFR and redder colors in the spheroidal remnant (Springel et al. 2004)

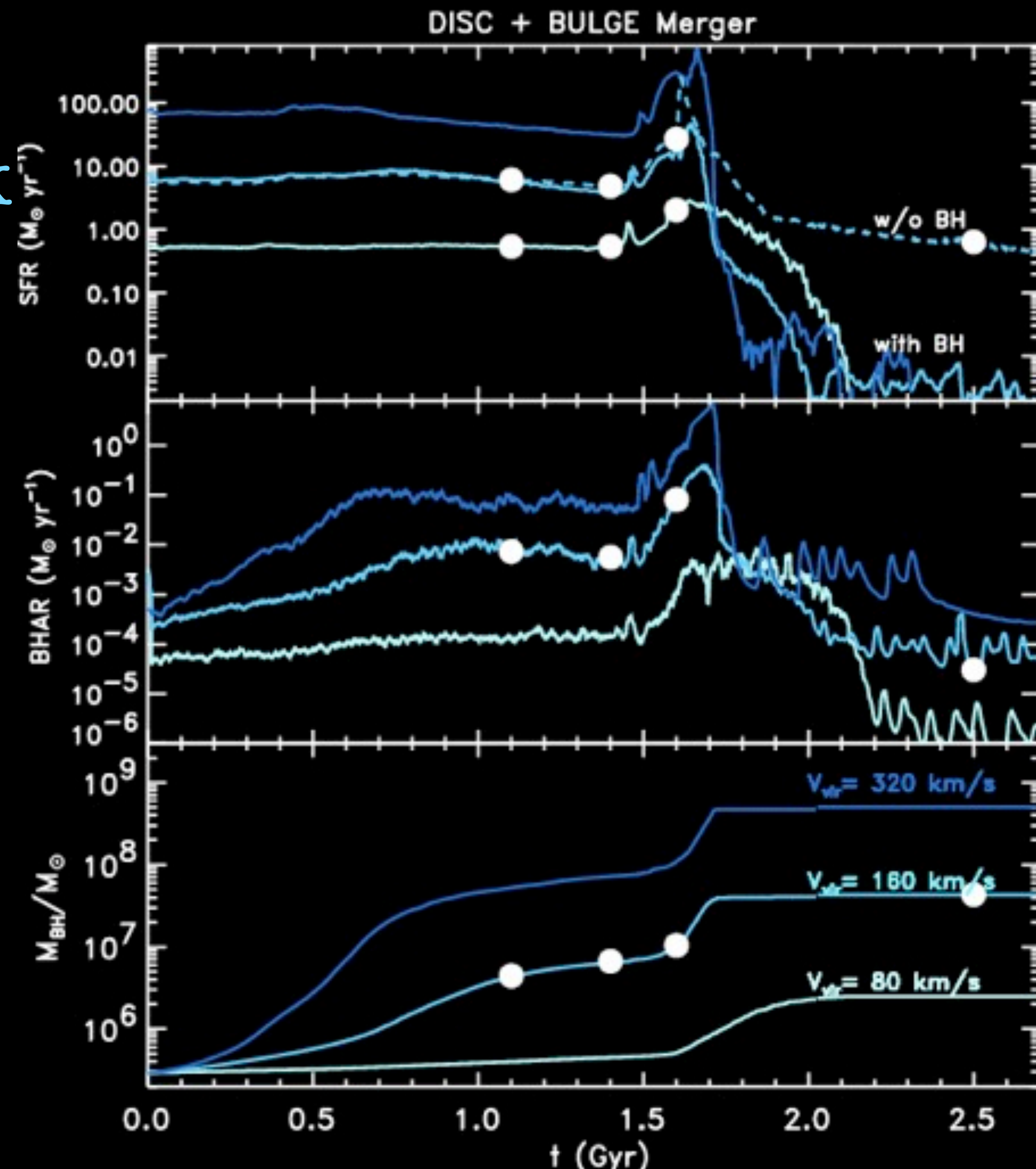

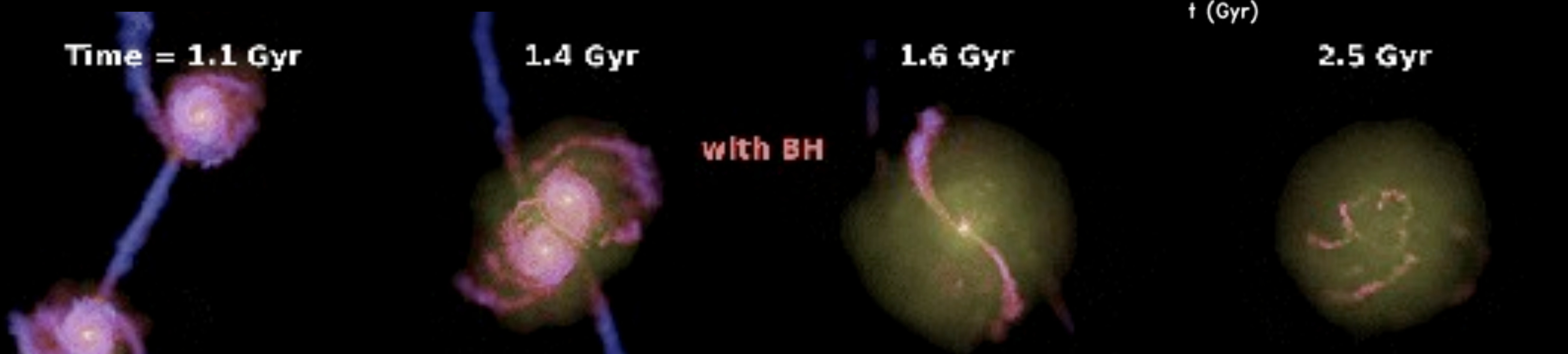

di Matteo, Springel & Hernquist 2005; Hopkins et al. 2006-

Color-Magnitude Diagram of EGS X-ray selected AGN

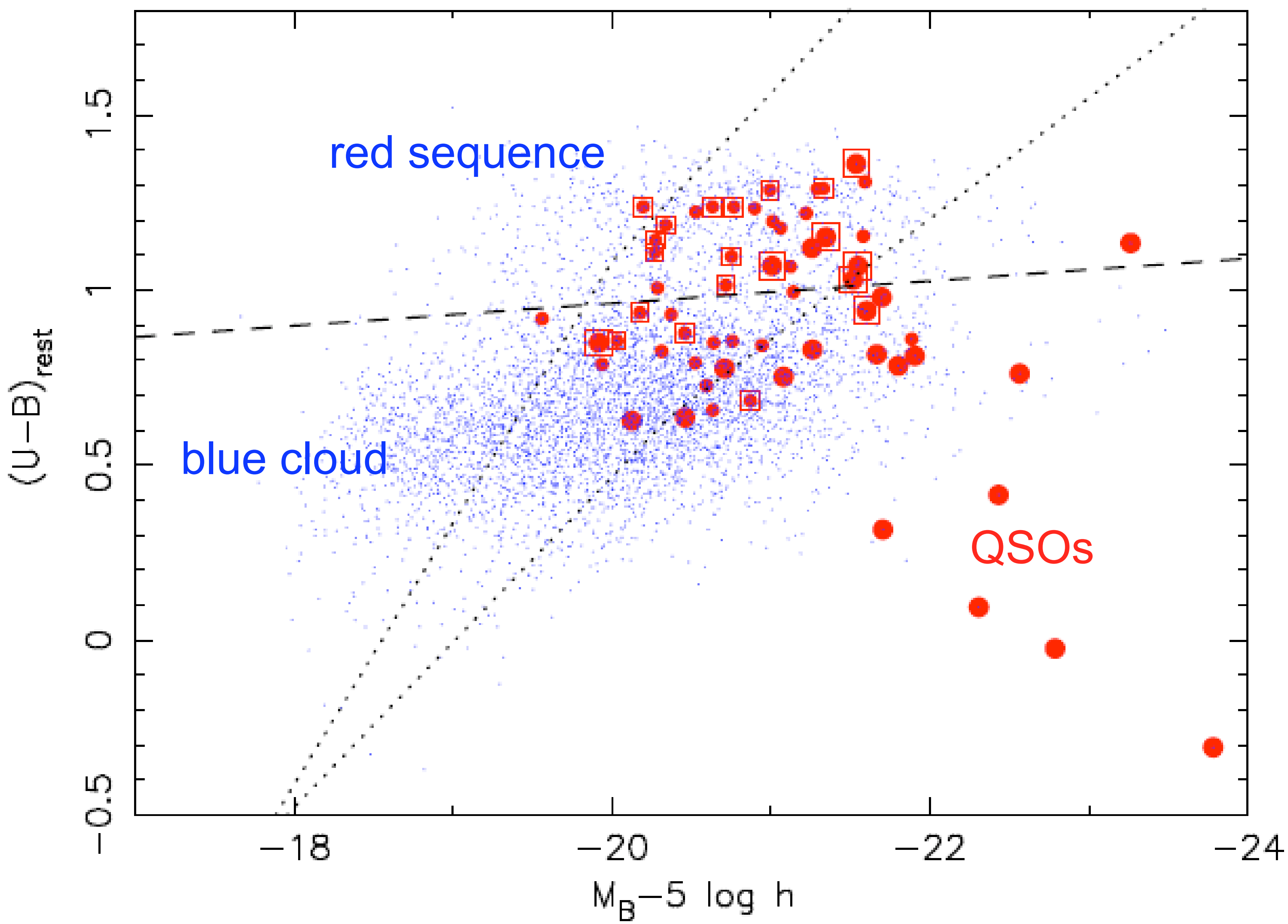

Rest-frame U-B colour is plotted against the B-band absolute magnitude for DEEP2 comparison galaxies (small blue dots) and X-ray sources (filled red circles) in the EGS in the range $0.7 < z < 1.4$. Squares around the symbols indicate hard X-ray sources, and more luminous systems ($L_X > 10^{43}$ erg s^{-1}) are plotted with larger symbols. The dashed line separates red and blue galaxies, and the dotted lines show the DEEP2 completeness limits at $z = 1.0$ and $z = 1.4$. (Nandra et al., ApJ Letters, 2007.)

Morphological distribution of EGS X-ray selected AGN

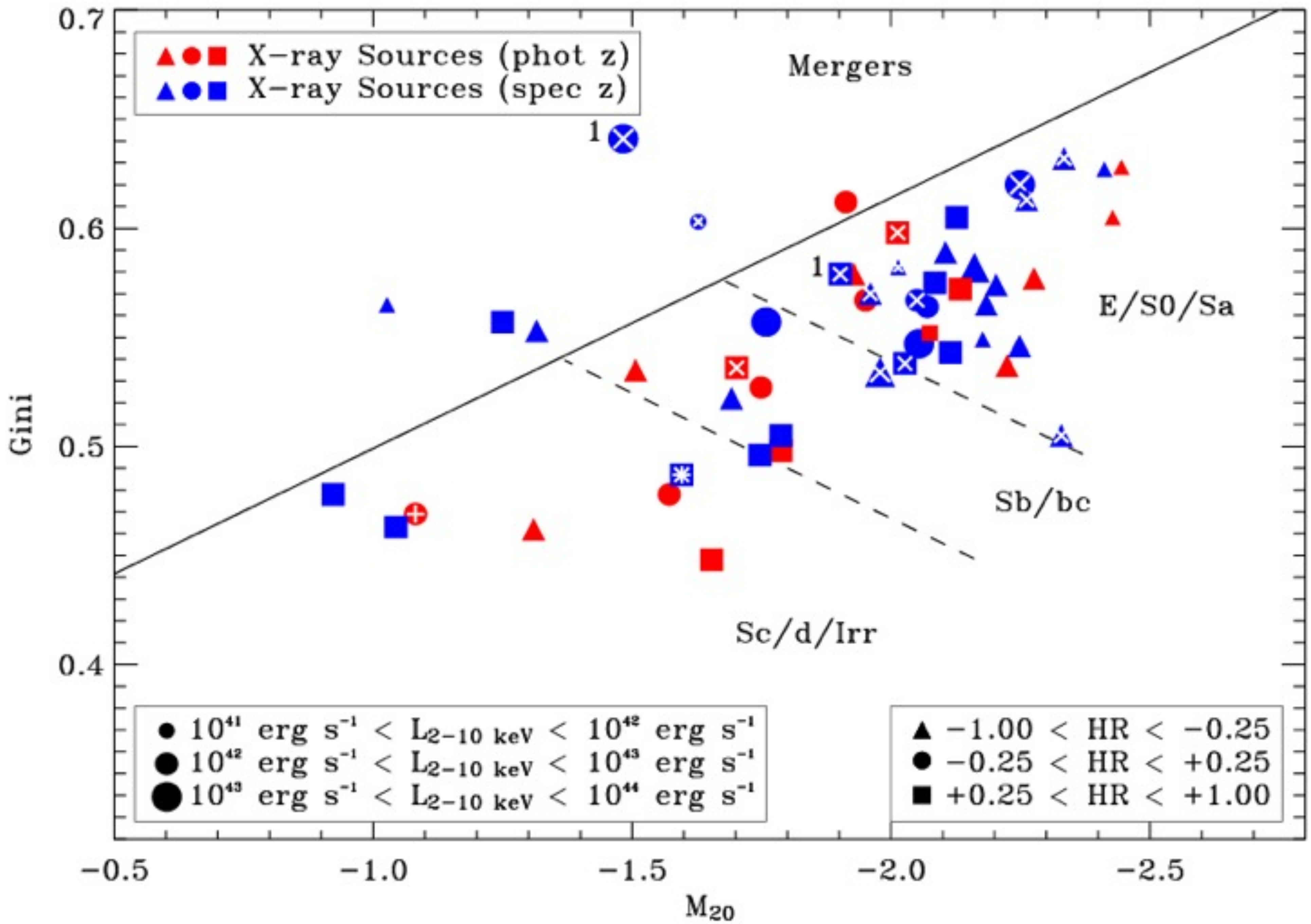

The highest fraction of EGS galaxies hosting AGN are early-types, not mergers. This suggests that the AGN activity is delayed, rather than occurring mainly during and immediately following mergers as the Hopkins et al. simulations predicted. (Christy Pierce et al., ApJ Letters, May 2007).

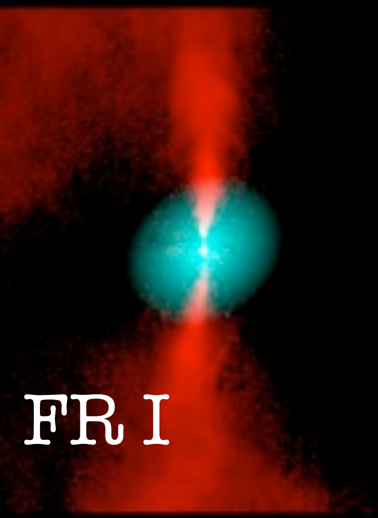

AGN feedback 2: Radio Mode

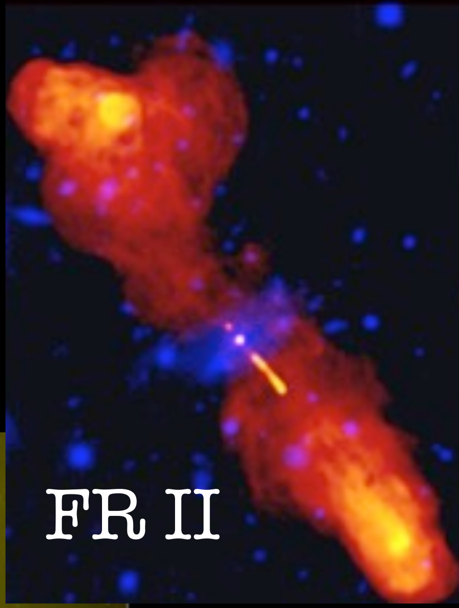

- some massive galaxies are ‘radio loud’
- radio activity believed to be associated with BH’s in ‘low accretion state’ (low Eddington ratio, $<10^{-3}$)
- jets often associated with cavities visible in X-ray images
- coupling of jet energy with hot gas very efficient

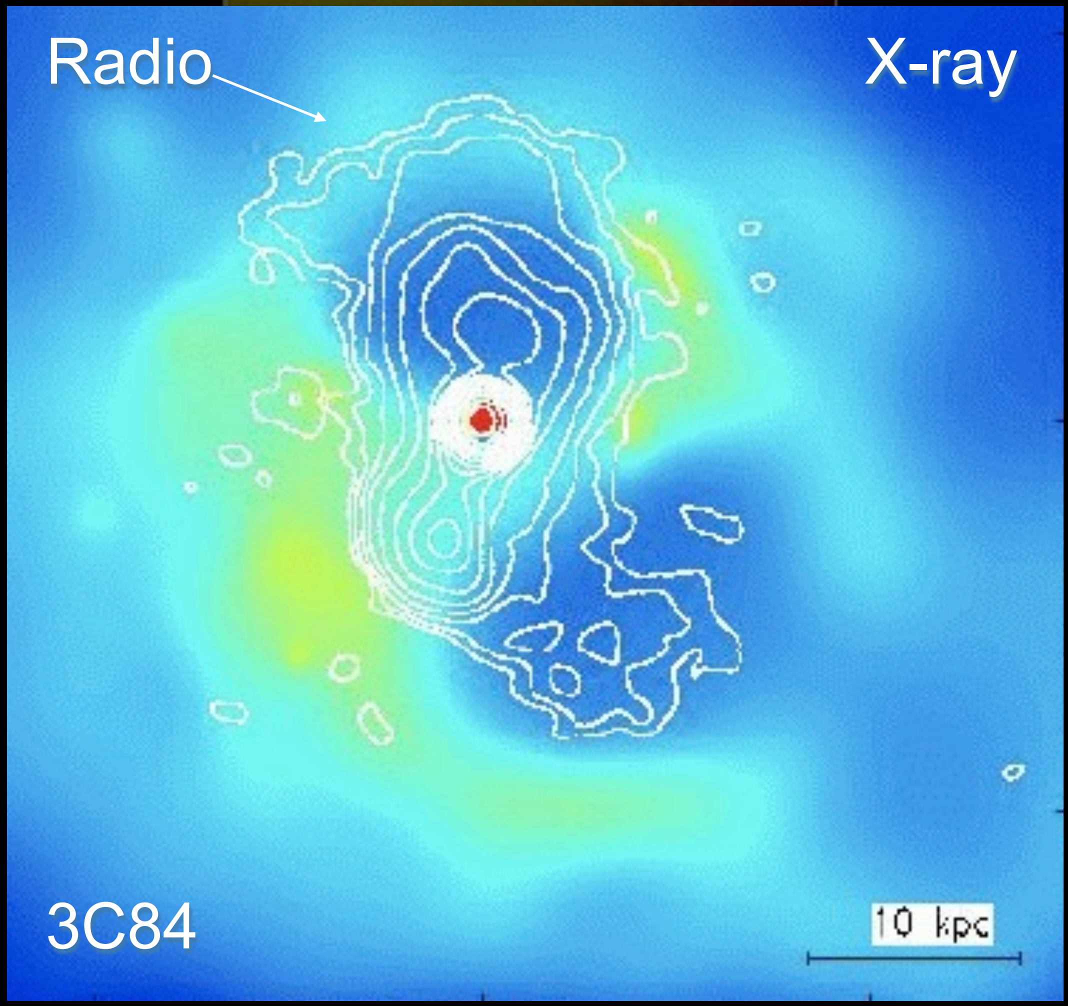

NEW Self-Consistent Model for the Co-Evolution of Galaxies, Black Holes, and AGN

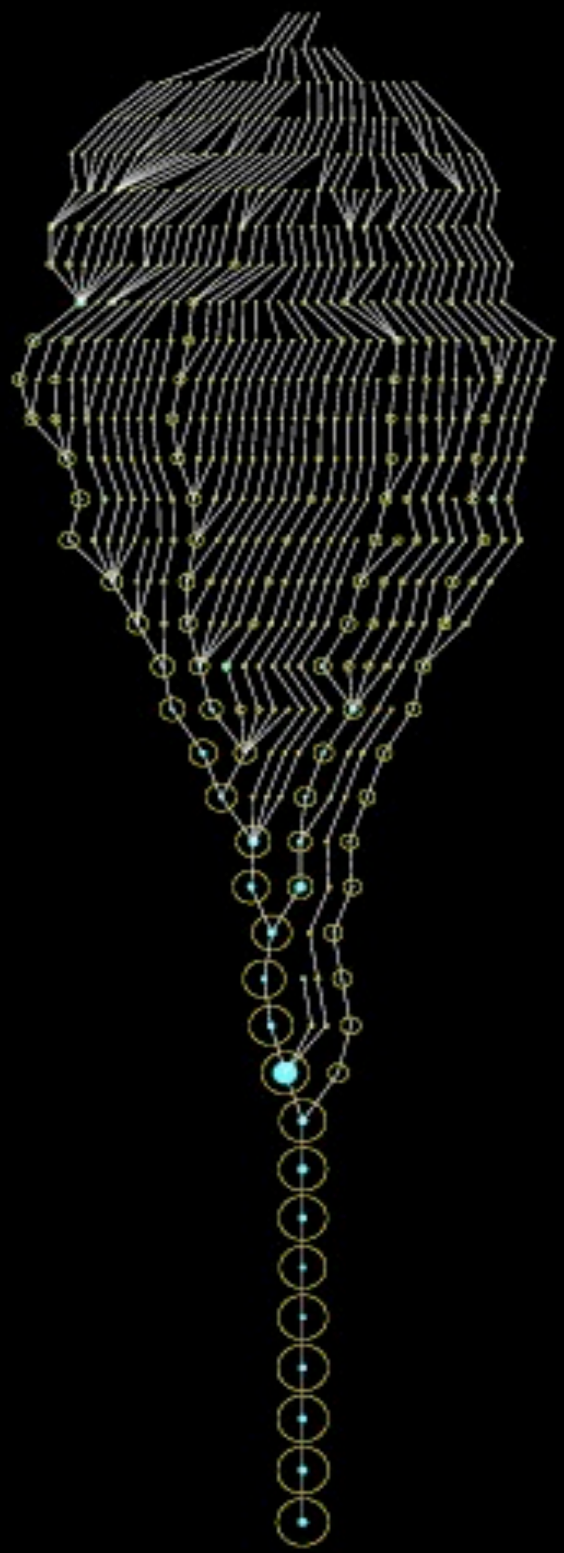

- Top-level halos start with a ~100 M_{sun} seed BH
- Mergers trigger bursts of star formation and accretion onto BH; efficiency and timescale parameterized based on hydrodynamical merger simulations (μ, B/T, V_c, f_g, z; Cox et al., Robertson et al.)
- BH accrete at Eddington rate until they reach 'critical mass', then enter 'blowout' (power-law decline) phase

$$dm_{acc}/dt = \dot{m}_{Edd}/[1+(t/t_Q)^{\beta}]$$

- Energy released by accretion drives a wind
- BH merge when their galaxies merge; mass is conserved

Somerville, Hopkins, Cox, et al. 2008 MN

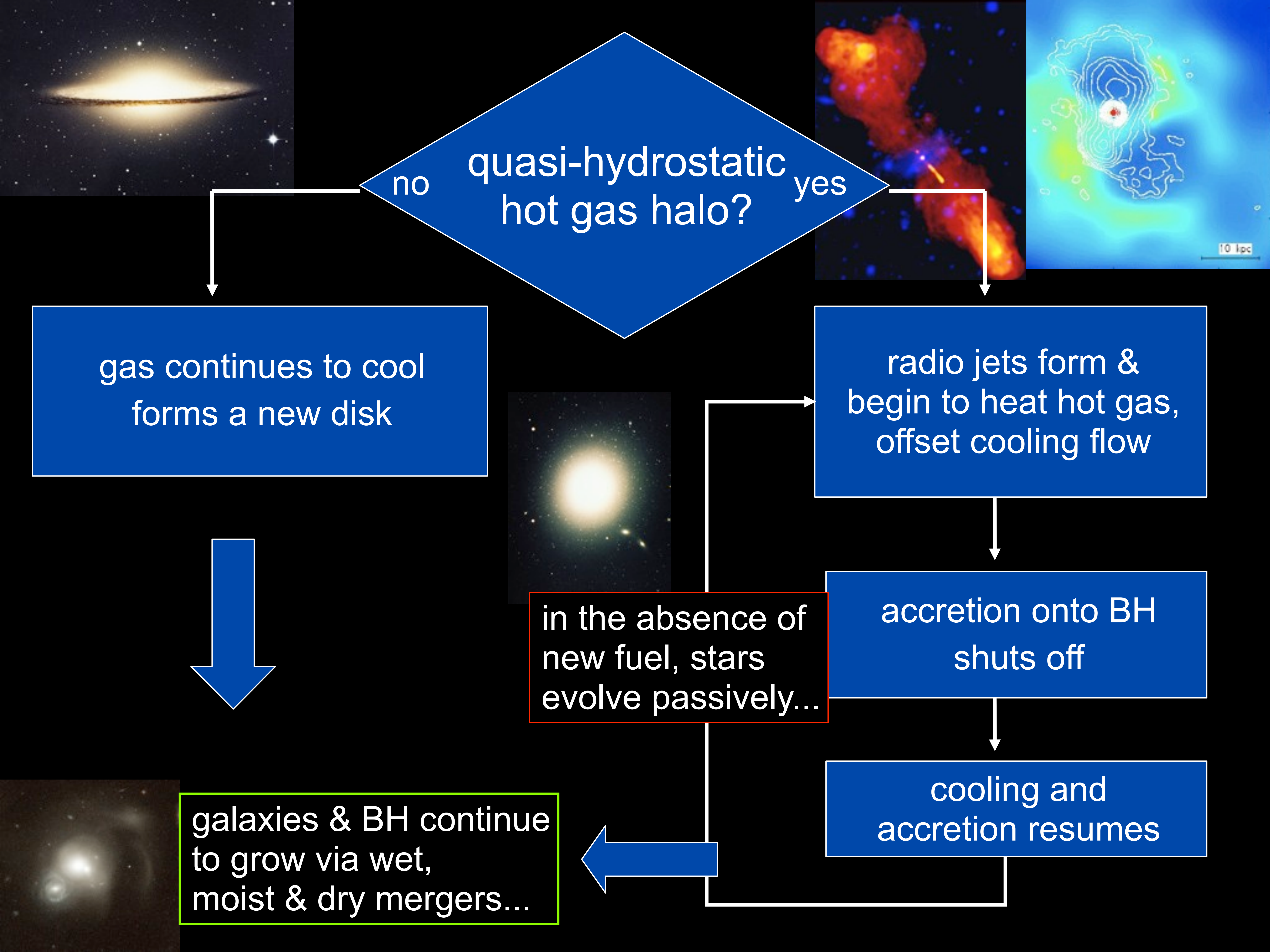
quasi-hydrostatic hot gas halo?
no
yes
10 kpc
gas continues to cool forms a new disk
radio jets form & begin to heat hot gas, offset cooling flow
accretion onto BH shuts off
cooling and accretion resumes
in the absence of new fuel, stars evolve passively...
galaxies & BH continue to grow via wet, moist & dry mergers...

Predicted M_{BH}-M_{bulge} relationship

in Somerville+08 model, arises from ‘bright mode’ feedback

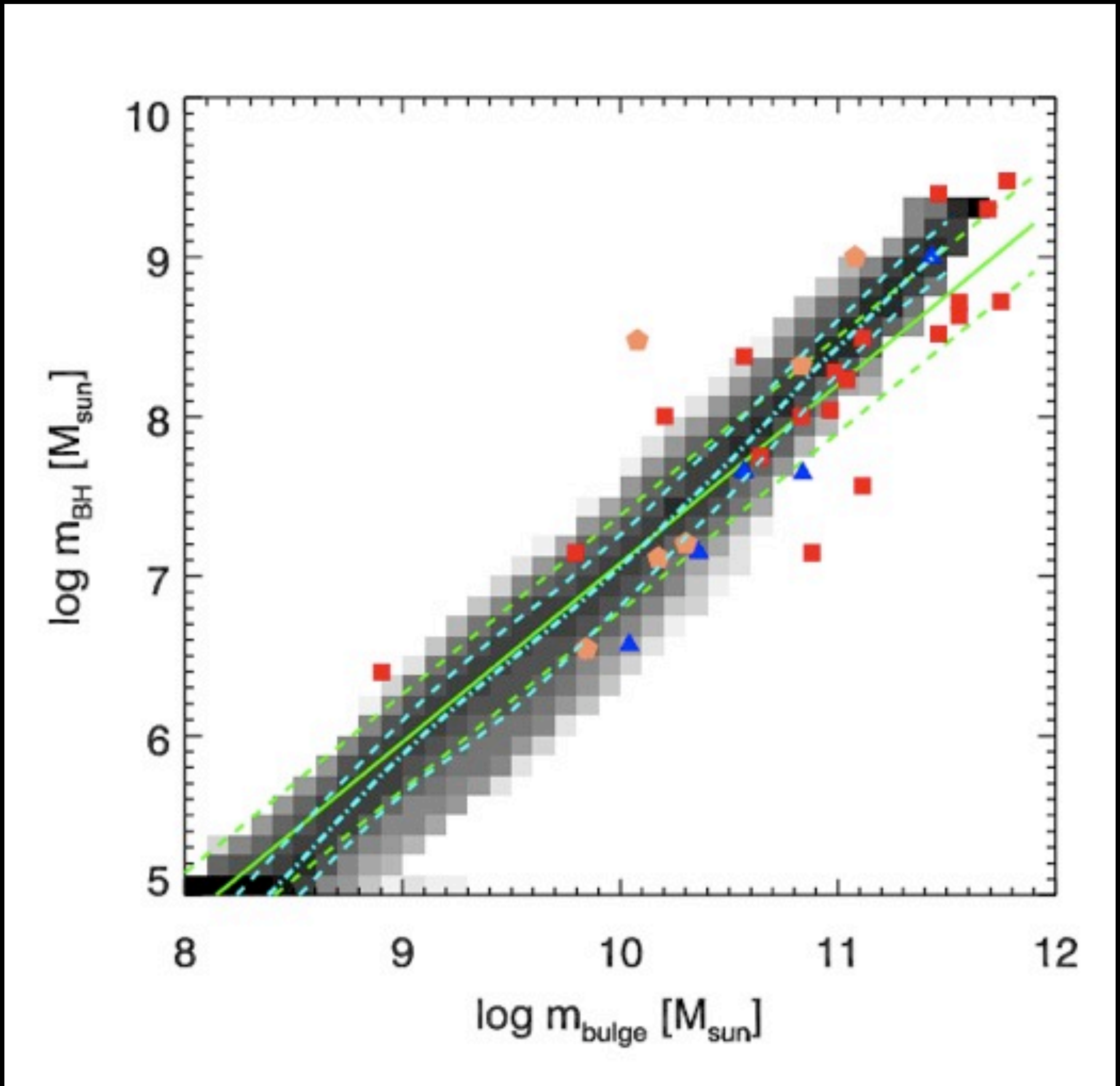

matches slope & scatter of observed relation

large symbols:
Haering & Rix data
green: H&R fit + scatter
intrinsic scatter: 0.3 dex

cyan: predicted median, 10th, & 90th percentile
predicted scatter:
~0.15 dex

Somerville et al. 2008

AGN Heating Leads to Galaxy Mass Functions at z~0 in Agreement with Observations

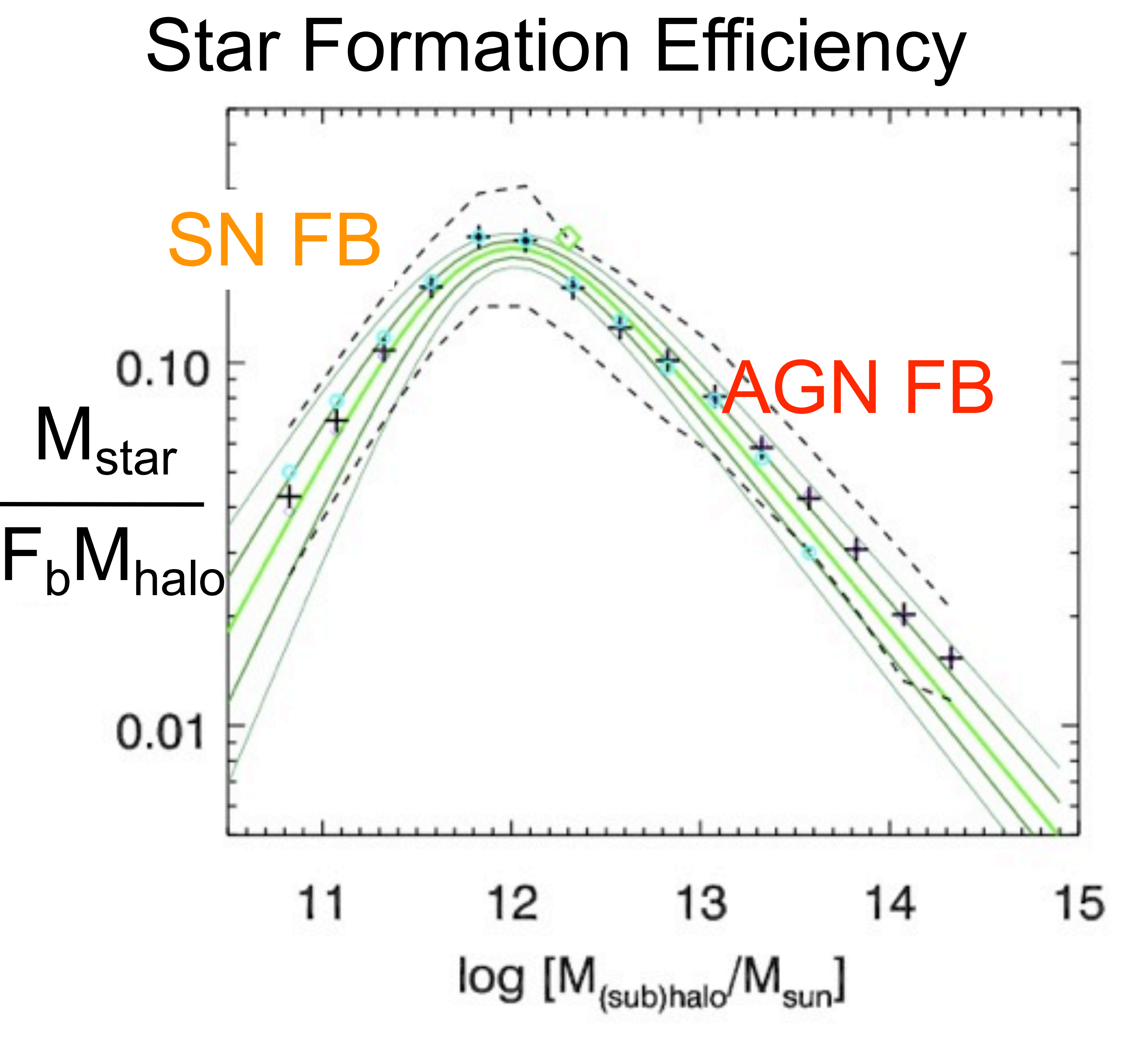

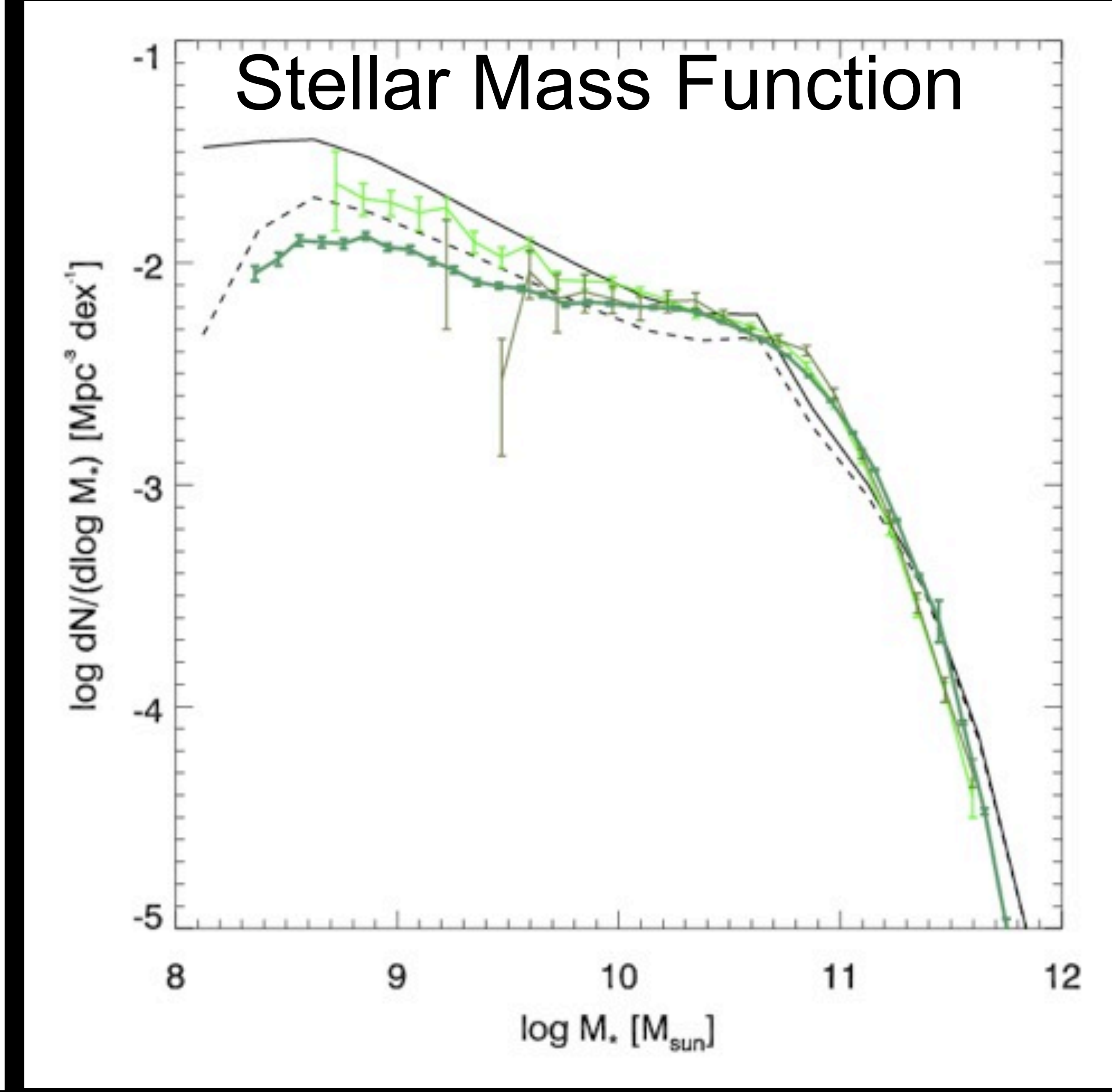

Somerville et al. 2008

Luminosity Functions

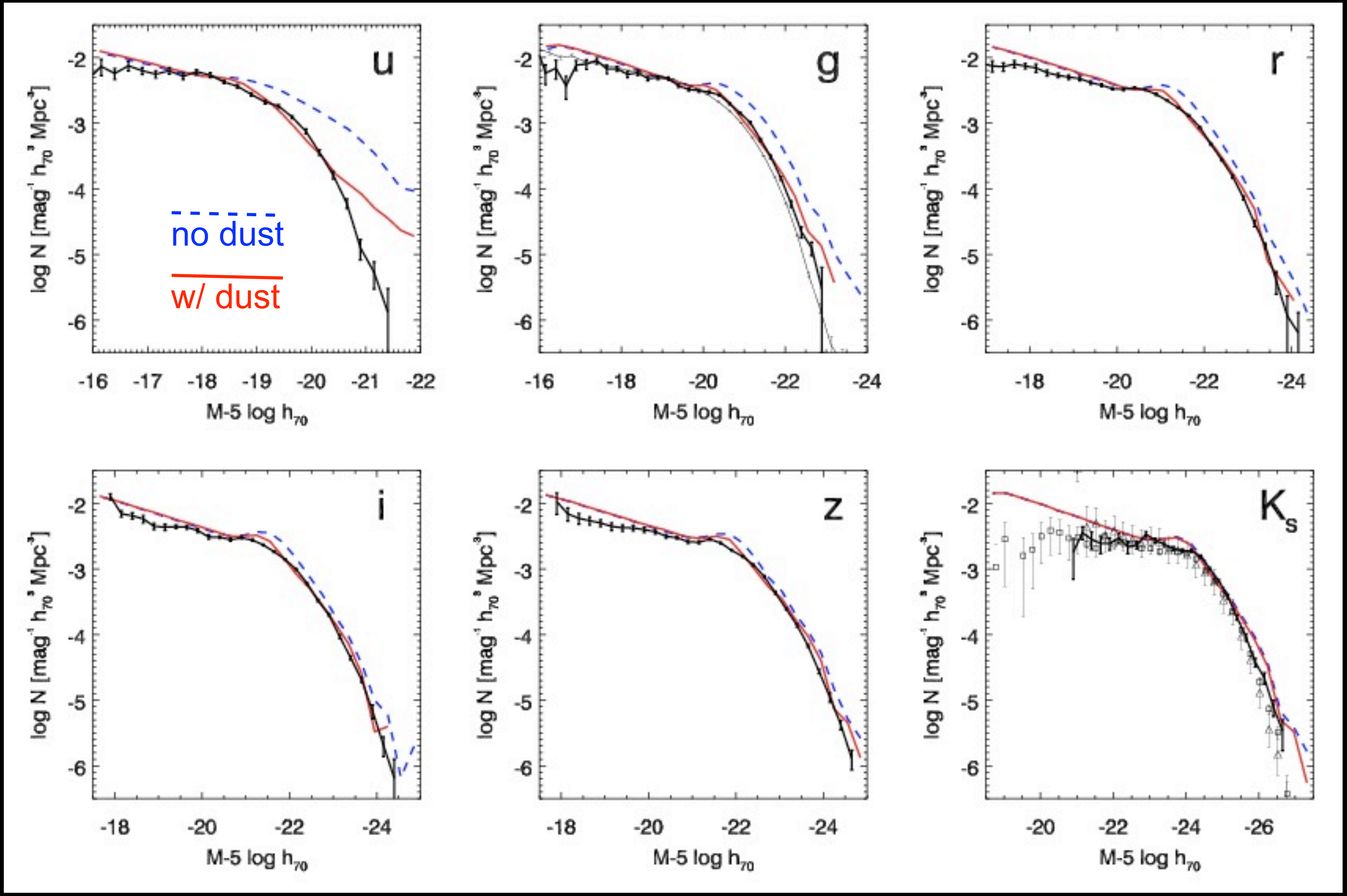

Somerville et al. 2008

Model produces enough massive galaxies at high redshift

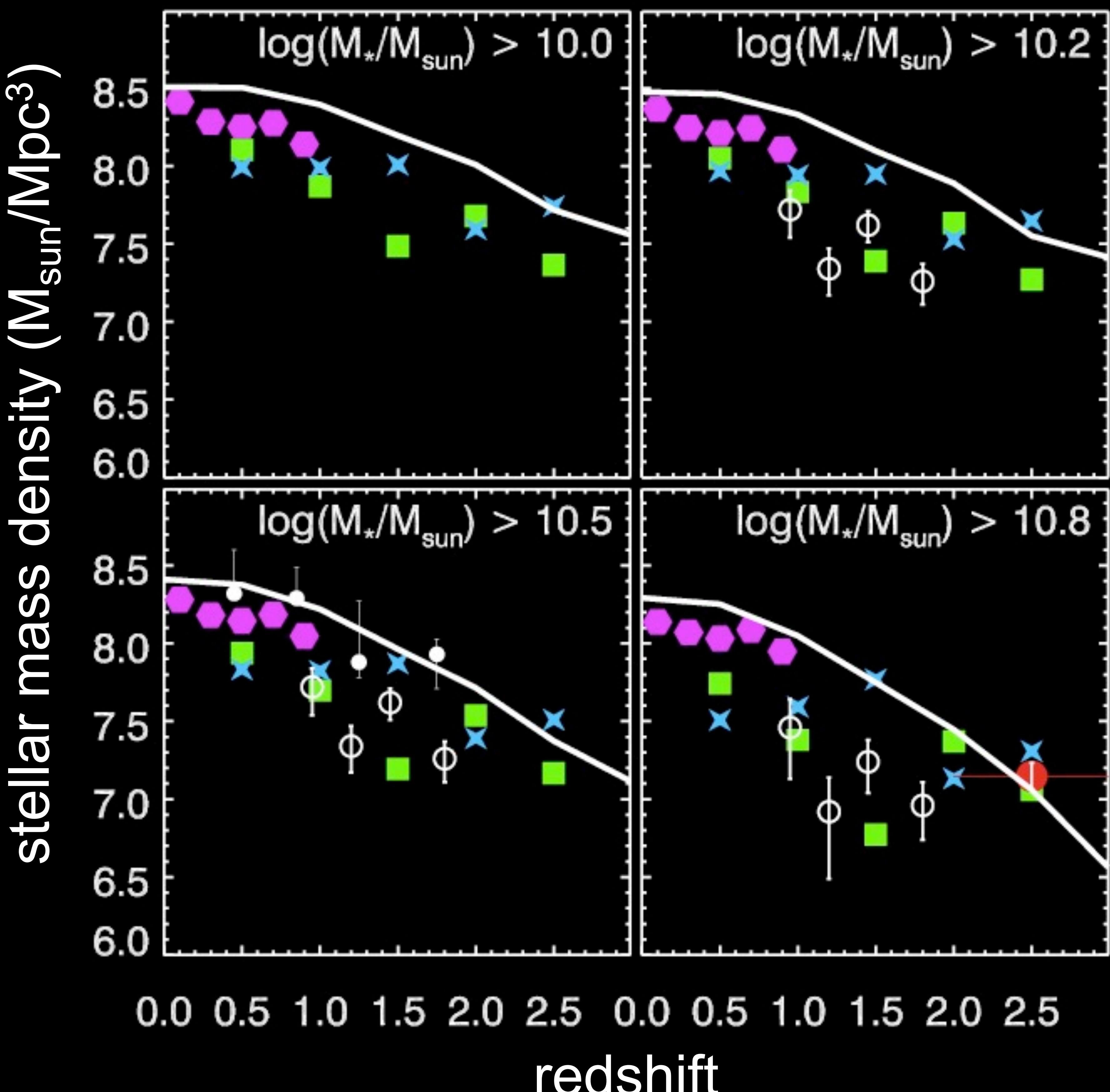

observations:
Borch et al. (COMBO-17)
Drory et al. (GOODS)
Glazebrook et al. (GDDS)
Fontana et al. (K20)
Papovich et al. (GOODS DRGs)

Somerville et al. 2008;
see also Bower et al.2006;
Kitzblicher & White 2006

Stellar Mass Function Evolution

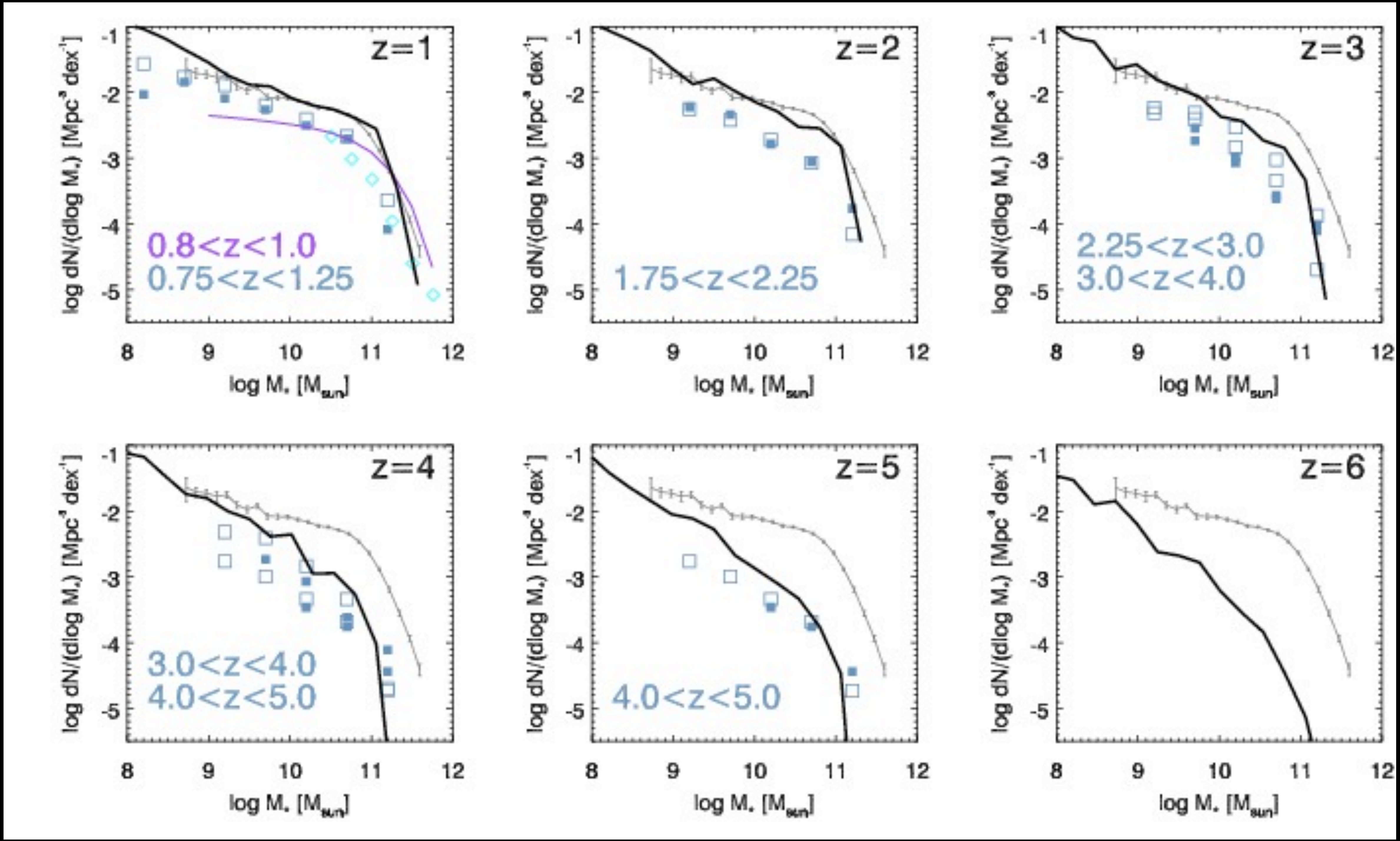

data from Borch et al. (COMBO-17);
Drory et al. (MUNICS, GOODS, FDF)

Somerville et al. in prep

A Physical Model for Predicting the Properties of Spheroidal Remnants of Binary Mergers of Gas Rich Disk Galaxies

We might expect that a more energetic encounter will cause increased tidal stripping and puff up the remnant.

NO! For our simulations, more energetic encounters create more compact remnants.

Why? Dissipative effects cause more energetic encounters to result in smaller remnants. The greater the impulse, the more the gas is disturbed, therefore the more it can radiate and form stars.

A number of physical mechanisms conspire to make this so (e.g., greater tidal effects, lower angular momentum, and more gas disk overlap).

Matt Covington, Cox, Dekel, & Primack MNRAS 2008

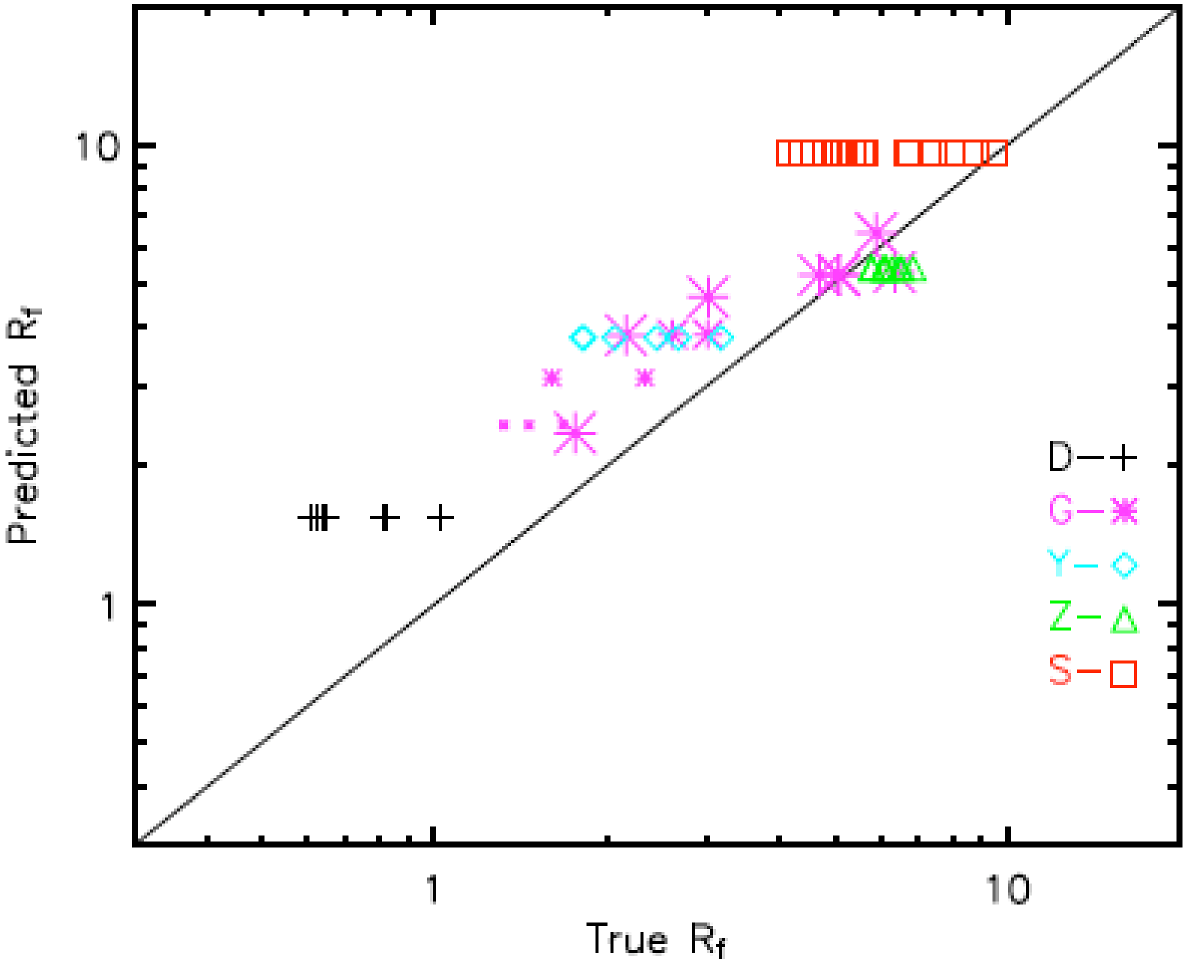

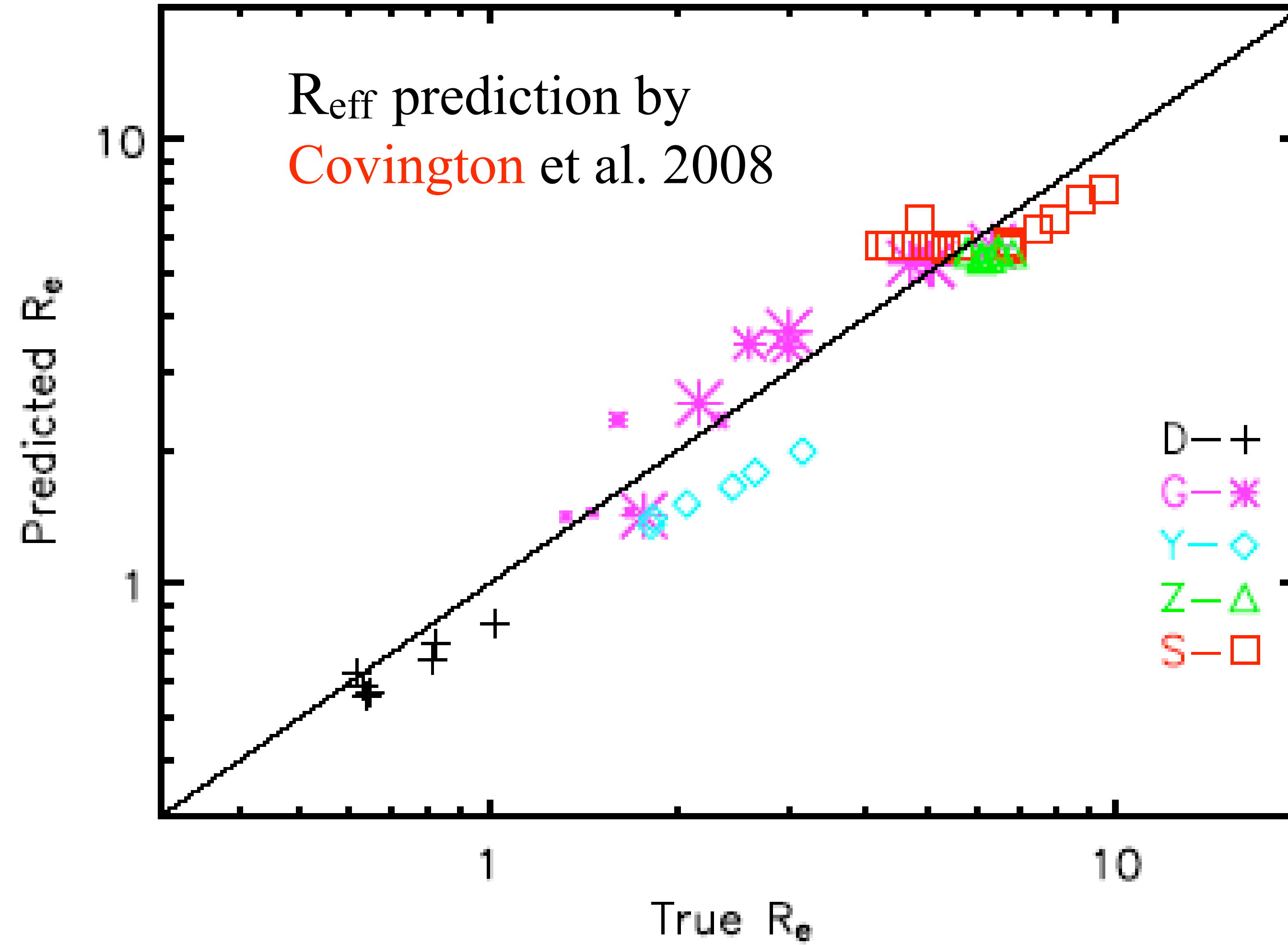

R$_{eff}$ prediction by
Cole et al. 2000
dissipationless model,
best for dry merging

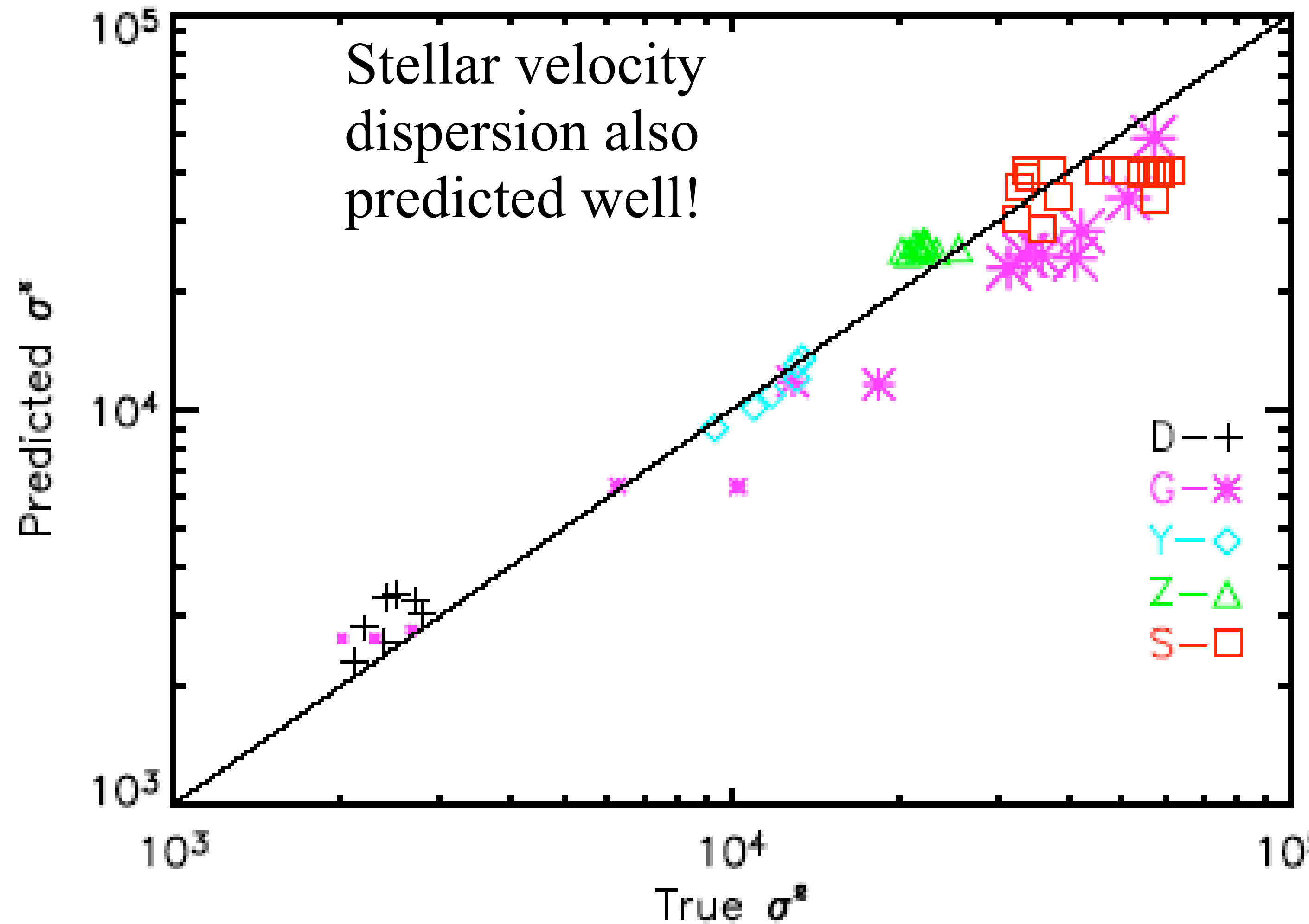

Covington et al. 2008 model takes dissipation into account, also works well for dry and non-equal mass mergers, including minor mergers!

Somerville+08 SAM + Mergers Predict Observed Size-Mass

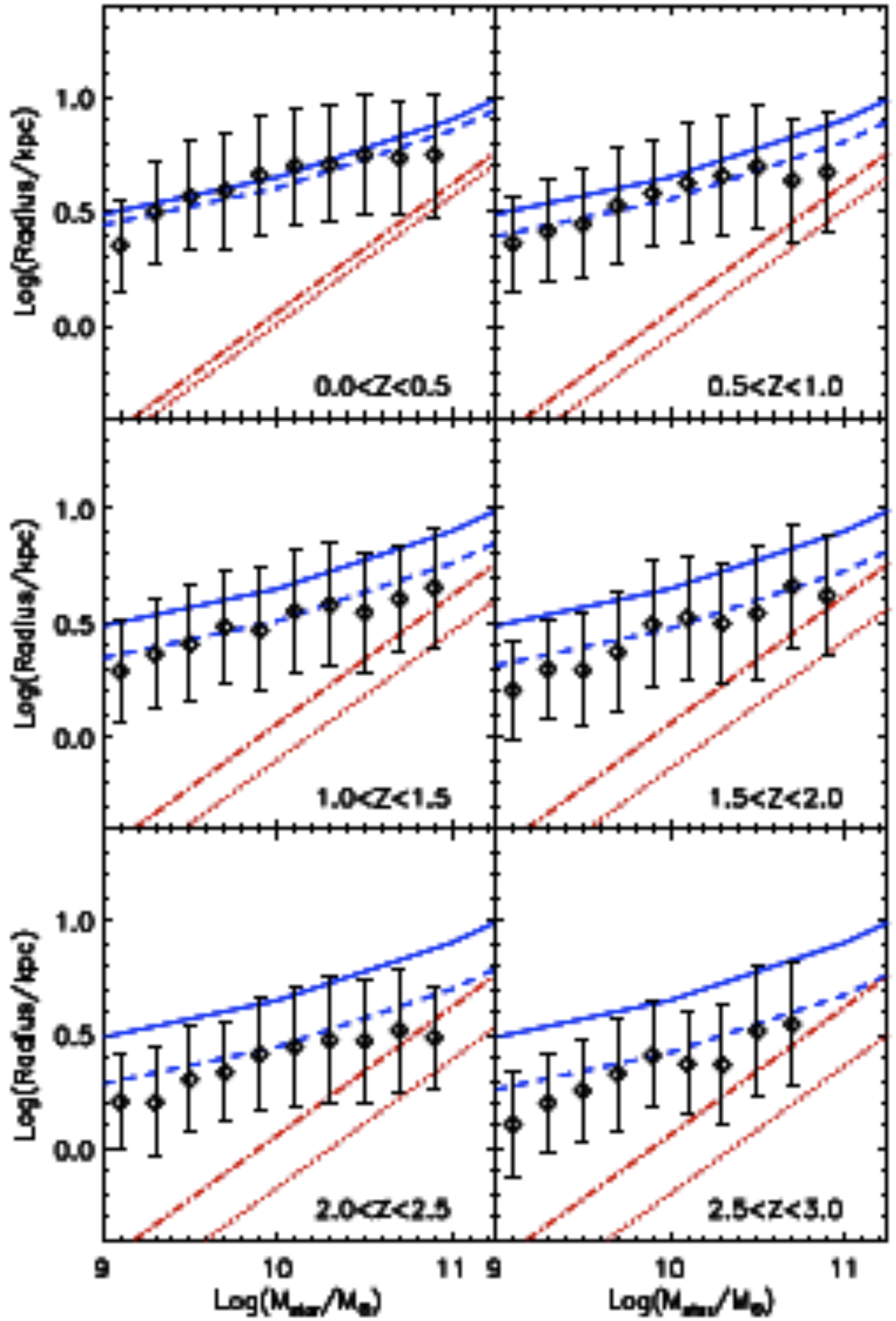

DISKS

z ~ 0 observations SDSS

higher z data Trujillo+06

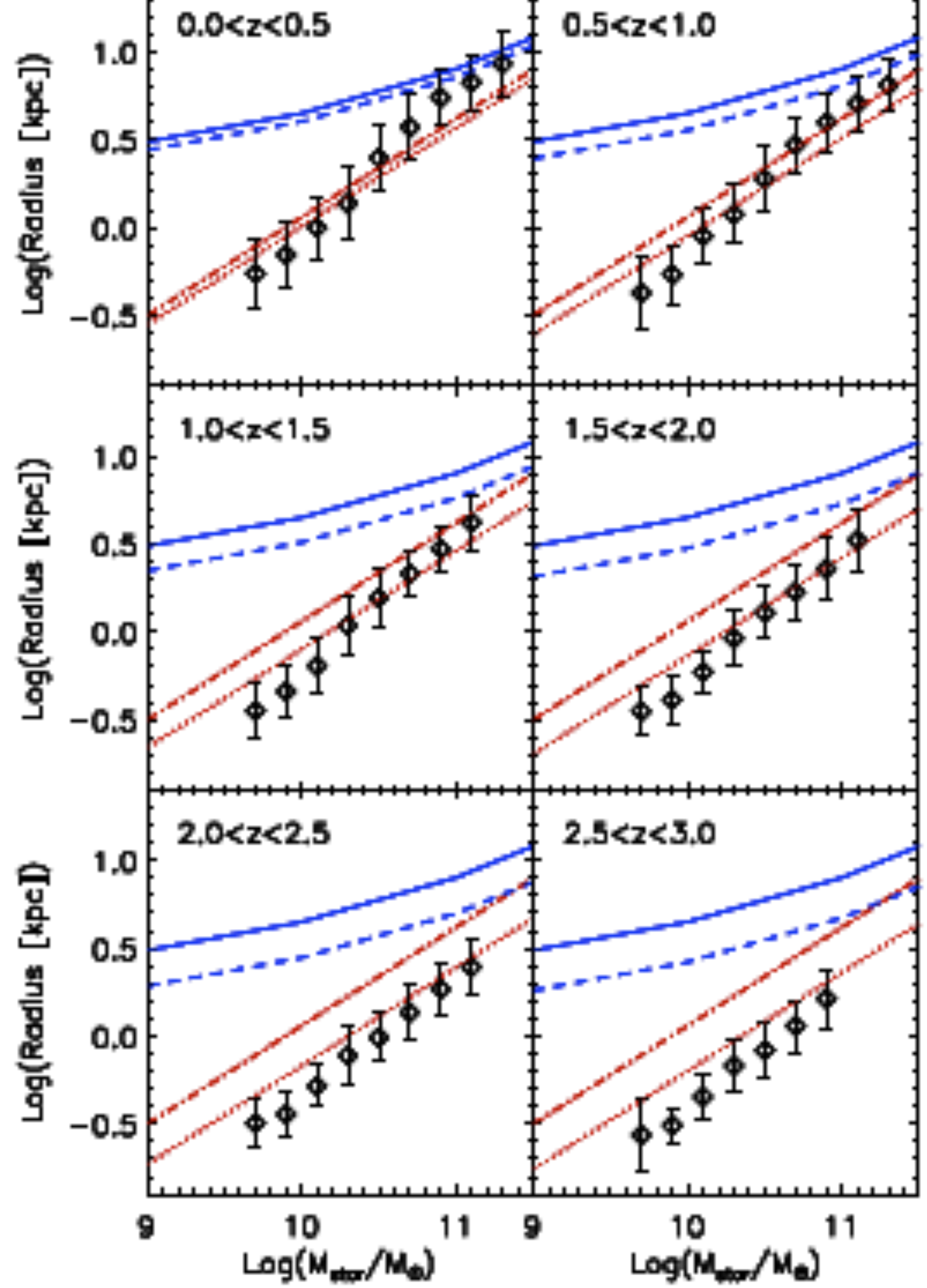

SPHEROIDS

z ~ 0 observations SDSS

higher z data Trujillo+06

Faber-Jackson relations for the remnants in the S08 SAM, binned by redshift. Model predicts little F-J evolution.

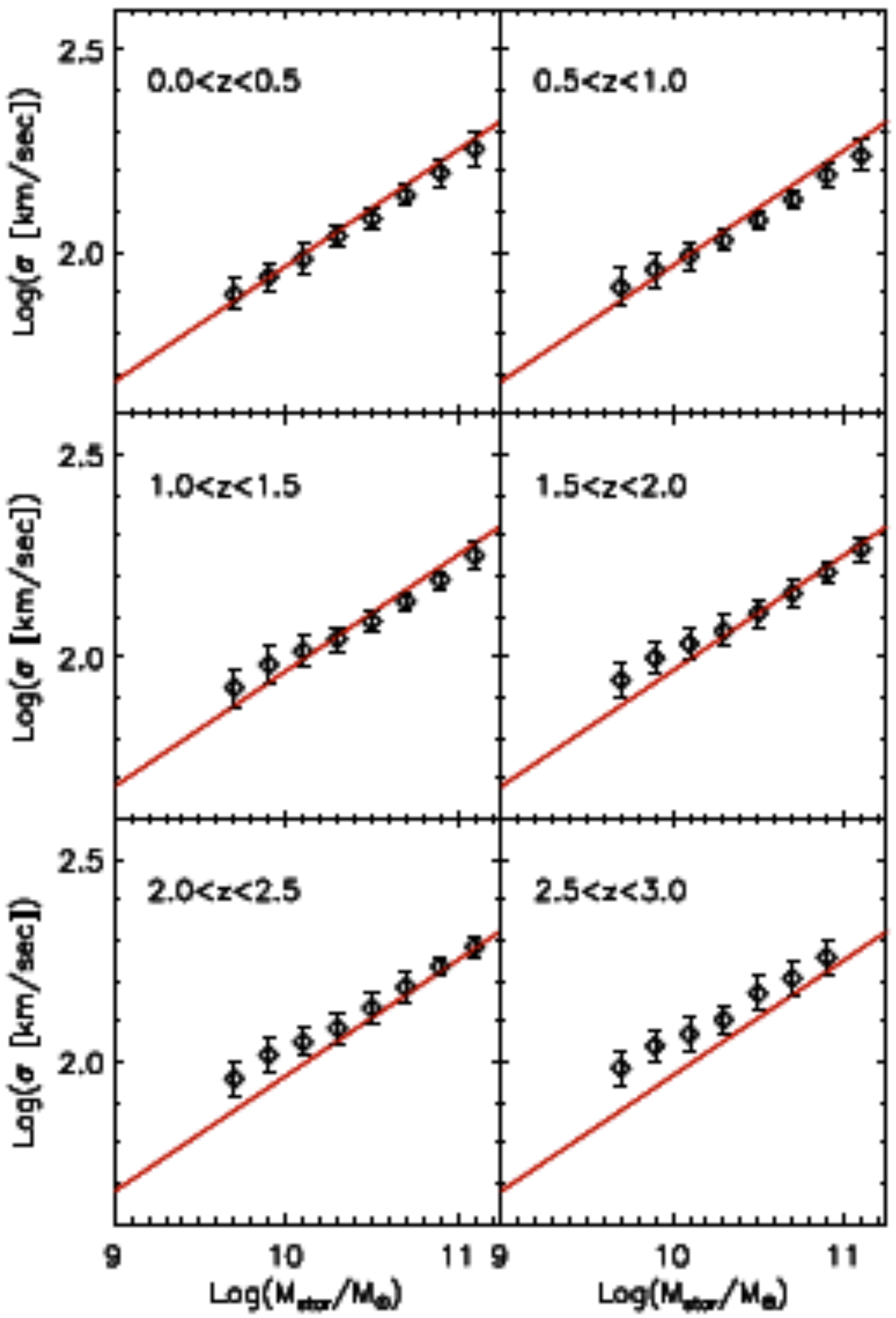

Red line is the observed relation at low redshift (Gallazzi et al., 2006).

Fundamental Plane plotted as M_* vs. M_{dyn} for the remnants in the S08 SAM, binned by redshift. Model reproduces observed tilt of the Fundamental Plane.

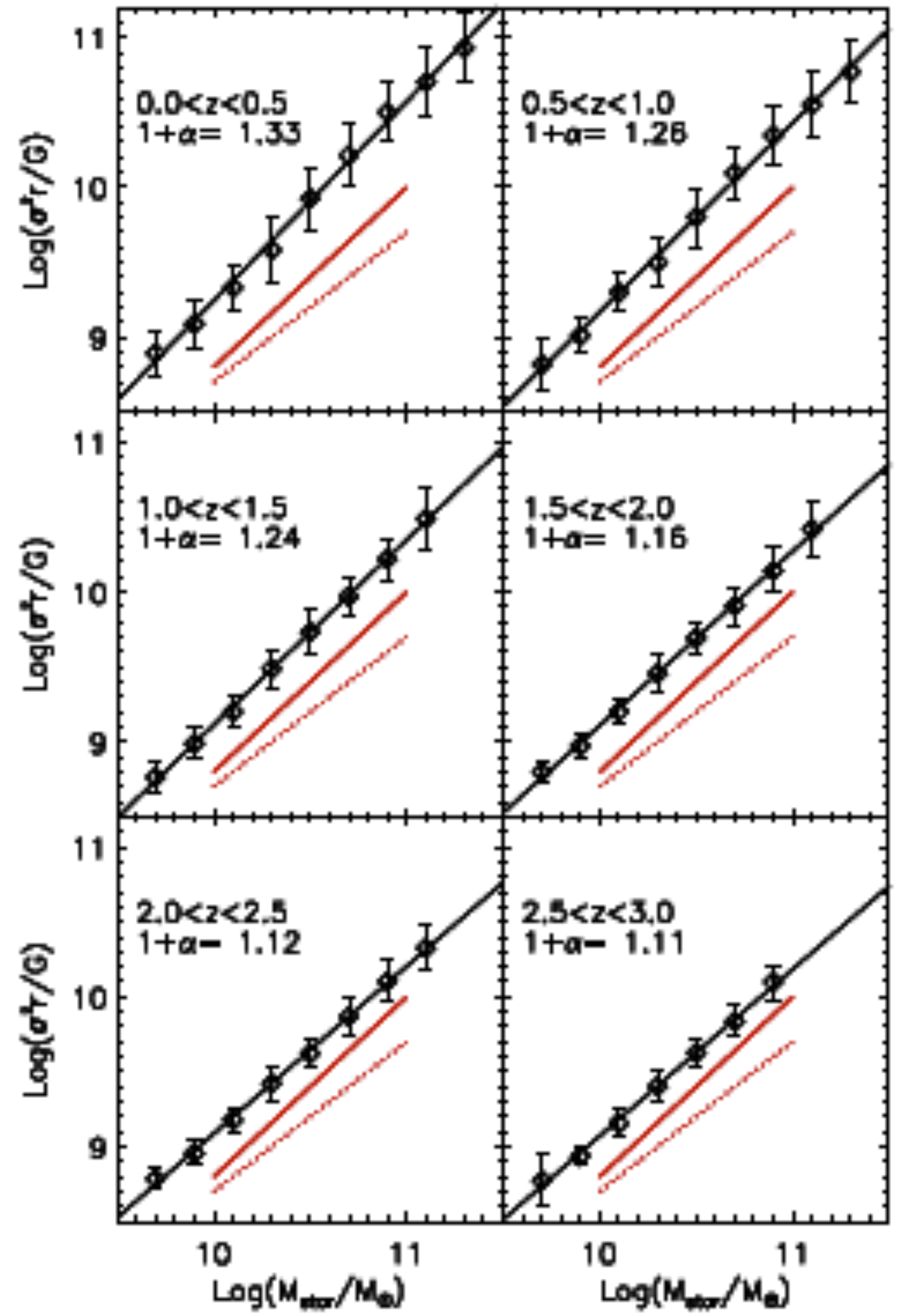

observed scaling $M_{dyn} \propto M_*^{1.2}$

virial scaling

Matt Covington dissertation 08

The black line is fit to the SAM remnants with $M_{dyn} \propto M_*^{1+\alpha}$ (1 + α is shown on the figure).

Covington et al. in prep.

Flow through the color-mass diagram for "central" galaxies

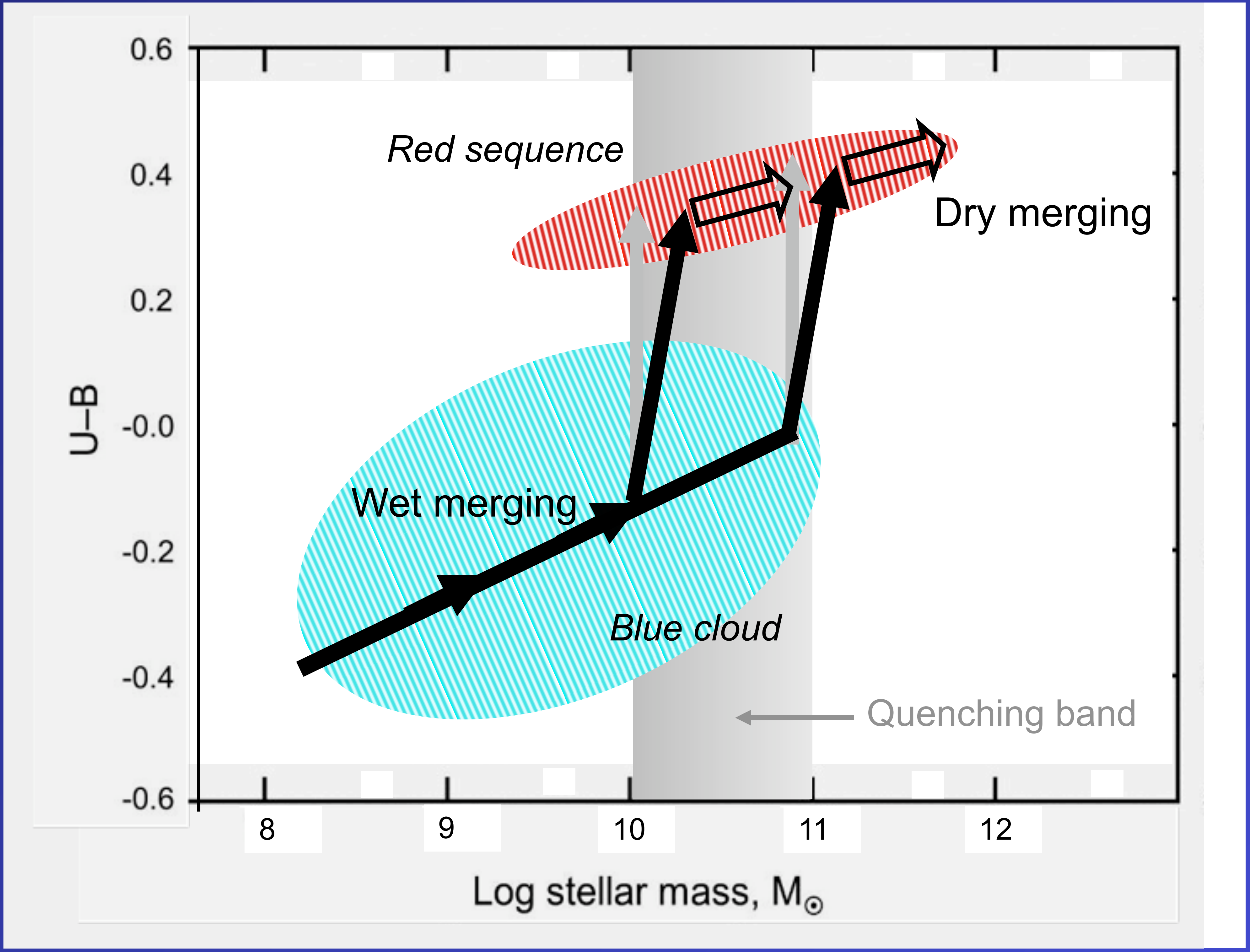

Sandra Faber

Flow through the color-mass diagram for "satellite" galaxies

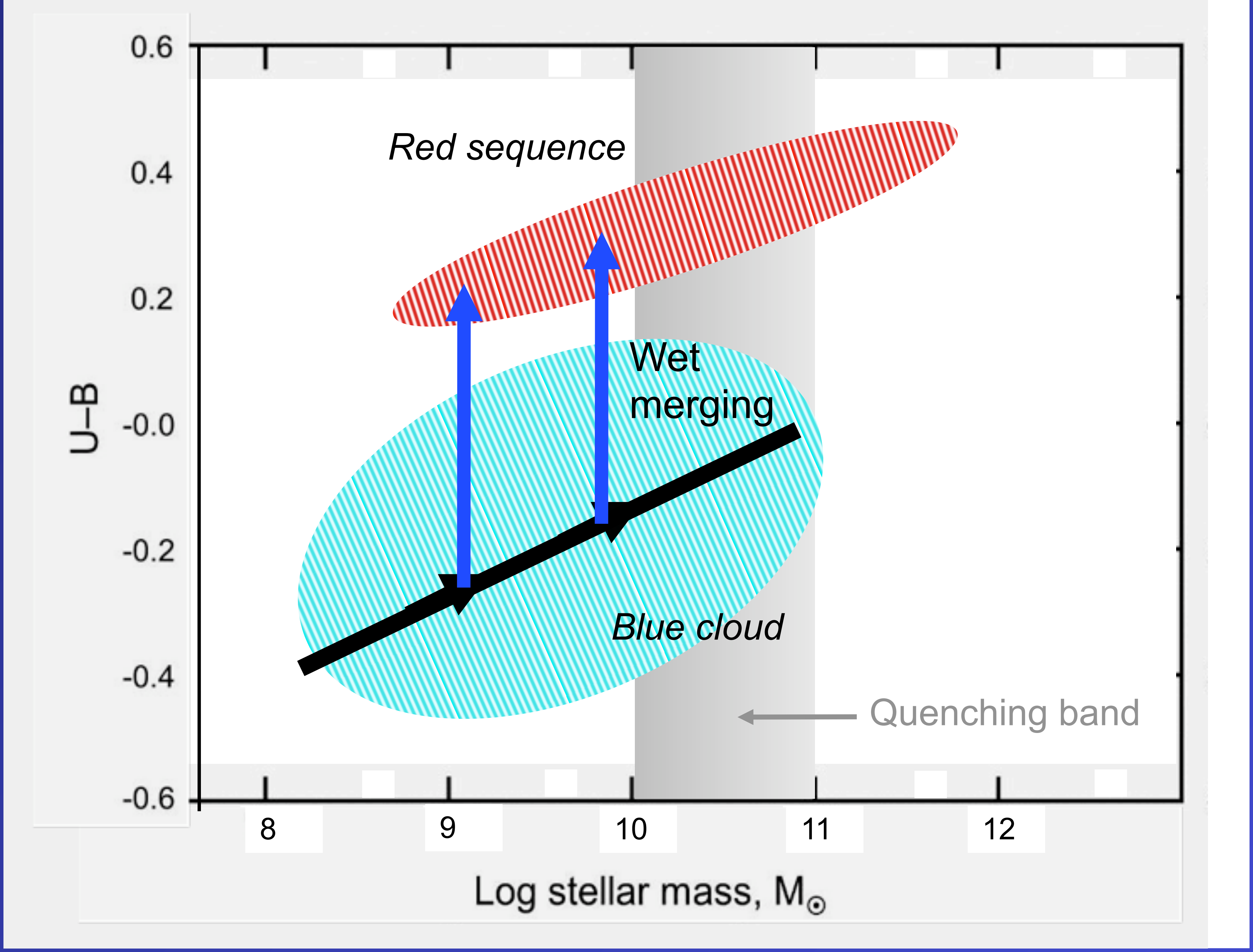

Sandra Faber

Flow through the CM diagram versus environment

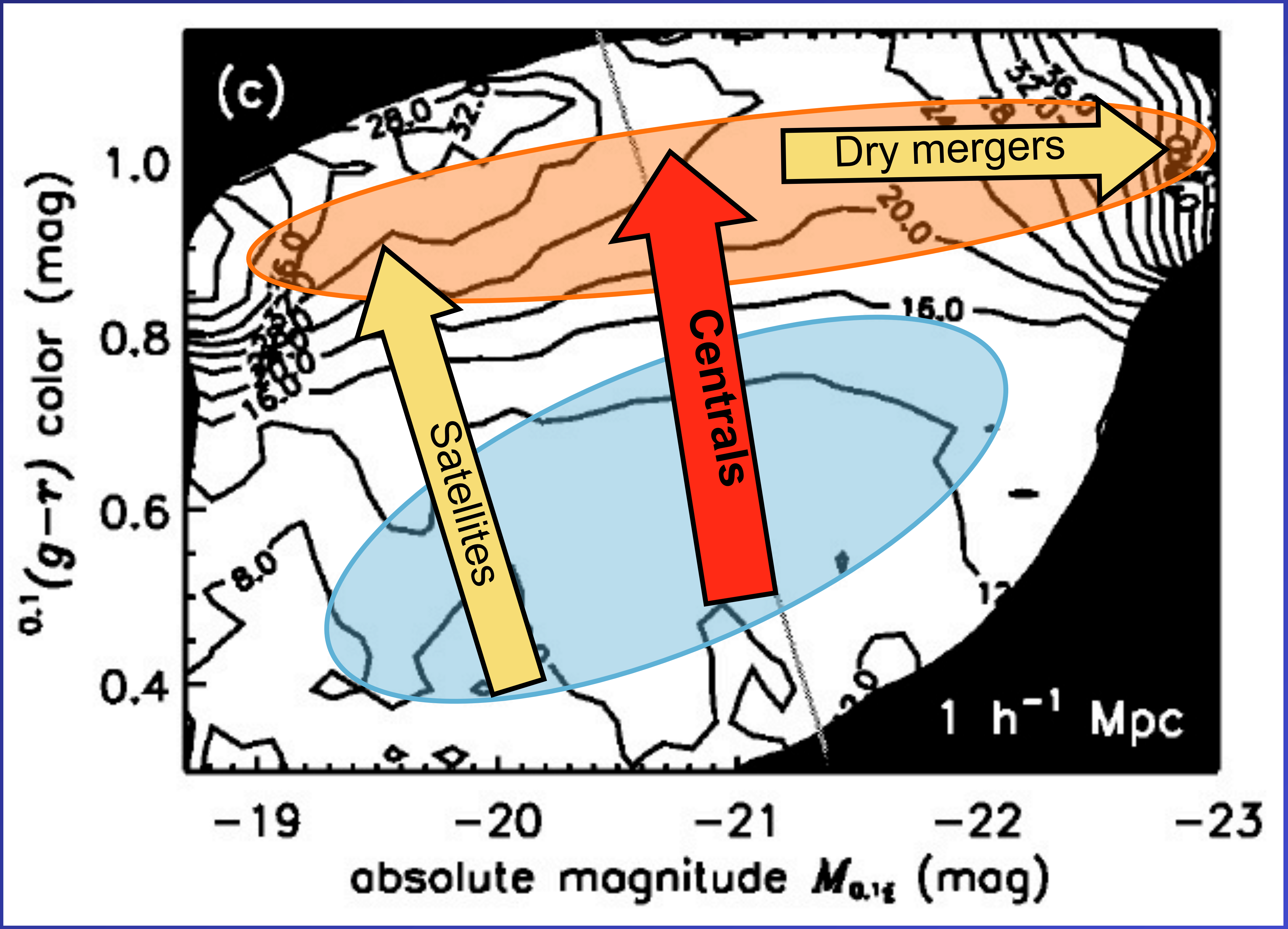

Hogg et al. 2003: Sloan Survey

All formed by environment

BH not avail?

$M_i^{0.1}$ = -19.3

Transition mass
3 x 10^{10} $M_\odot$

$M_i^{0.1}$ ~ -21.0

Satellite/Central
wet/dry transition

$M_i^{0.1}$ > -22.1

All boxy/dry

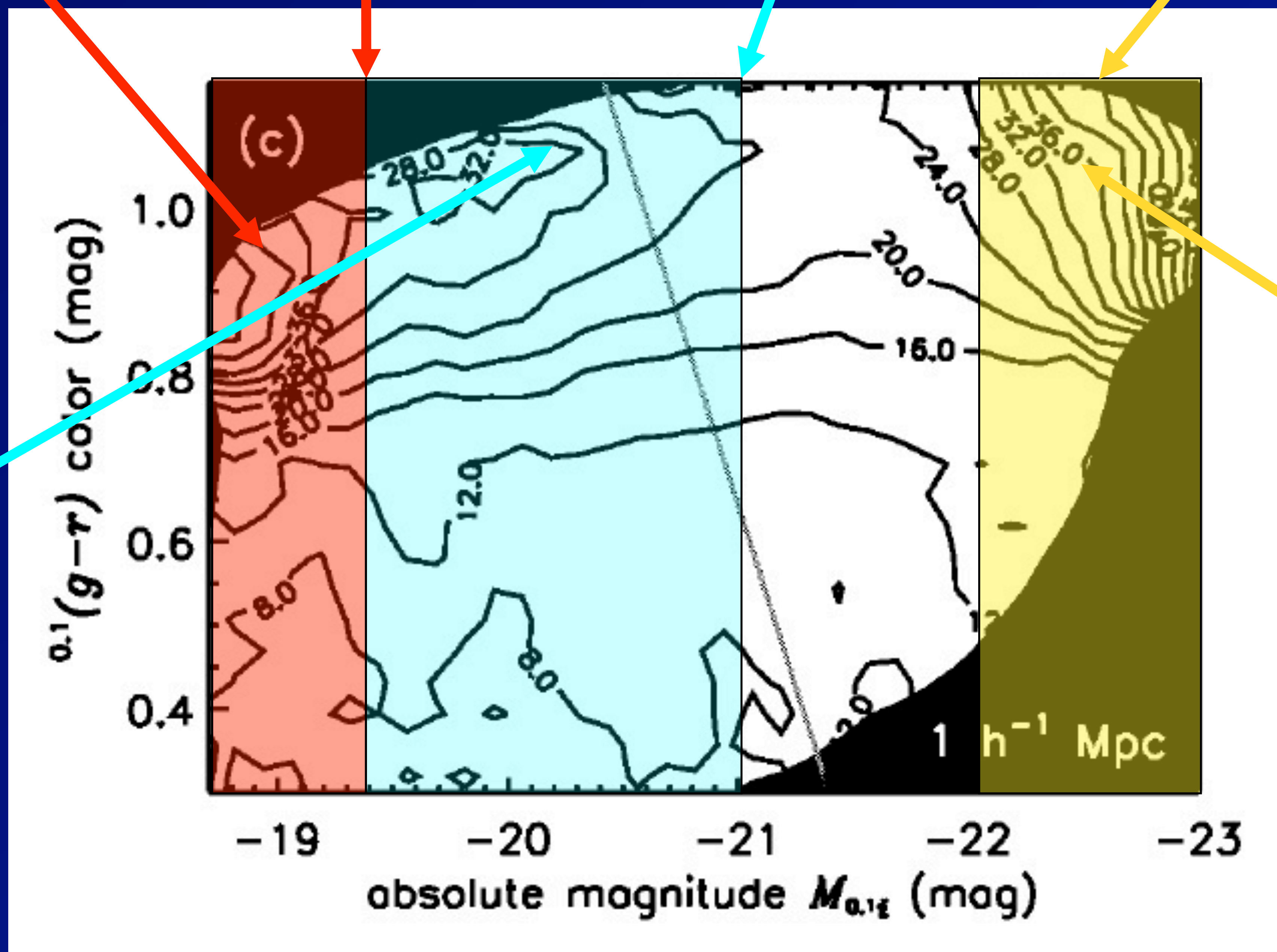

Some by env,
some by wet
mergers

All by dry
mergers

Sandra Faber

History of Star Formation and Stellar Mass Build-up

Star Formation History

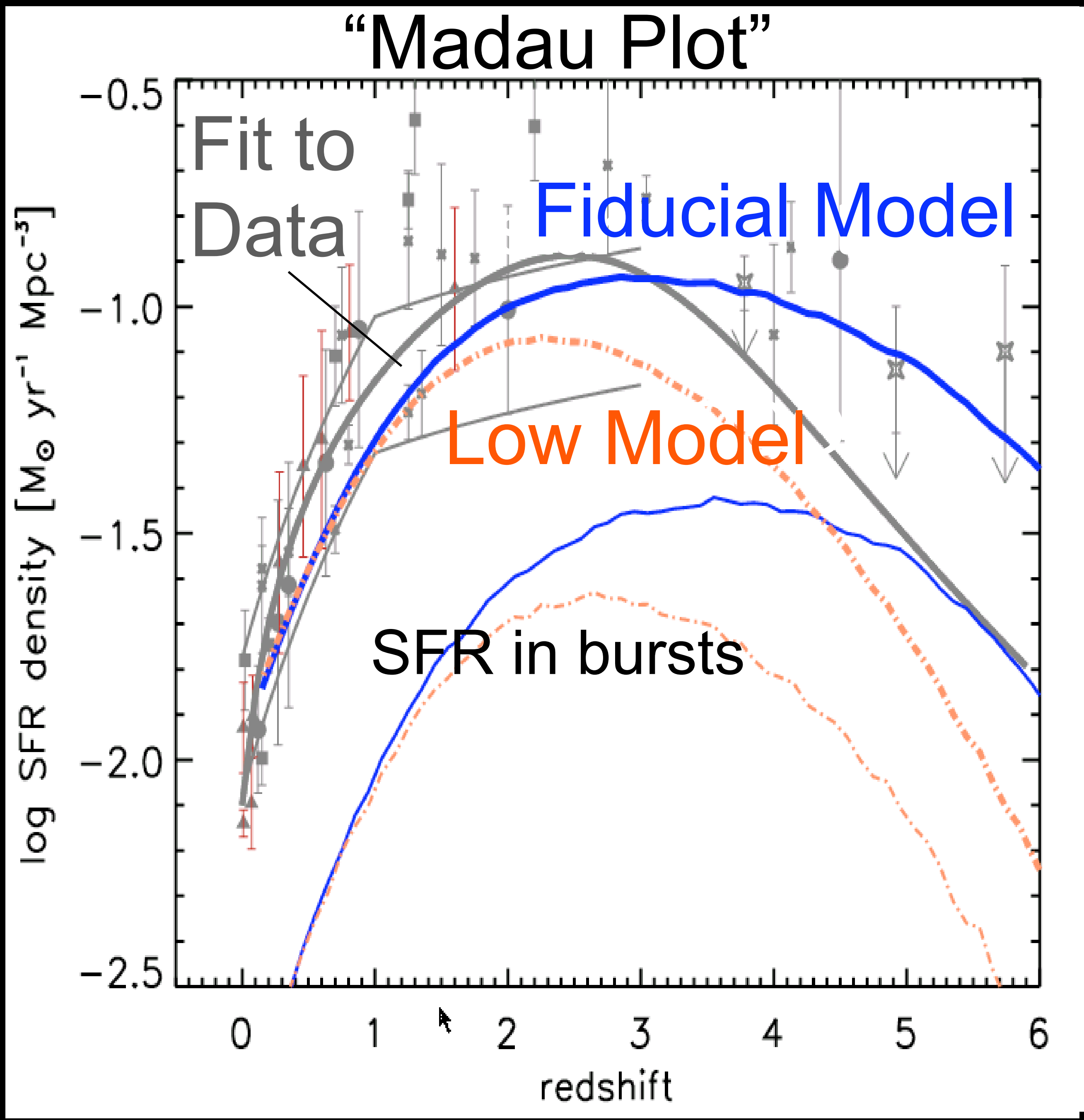

Stellar Mass Build-up

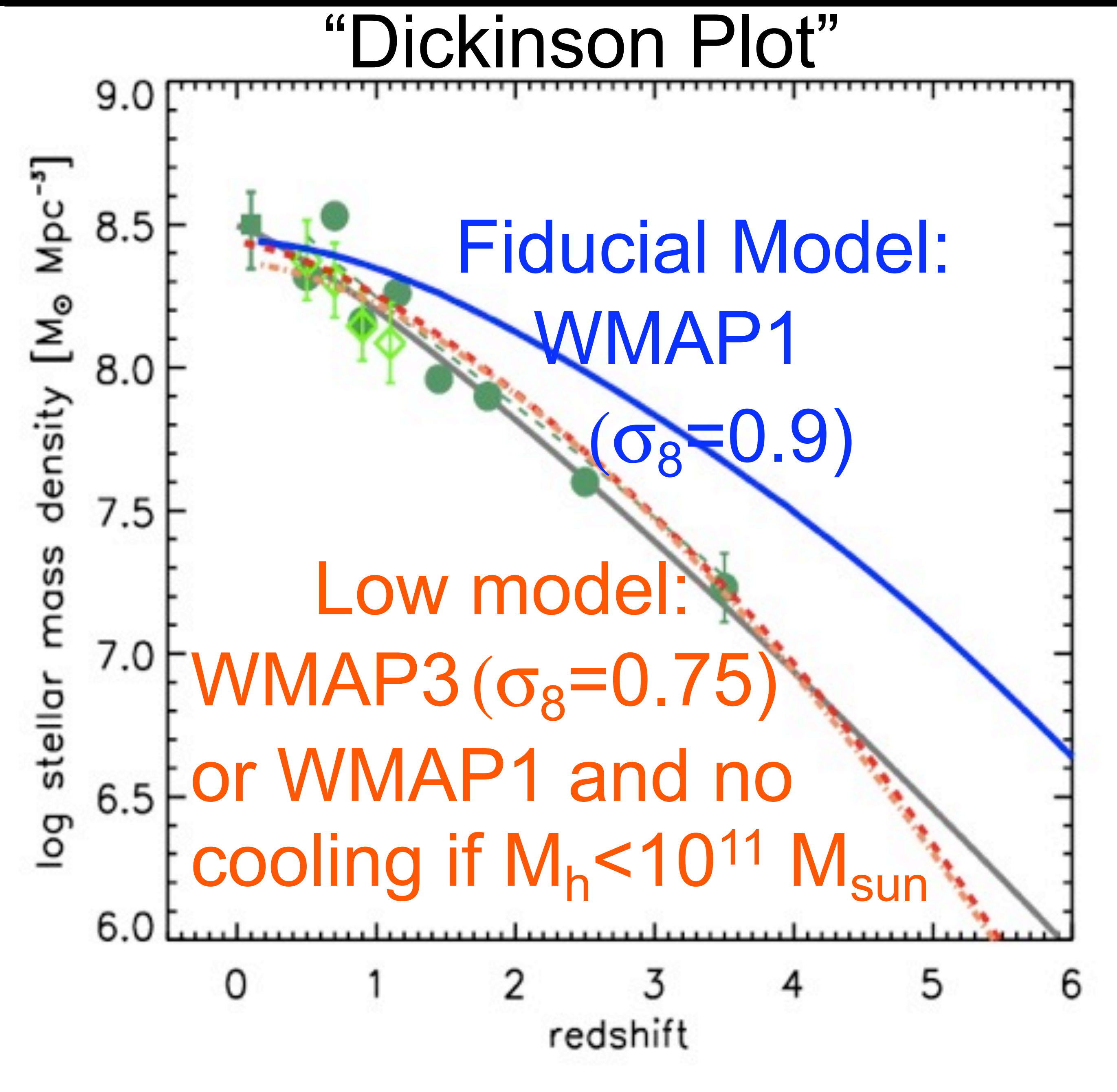

Discrepancy: SFR indicators or IMF evolution?

Somerville et al. 2008

SFR tracers available for large numbers of galaxies at z~1:

1) Thermal IR 24mum + UV continuum :

Advantage: In principle, self-correcting for extinction

Problems: Obscured AGN posing as SF (Daddi et al. 2007)

Are local IR SED templates correct at z>~1?

Hope: longer λ data (FIDEL, Herschel, LMT, ALMA)

2) UV continuum

Advantage: widely available from broad-band imaging to high z

Problems: extinction correction (UV slope, ...) uncertain

Hope: SED fits (Salim et al.), calib from other tracers

3) Emission lines (Balmer, OII, OIII)

Advantage: Robust extinction correction from Balmer decrement

Problems: Balmer lines need NIR spectroscopy at z~1

OII, OIII depend on T,O/H, calibration problematic

Hope: NIR, massively Multi-Object spectrographs

Kai Noeske

Fiducial Model

Low Model

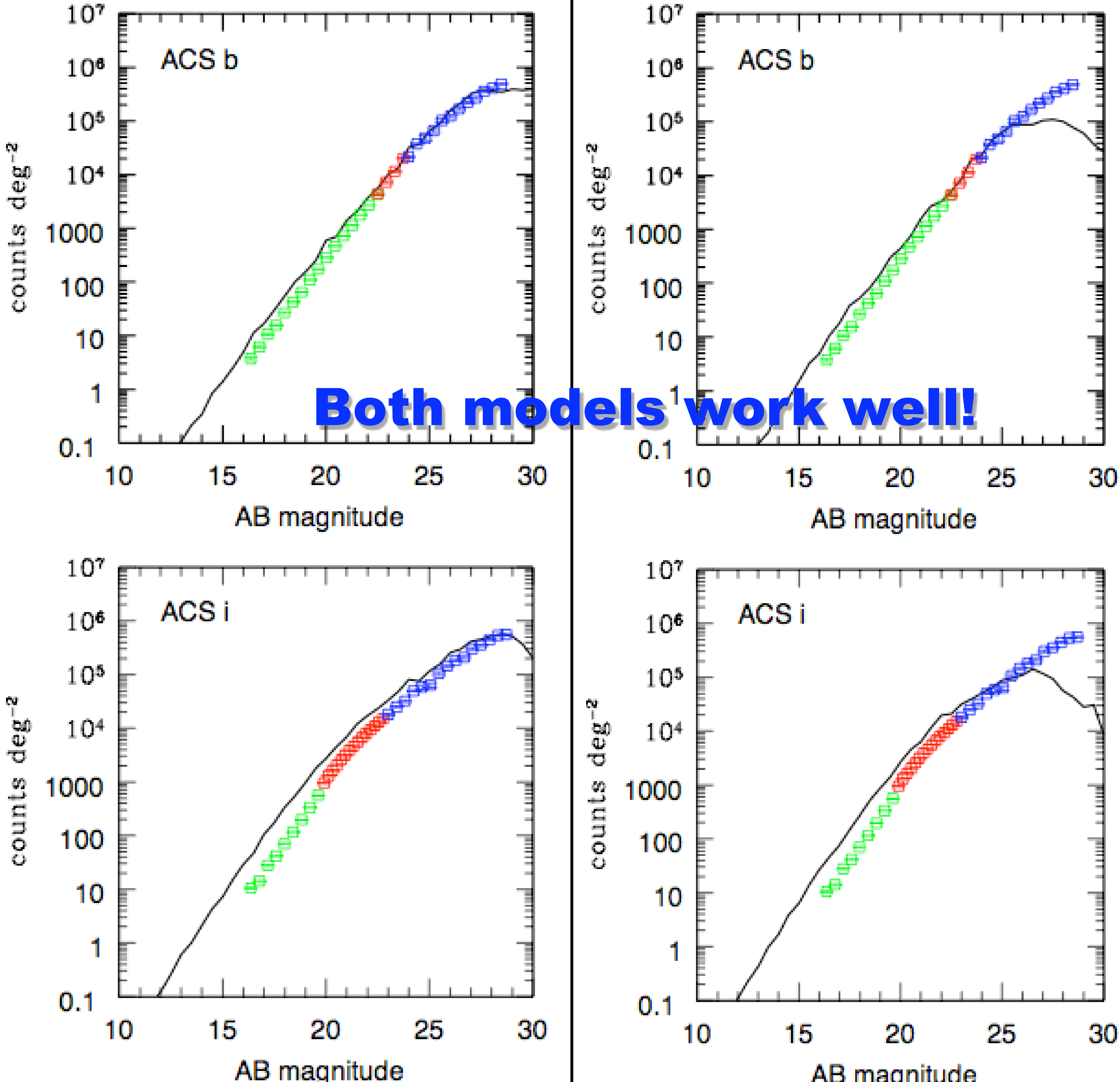

Both models work well!

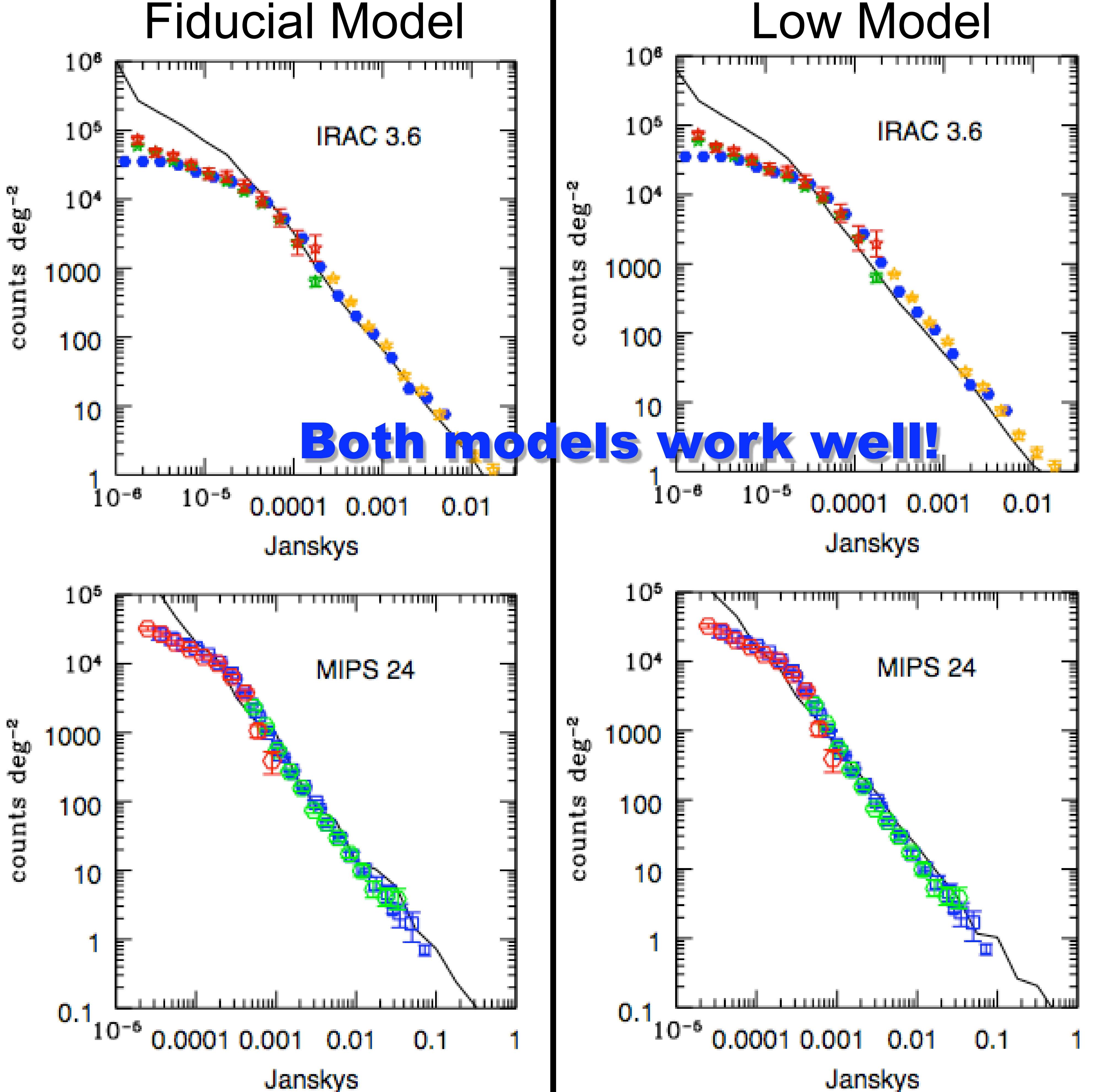
Fiducial Model
Low Model
IRAC 3.6
MIPS 24
counts deg^{-2}
Janskys
Both models work well!

08SAM **Fails** to Predict Observed 850 μm Number Counts

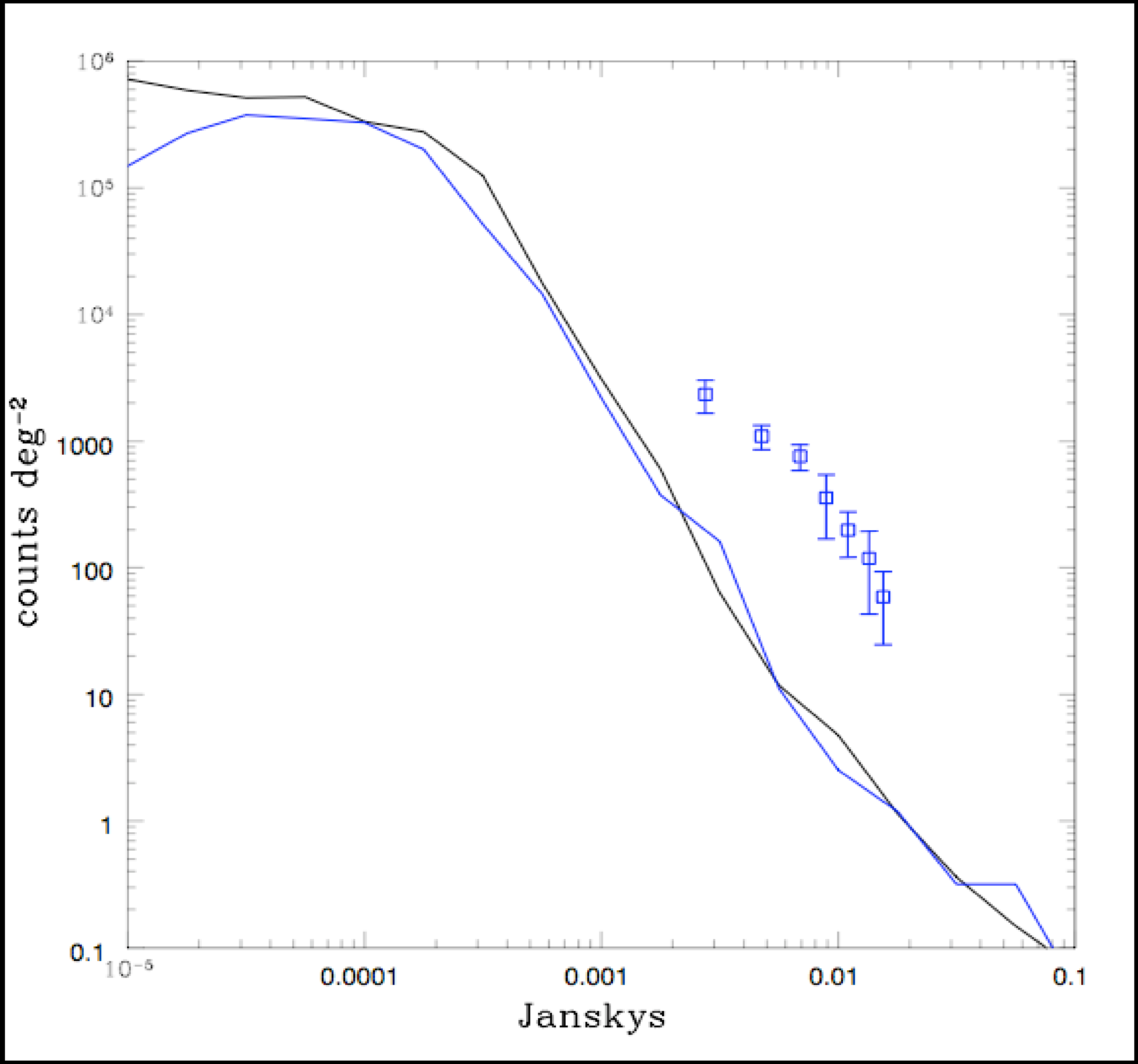

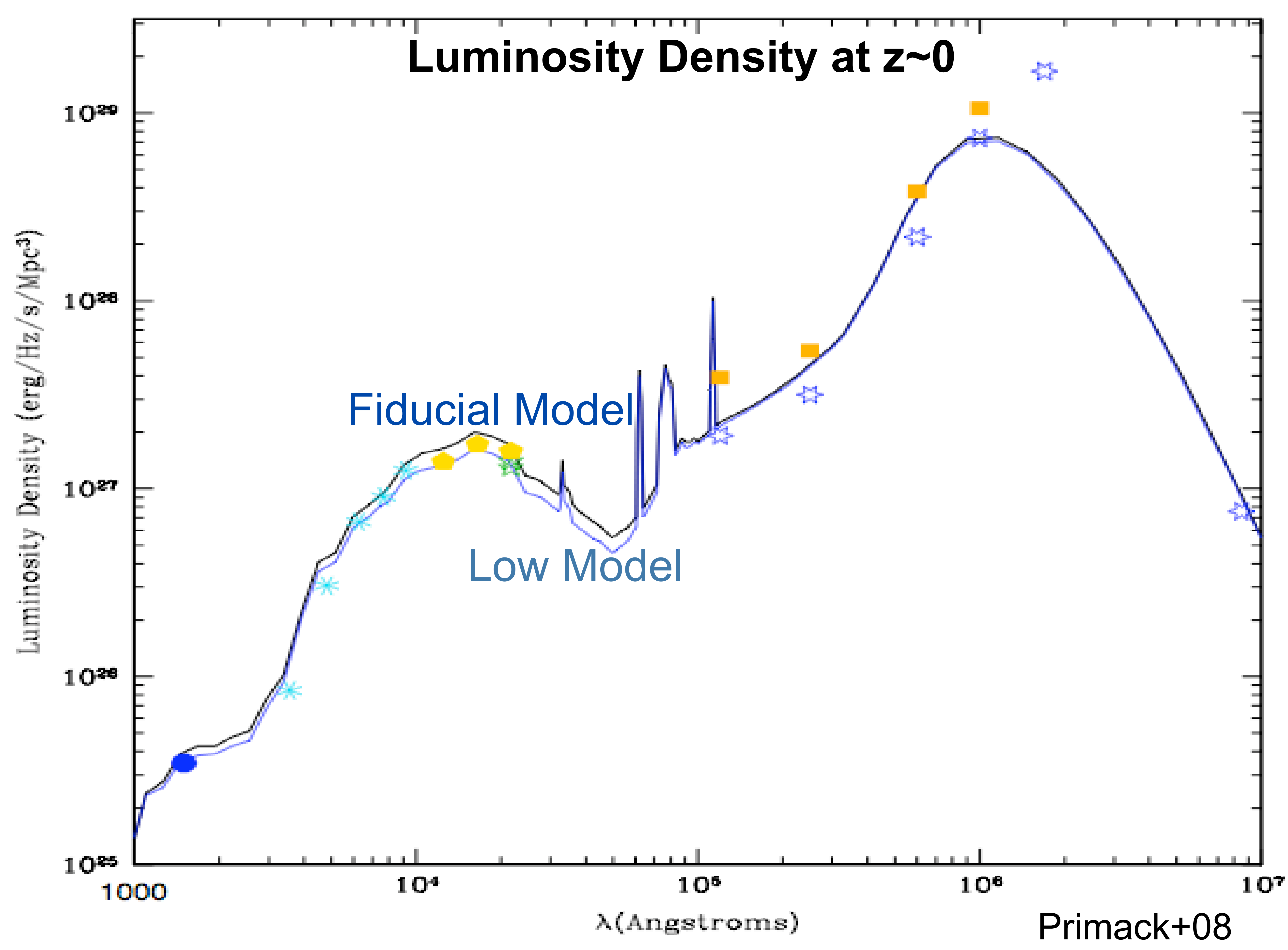
Luminosity Density at z~0
Luminosity Density (erg/Hz/s/Mpc^3)
10^{29}
10^{28}
10^{27}
10^{26}
10^{25}
Fiducial Model
Low Model
1000
10^4
10^5
10^6
10^7
λ(Angstroms)
Primack+08

Extragalactic Background Light

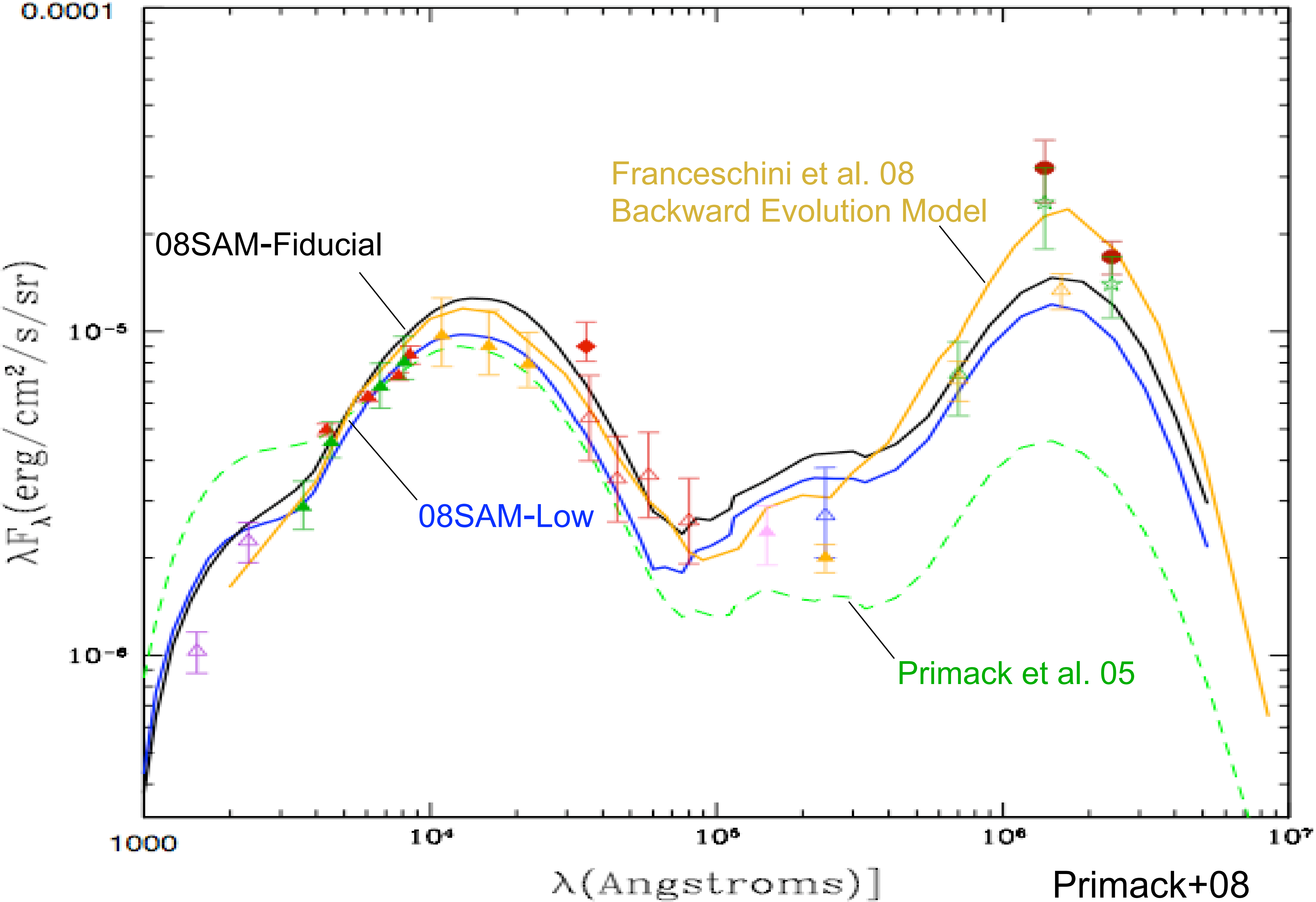

Primack+08

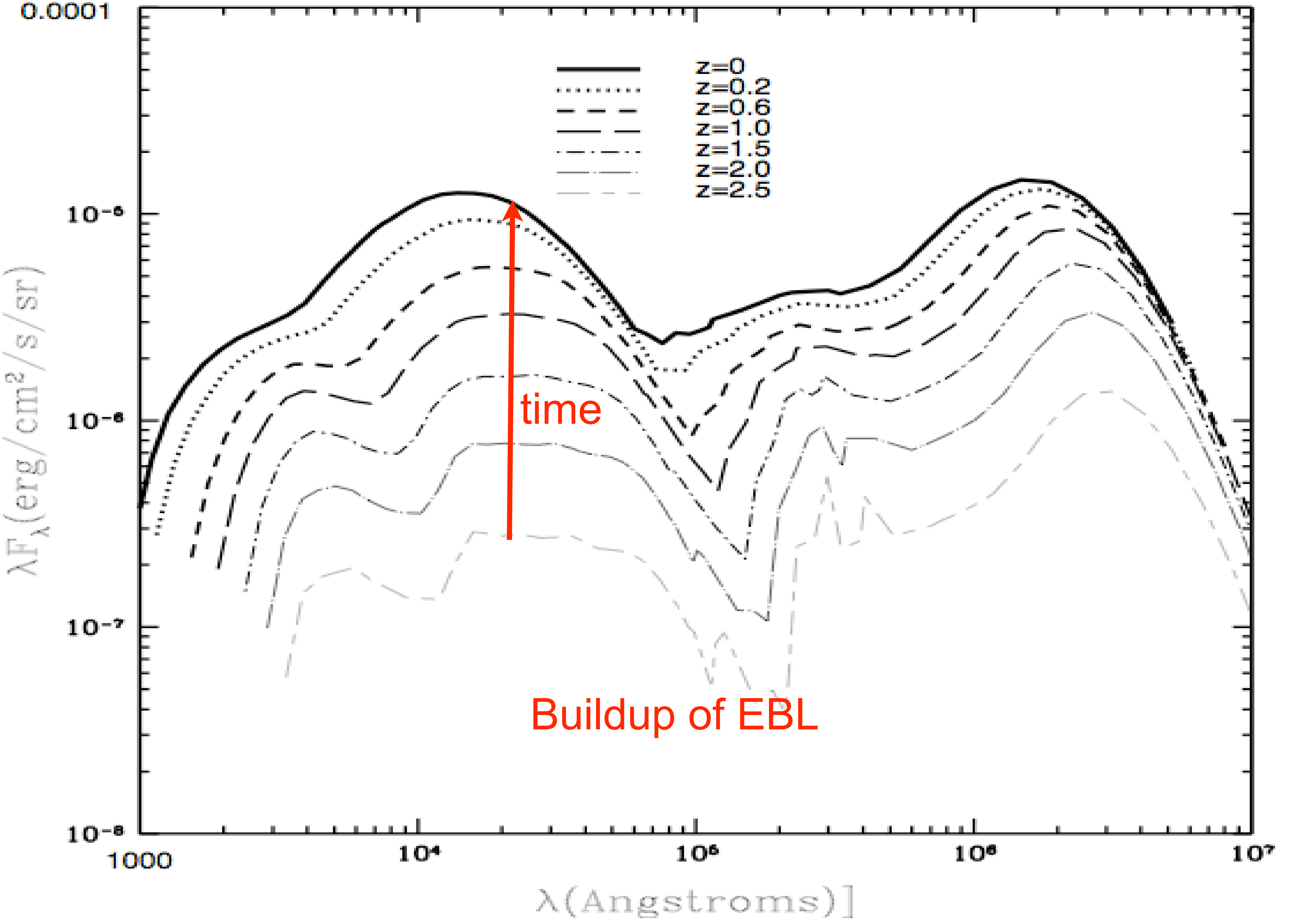

0.0001
z=0
z=0.2
z=0.6
z=1.0
z=1.5
z=2.0
z=2.5
time
Buildup of EBL
10^{-5}
10^{-6}
10^{-7}
10^{-8}
λF_λ(erg/cm^2/s/sr)
1000
10^4
10^5
10^6
10^7
λ(Angstroms)]

Upper Limits on EBL from z~0.2 Blazars and z=0.53 Quasar

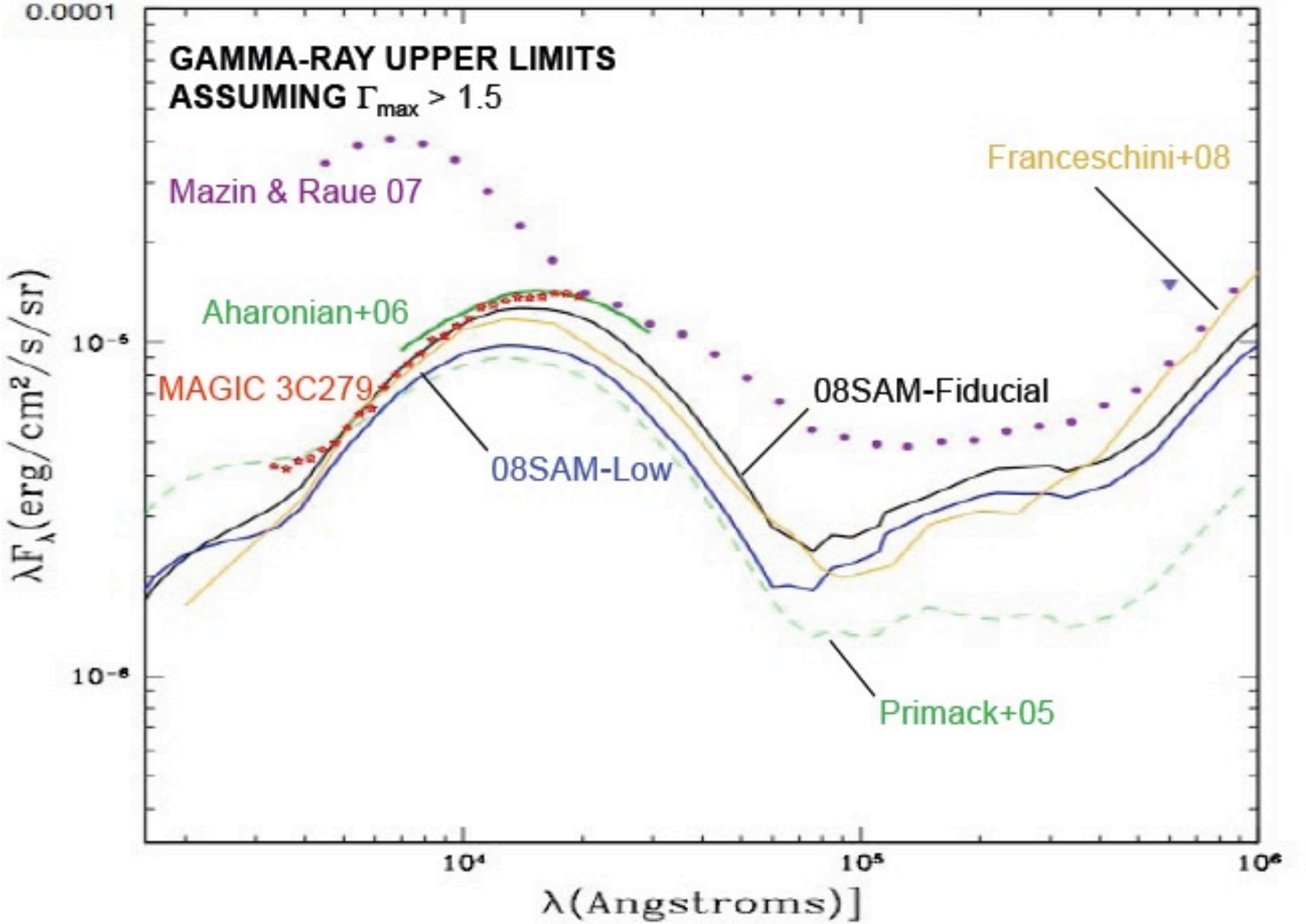

Gamma Ray Attenuation Due to **Fiducial** and **Low** Models

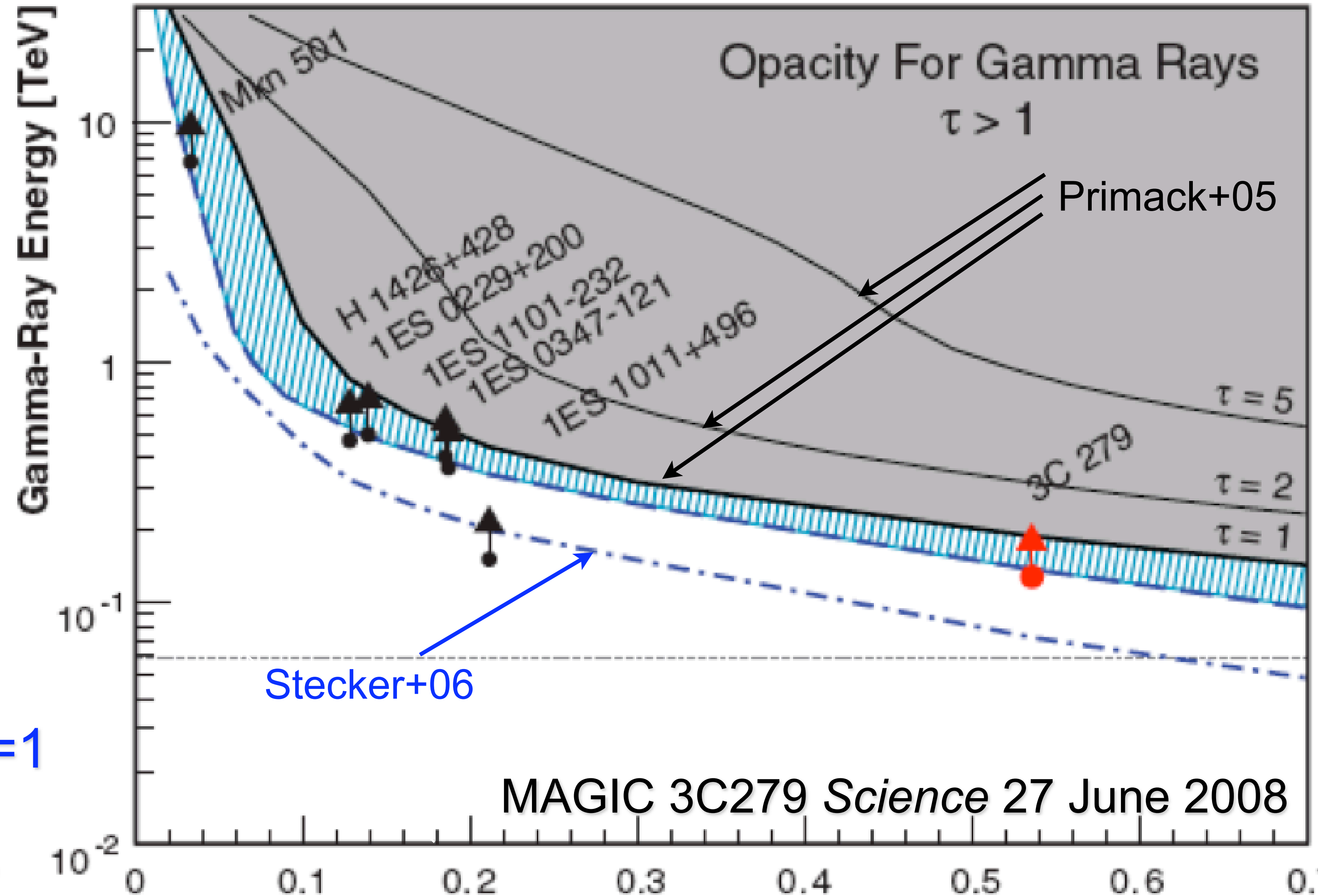

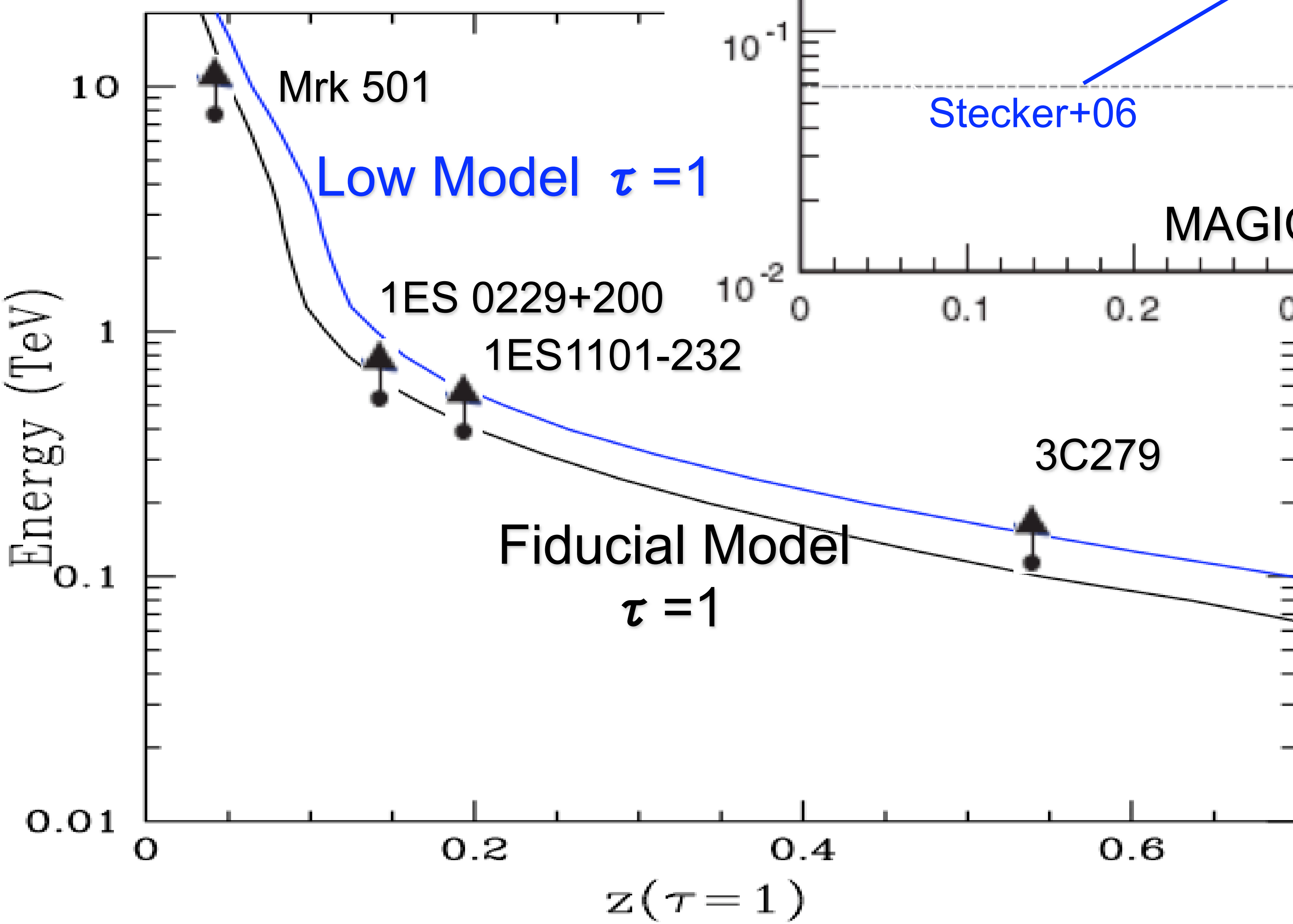

Gilmore, Primack, Somerville 2009
Low Model is well within observational constraints

Fiducial Model also looks OK!

Conclusions

- High resolution DM simulations show halo substructure. New hydrodynamic simulations are increasingly able to explain galaxy formation. At z>2, even massive halos have cold streams bringing in gas that quickly forms stars. At z<2 this only happens for $M_{halo} < 10^{12}$.
- Spheroids from mergers have the observed size-mass relation and lie in the observed Fundamental Plane.
- New self-consistent semi-analytic galaxy formation models based on physical scaling from numerical simulations and calibrated against empirical constraints now enable us to predict and interpret the relationship between galaxies, BH, and AGN across cosmic history.
- Such models accurately predict number counts and luminosity functions in all spectral bands and all redshifts except for sub-mm galaxies.
- The predicted range of EBLs is consistent with the best estimates of EBL evolution inferred from observations.